Research Project on CO_2 Geological Storage and Groundwater Resources

Water Quality Effects Caused by CO_2 Intrusion into Shallow Groundwater

Appendices A-F

Appendix A:
Lists of Analytical Methods for Groundwater Analysis

Table A1. Summary of Groundwater Analyses Data Available for Trace Elements (see list of analytical methods in Table A2)

(a) Summary of Arsenic (As) Analyses

Analytical Method Code	PCode	Total No. of Analyses	Detection Limit (mg/L)	No. below Detn Limit	No. at or above Detn Limit	Percentage at or above Detn. Limit (%)	Notes
GF042	01000	135	0.001	124	11	8.15	
GF044	01002	2	0.001	1	1	50.00	
GF073	01002	9	0.005	1	8	88.89	
PL120	01002	2	0.001	1	1	50.00	
PLA06	01000	5	0.002	4	1	20.00	
GF085	01000	652	0.001 0.002 0.004	175 91 1	385	59.05	
GF096	01002	157	0.002 0.003 0.004 0.008	60 2 2 1	92	58.60	
GF031	01002	69	0.001	44	25	36.23	
HY010	01000	5522	0.001 0.005 0.01	2309 1 9	3203	58.00	
HY013	01002	137	0.001	81	56	40.88	
PLA07	01002	117	0.002 0.004	33 66	99	84.62	
PLM10	01000	76	0.00012	6	70	92.11	
PLM27	01000	174	0.002 0.001 0.01	104 24 2	144	82.76	
PLM40	01000	2782	0.0002 0.0003 0.0004 0.0009	201 72 1 87	2421	87.02	
Unknown		11610	>0.1 0.01-0.1 0.01 0.005-0.01 0.005 0.004 0.003-0.004 0.003 0.002 0.001 0.000001-0.001 0	82 131 3366 11 593 36 1 10 94 2586 149 14	3688	31.77	40 presence verified but not quantified. 788 analyzed but not detected 1 greater than 1.e6 mg/L

(b) Summary of Barium (Ba) Analyses

Analytical Method Code	PCode	Total No. of Analyses	Detection Limit (mg/L)	No. below Detn Limit	No. at or above Detn Limit	Percentage at or above Detn. Limit (%)	Notes
AA003	01005	117	0.10	70	47	40.17	
GF046	01005	16	-	0	16	100.00	
PLA06	01005	24	0.0005	1	23	95.83	
PLM27	01005	177	0.1	18	159	89.83	
PLA11	01005	5178	0.0009 0.001 0.002 0.003 0.006 0.1	6 9 100 3 1 6	5053	97.59	
PLM43	01005	1252	0.0002 0.001	2 29	1206	96.33	15 Presence verified but not quantified
PLM47	01007	87	0.0002	1	86	98.85	
GF033	01007	18	-	0	18	100.00	
PLA15	01007	13	-	0	13	100.00	
PLA07	01007	120	-	0	120	100.00	
PLA06	01007	24	-	0	24	100.00	
unknown		7337	0.0001 0.0002 0.001 0.002 0.005 0.01 0.025 0.03 0.04 0.05 0.06 0.07 0.1 0.2 0.3 0.4 0.5 10	2875	4462	60.82	

(c) Summary of Cadmium (Cd) Analyses

Analytical Method Code	PCode	Total No. of Analyses	Detection Limit (mg/L)	No. below Detn Limit	No. at or above Detn Limit	Percentage at or above Detn. Limit (%)	Notes
AA005	01025	39	0.01	38	1	2.56	
CX002	01025	39	0.001 0.004 0.01	31 1 1	6	15.38	
GF086	01025	2421	0.00001 0.001	1 2405	15	0.62	
CX013	01027	27	0.001	19	8	29.63	
GF097	01027	67	0.001	67	0	0.00	
PLA06	01025	23	0.0005	22	1	4.35	
PLA07	01027	118	0.0005	114	4	3.39	
PLA11	01025	2403	0.001 0.002 0.003 0.005 0.008 0.009 0.01	1964 12 18 7 49 1 4	348	14.48	
PLM27	01025	177	0.001 0.002	31 145	1	0.56	
PLM43	01025	3290	0.00004 0.001 others	1385 1093 15	797	24.22	
PLM47	01027	64	0.00004	53	11	17.19	
Unknown	01025 or 01027	12201	0 0-0.0002 0.0002 0.0005 0.0006 0.001 0.001-0.005 0.005 0.005-0.01 0.01 0.02	225 89 229 1339 117 2653 2628 484 11 940 1095	319	2.6	1118 Analyzed for but not detected 953 Presence verified but not quantified

(d) Summary of Mercury (Hg) Analyses

Analytical Method Code	PCode	Total No. of Analyses	Detection Limit (mg/L)	No. below Detn Limit	No. at or above Detn Limit	Percentage at or above Detn. Limit (%)	Notes
CV013	71890	2534	0.0001 0.0002 0.0003 0.001	2210 14 1 6	303	11.96	
CV014	71890	112	0.0001 0.0002	78 24	10	8.93	
CV016	71900	111	0.0001 0.0002	94 1	16	14.41	
CV017	71900	58	0.0001	58	0	0.00	
CV018	71900	69	0.0001 0.0002	36 25	8	11.59	

(e) Summary of Lead (Pb) Analyses

Analytical Method Code	PCode	Total No. of Analyses	Detection Limit (mg/L)	No. below Detn Limit	No. at or above Detn Limit	Percentage at or above Detn. Limit (%)	Notes
AA019	01049	74	0.1	71	3	4.05	
CX007	01049	501	0.001 0.004 0.005 0.01	300 1 54 11	135	26.95	
CX017	01049	40	0.005	22	18	45.00	
GF031	01051	47	0.001	29	18	38.30	
GF056	01051	1	0.005	1	0	0.00	
GF078	01049	1	0.005	1	0	0.00	
GF089	01049	2876	0.001 0.002 0.1	2531 1 1	341	11.86	2 empty values
GF100	01051	94	0.001 0.005	36 1	57	60.64	
PLA06	01049	23	1.001 0.002	16 5	2	8.70	
PLA07	01051	123	0.001 0.002	39 76	8	6.50	
PLA11	01049	1657	0.001 0.01 0.02 0.03 0.05 0.1	1 1368 9 15 7 40	215	12.98	2 empty values
PLM43	01049	1970	0.0001 0.0001- 0.001 0.001 0.002 0.004	285 6 701 7 1	970	49.24	
PLM48	01051	100	0.00006 0.001	6 12	82	82.00	
Unknown		12374	0 0.000001 0.00001 0.00001- 0.0001 0.0001- 0.001 0.001 0.001-0.01 0.01 0.01-0.1 0.1 0.1-1 >1	187 55 4 24 81 417 3932 (3337 of them are 0.005) 3466 499 271 18 11	438	3.54	971 Analyzed for but not detected 2000 Presence verified but not quantified

(f) Summary of Antimony (Sb) Analyses

Analytical Method Code	PCode	Total No. of Analyses	Detection Limit (mg/L)	No. below Detn Limit	No. at or above Detn Limit	Percentage at or above Detn. Limit (%)	Notes
GF032	01095	1	0.001	1	0	0.00	
GF040	01097	115	0.001	115	0	0.00	
PLM48	01097	54	0.0002 0.0006 0.0009	49	5	9.26	
HY009	01095 01097	516	0.001	432	84	16.28	
PLM43	-	1274	0.00005 0.0001 0.0002 0.0003 0.0004 0.0006 0.0008 0.001 0.002 >=0.003	105 1 219 148 1 1 2 555 7 2	233	18.29	Trivial No. of other misc. detn limits
Unknown	01095	790	Misc: 0.00005-0.3	761	29	3.67	

(g) Summary of Selenium (Se) Analyses

Analytical Method Code	PCode		Detection Limit (mg/L)	No. below Detn Limit	No. at or above Detn Limit	Percentage at or above Detn. Limit (%)	Notes
GF060	01145		0.001	16	6	27.27	
PLM10	01145		0.0008	17	52	75.36	
GF091	01145		0.001 0.002 0.006 0.014	297 41 6 4	80	18.69	
PLM27	01145		0.01	153	21	12.07	
HY011	01145		0.001 0.002 0.003 0.005 0.01	3240 61 1 3 10	752	18.49	
PLM40	01145		0.0003 0.0004 0.0005 0.0007 0.002	365 250 230 160 1	1411	58.38	
Unknown	01145		0 <0.001 0.001 0.001-0.01 0.01 0.01-0.1 >=0.1	192 112 932 248 2170 53 53	1108	22.76	

(h) Summary of Uranium (U) Analyses

Analytical Method Code	PCode	Total No. of Analyses	Detection Limit (mg/L)	No. below Detn Limit	No. at or above Detn Limit	Percentage at or above Detn. Limit (%)	Notes
PHOS1	22703	218	0.0004	72	146	66.97	
PHOS2	22703	4	0.09	1	3	75.00	
PHOS3	22703	141	0.00001	10	131	7.09	
PHOS4	22703	1	0.00024	1	0	0.00	
PHOS5	22703	162	0.00	8	149	4.94	5 of them are "Presence verified but not detected"
PHOS6	22703	61	0.001	44	2	3.28	15 of them are "Presence verified but not detected"
PLM43	22703	1310	0.004 0.003 0.002 0.001 0.00016 0.00007 0.00004 0.00002	1 1 4 315 1 1 31 43	913	69.70	
PLM48	28011	62	-	0	62	100.	
FL001	22703	163	0.001	120	43	26.38	
FL002	75990	122	-	0	122	100.00	
FL003	28011 28011 75993	56	0.001	21	35	60.00	
FL004	22703	4	-	0	4	100.00	
FL006	22703	59	0.0004	18	41	69.49	
FL007	80020	33	0.00001	1	32	96.97	
Unknown		848	0.00001 0.0001 0.0002 0.0003 0.0004 0.0005 0.0006 0.0007 0.0011 0.007 0.013 0.02	11 56 38 1 12 16 20 3 2 1 63 6	618	72.88	

(i) Summary of Zinc (Zn) Analyses

Analytical Method Code	PCode	Total No. of Analyses	Detection Limit (mg/L)	No. below Detn Limit	No. at or above Detn Limit	Percentage at or above Detn. Limit (%)	Notes
AA039	01090	187	0.01	75	112	59.89	
AA071	01092	125	0.01	26	99	79.20	
PLM48	01092	89	0.002	9	80	89.89	
GF084	01090	1		0	1	100.00	
PLA06	01090	83	0.001 0.002 0.01	2 16 1	64	77.11	
PLA07	01092	141	0.001 0.002	4 14	123	87.23	
PLA15	01092	17	0.006 0.031 0.04	6	11	64.71	
PLM10	01090	11	0.0006	2	9	81.82	
PLM27	01090	175	0.01	120	55	31.43	
PLA11	01090	5407	0.003 0.004 0.005 0.006 0.007 0.009 0.01 0.014 0.02 0.024 0.06 0.08	587 8 7 5 1 5 11 1 342 7 6 1	4426	81.86	
PLM43	01090	1554	0.0006 0.001 0.001-0.01 0.0101	4 87 7 1	1455	93.63	
Unknown	01090 01092	14304	0 0-0.0001 0.001 0.001-0.01 0.01 0.02 0.03 0.04 0.05 0.05-0.1 0.1 >0.1	64 21 9 392 1378 1924 8 13 2010 65 103 16	8301(1225 are zeros)	58.03	

Table A2. List and Explanation of Analytical Methods from USGS NWIS Database Used in Table A

Analytical Method Code	Short Info	Long Info	Database Citation	Method Number	Method Owner
AA003	Barium, wf, direct AAS	Barium in filtered water by direct AAS	TWRI 5-A1/1989, p. 89	I-1084-85:USGS	USGSNWQL
AA005	Cadmium, wf, direct AAS	Cadmium in filtered water by direct AAS	TWRI 5-A1/1989, p. 127	I-1135-85:USGS	USGSNWQL
AA019	Lead, wf, direct AAS	Lead in filtered water by direct AAS	TWRI 5-A1/1989, p. 247	I-1399-85:USGS	USGSNWQL
AA039	Zinc, wf, direct AAS	Zinc in filtered water by direct AAS	TWRI 5-A1/1989, p. 507	I-1900-85:USGS	USGSNWQL
AA071	Zinc, wu, USGS digest, AAS	Zinc recoverable from unfiltered water by dilute HCl (USGS) digestion and direct AAS	TWRI 5-A1/1989, p. 507	I-3900-85:USGS	USGSNWQL
CV013	Mercury, wf, auto CVAAS	Mercury in filtered water by automated-sequential CVAAS	TWRI 5-A1/1989, p. 289	I-2462-85:USGS	USGSNWQL
CV014	Mercury, wf, CV-AFS	Mercury in Filtered Water by Cold Vapor-Atomic Fluorescence Spectrometry	WRI 01-4132	I-2464-01:USGS	USGSNWQL
CV016	Mercury, wu, CVAAS (NWQL)	Mercury recoverable from unfiltered water by CVAAS	TWRI 5-A1/1989, p. 285	I-3462-85:USGS	USGSNWQL
CV017	Mercury, wu, CVAAS (NWQL)	Mercury recoverable from unfiltered water by CVAAS	TWRI 5-A1/1989, p. 285	I-3462-85:USGS	USGSOCFL
CV018	Mercury, wu, CV-AFS	Mercury in Unfiltered Water by Cold Vapor-Atomic Fluorescence Spectrometry	WRI 01-4132	I-4464-01:USGS	USGSNWQL
CX002	Cadmium, wf, APDC & MIBK, AAS	Cadmium in filtered water by chelation-extraction with APDC and MIBK, and AAS	TWRI 5-A1/1989, p. 125	I-1136-85:USGS	USGSOCFL
CX007	Lead, wf, APDC & MIBK, AAS	Lead in filtered water by chelation-extraction with APDC and MIBK, and AAS	TWRI 5-A1/1989, p. 245	I-1400-85:USGS	USGSOCFL
CX013	Cadmium, USGS digest,extract AAS	Cadmium recoverable from unfiltered water by dilute HCl (USGS) digestion, chelation-extraction with APDC and MIBK, and AAS	TWRI 5-A1/1989, p. 125	I-3136-85:USGS	USGSOCFL
CX017	Lead, USGS digest, extract AAS	Lead recoverable from unfiltered water by dilute HCl (USGS) digestion, chelation-extraction with APDC and MIBK, and AAS	TWRI 5-A1/1989, p. 245	I-3400-85:USGS	USGSOCFL
FL001	U (natural), wf, fluorometric	Dissolved fluorometric			USGSNWQL
FL002	U (natural) 2SPE, wf,fluorimetry	Fluorimetry, Uranium, FIL			USGSNWQL
FL003	U (natural), water, fluorometric	U, Fluorometric, TOT			USGSNWQL
FL004	U (natural), wf, FL-DIR GR-W	U-FIL, fluorometric method--direct (FL-DIR.), ground water (GR-W)			USGSNWQL
FL006	U (natural), wf, direct fluorom	U-FIL, fluorometric method--direct (FLUOR-direct)			USGSNWQL
FL007	Uranium, wf,extract fluorometric	U-FIL, fluorometric method--extracted sample (FLUOR-ext)			USGSNWQL
GF031	Elements, drinking water, GFAA	EPA 200.9 determination of total recoverable trace elements in drinking water by GFAA		200.9:USEPA	USGSNWQL
GF032	Antimony, drinking wtaer, GFAA	GFAA, Antimony, dissolved, EPA 200.9, Drinking Water		200.9:USEPA	USGSNWQL
GF040	Antimony, wu, GFAA	ANTIMONY TOTAL (GFAA)		204.2:USEPA	USGSOCFL
GF042	Arsenic, wf, GFAA	ARSENIC DISSOLVED (GFAA)		206.2:USEPA	USGSOCFL
GF044	Arsenic, wu, GFAA	ARSENIC TOTAL GFAA		206.2:USEPA	USGSOCFL
GF046	Barium, wf, GF	BARIUM DISSOLVED (GF)		208.2:USEPA	USGSOCFL
GF056	Lead, LL, wu, GFAA	LEAD TOTAL LL (GFAA)		239.2:USEPA	USGSOCFL

GF060	Selenium, wf, GFAA (Ocala)	SELENIUM DISSOLVED (GFAA)		270.2:USEPA	USGSOCFL
GF073	Arsenic and selenium, wu, GFAA	Graphite furnace atomic absorption		I-0000-91:USGS	USGSNWQL
GF078	Lead, LIS, GFAAS	Lead in low ionic strength water by GFAAS	TWRI 5-A1/1989, p. 249	I-1401-85:USGS	USGSNWQL
GF084	Zinc, LIS, GFAAS	Zinc in low ionic strength water by GFAAS	TWRI 5-A1/1989, p. 509	I-1901-85:USGS	USGSNWQL
GF085	Arsenic, wf, GFAAS	Arsenic in Filtered Water by GFAAS	OF 98-639	I-2063-98:USGS	USGSNWQL
GF086	Cadmium, wf, GF-AAS	Cadmium in filtered water, by GF-AAS	OF 93-125, p. 53	I-2138-89:USGS	USGSNWQL
GF089	Lead, wf, GF-AAS	Lead in filtered water, by GF-AAS	OF 93-125, p. 87	I-2403-89:USGS	USGSNWQL
GF091	Selenium, wf, GFAAS (NWQL)	Selenium in Filtered Water by GFAAS	OF 98-639	I-2668-98:USGS	USGSNWQL
GF096	Arsenic, wu, GFAAS	Arsenic Recoverable from Unfiltered Water by GFAAS	OF 98-639	I-4063-98:USGS	USGSNWQL
GF097	Cadmium, wu, GF-AAS	Cadmium in unfiltered water, by GF-AAS	OF 93-125, p. 53	I-4138-89:USGS	USGSNWQL
GF100	Lead, wu, GF-AAS	Lead recoverable from unfiltered water, by GF-AAS	OF 93-125, p. 87	I-4403-89:USGS	USGSNWQL
HY010	Arsenic, wf, auto hydride AAS	Arsenic in filtered water by automated sulfuric acid potassium persulfate digestion or ultraviolet radiation, hydride generation, and tube furnace AAS	TWRI 5-A1/1989, p. 77	I-2062-85:USGS	USGSNWQL
HY011	Selenium, wf, auto hydride AAS	Selenium in filtered water by automated hydride generation and AAS	TWRI 5-A1/1989, p. 403	I-2667-85:USGS	USGSNWQL
HY013	Arsenic, wu, digest & hydrideAAS	Total arsenic in unfiltered water by automated sulfuric acid potassium persulfate digestion or ultraviolet radiation, hydride generation, and tube furnace AAS	TWRI 5-A1/1989, p. 77	I-4062-85:USGS	USGSNWQL
PHOS1	Laser phosphorim, dir (Eberline)	Laser-induced phosphorimetry, direct (analysis by Eberline Services)			USGSNWQL
PHOS2	Laser phosphorimetry, dir (NWQL)	Laser-induced phosphorimetry, direct (analysis by NWQL)			USGSNWQL
PHOS3	Laser phosphorim, ext (Eberline)	Laser-induced phosphorimetry, extracted (analysis by Eberline Services)			USGSNWQL
PHOS4					
PHOS5	Uranium, wf, dir phosphorescence	Uranium, Water, Filtered, by Direct Laser Induced Phosphorescence			USGSNWQL
PHOS6	Uranium, wf, ext phosphorescence	Uranium, Water, Filtered, by Extraction and Laser Induced Phosphorescence			USGSNWQL
PL120	Metals, wu, ICP-OES or ICP-MS	Metals Recoverable from Unfiltered Water ICP-OES or ICP-MS	OF 98-165	I-4471-97:USGS	USGSNWQL
PLA06	Trace elements, wf, ICP/T (Ocala	Ocala Lab analysis of dissolved trace elements by Inductively Coupled Plasma--Atomic Emission Spectrometry (ICP/T)		200.7:USEPA	USGSOCFL
PLA07	Trace elements, wu,ICP/T (Ocala)	Ocala Lab analysis of total trace elements by Inductively Coupled Plasma--Atomic Emission Spectrometry (ICP/T)		200.7:USEPA	USGSOCFL
PLA11	Metals, wf, ICP-AES	Metals, filtered water, Inductively coupled plasma-atomic emmission spectrometry	OF 93-125, p. 101	I-1472-87:USGS	USGSNWQL
PLA15	Metals, wu, ICP-AES	Metals, unfiltered water, Inductively coupled plasma-atomic emission spectrometry	OF 98-165	I-4471-97:USGS	USGSNWQL
PLM10	Collision/reaction cell ICPMS	Elements in Natural-Water, Biota, Sediment, and Soil Samples Using Collision/Reaction Cell Inductively Coupled Plasma-Mass Spectrometry	USGS TMR 5-B1	:USGS	USGSNWQL
PLM27	Elements, wf, ICP-MS w/o digest	Trace elements in water and wastes by inductively coupled plasma - mass spectrometry without digestion	EPA-600/R-94/111	200.8:USEPA	USGSOKWC
PLM40	Metals, water, ICP-MS	Metals in Water by ICP-MS	OF 92-634	I-2477-92:USGS	USGSNWQL

PLM43	Metals, wf, ICP-MS	Metals, filtered water, Inductively coupled plasma-mass spectrometry	OF 92-634	I-2477-92:USGS	USGSNWQL
PLM47	Metals, wu, ICP-MS	Metals, unfiltered water, Inductively coupled plasma-mass spectrometry	OF 98-165	I-4471-97:USGS	USGSNWQL
PLM48	Metals, wu, ICP-MS	Metals, unfiltered water, Inductively coupled plasma-mass spectrometry	OF 98-165	I-4471-97:USGS	USGSNWQL

Appendix B:
Discussion of Spatial Distributions and Analytical Artifacts in Groundwater Analyses from NWIS Database

B1. Spatial Distribution of Groundwater Analyses from NWIS Database

With reference to discussion in Section 3.3.3, we further analyze here the spatial distributions of measured aqueous concentrations of lead in groundwater analyses from the NWIS database (Figure 3.8(a) and Figure B.1(a)). The question is why the measurable lead concentrations are so sparsely distributed over many parts of the country. A possible reason is that less water quality analyses for hazardous inorganic constituents have been conducted in certain parts of the country or that analyses have been conducted using analytical methods with insufficient detection limits. For evaluation, we have plotted in Figure B1(b) the spatial distribution of all samples that have been declared "non-detects" for lead, with the color scheme indicating the detection limit of the analytical method used (in Log mg/L). In Figure B1(c), we furthermore plot the location of samples that have been declared in the NWIS database as "presence verified, but not quantified".

Figures B1(a) through B1(c) together indicate that both possible reasons stated above are valid. Clearly, there are many states and regions where almost no water analyses for lead have been conducted, or at least these analyses have not been reported in the NWIS database. There are furthermore several states and regions with many lead analyses in the NWIS database, but the majority of those with insufficient detection limits. A good example are the states of Iowa and Illinois, where numerous samples have detection limits of about 0.01 mg/L, two orders of magnitude above the expected equilibrium lead concentration of 0.0001 mg/L for a typical reducing groundwater where galena coexists with pyrite and goethite (Section 3.3.5). The "hot spots" of measurable lead concentrations in Figure B1(a) are clearly correlated to states or regions where large numbers of high-quality analyses (i.e., with low enough detection limits) have been conducted. In contrast, states or regions with no or only few detectable lead concentrations in Figure 3B1(a) correspond to locations with either no measurements or analyses

with insufficient detection limits. We may conclude that almost all groundwaters in the United States would exhibit small (mostly below MCLs), but non-zero lead concentrations if measured with appropriate analytical techniques, which is consistent with the above finding that lead occurs ubiquitously in soils, sediments and aquifer rocks throughout the United States. While not reported here, the same conclusions can be drawn for the other hazardous inorganic constituents of interest in this study.

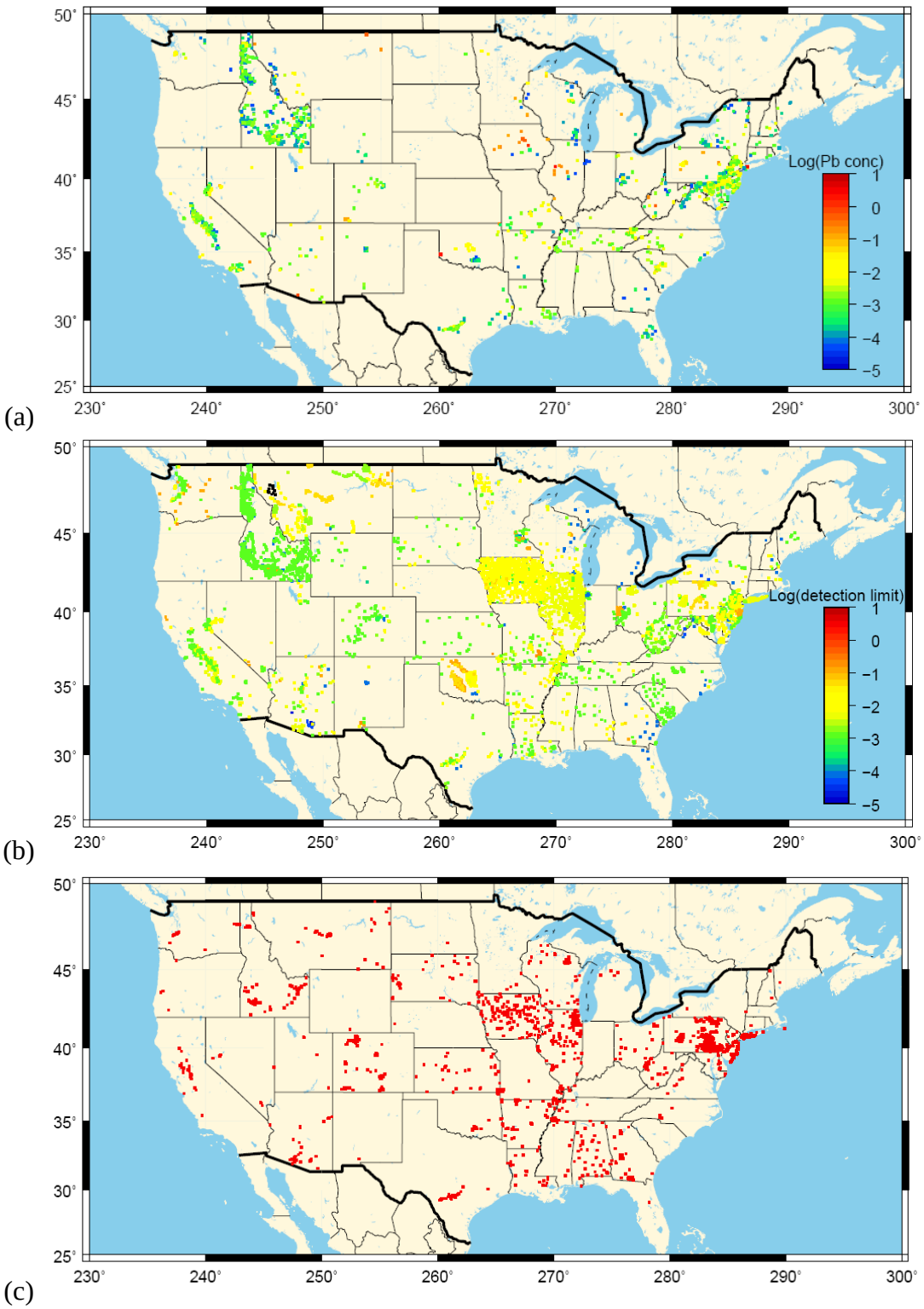

Fig. B1. Spatial distribution of (a) samples with measured aqueous concentration (Log mg/L) of lead, (b) samples with non-detects for lead with color scheme indicating the detection limit of the analytical method (in Log mg/L), and (c) samples with text stating "presence verified, but not quantified". The plots were drawn from more than 38,000 groundwater quality analyses downloaded from the National Water Information System Database (NWIS).

B2. Characterization of Analytical Artifacts in the Measurement of Concentrations of Hazardous Inorganic Constituents

Section 3.3.5 discusses the possibility and the implications of analytical artifacts introduced by the differing accuracy and sensitivity of analytical methods. The Cd concentrations in Figure 3.6(d) were mentioned there as an example where almost all analyses may have been affected. The figure shows essentially two sets of measurements, with each set starting an initially high frequency, apparently corresponding to the detection limit for some of the analyses, which then falls off with increasing concentration until a relatively low frequency is recorded. This is, of course, very different from a normal or possibly log-normal distribution of concentrations to be expected in natural groundwaters.

The analogy of the observations in Figure 3.6(d) with radioactive decay suggests a similar process involving Poisson statistics. This is illustrated by Figures B2(a) and B2(b), which display the normalized analytical frequency versus log concentration for two selected analytical methods (i.e., PLA11 with a detection limit of 0.001 mg/L and up, and PLM43 with a detection limit of 0.00002 mg/L and up, see Table A1). A linear regression of the plots indicates a very good correlation between frequency and concentration, with $R^2 = 0.98$ for both analytical methods. The normalized frequency of "non-detects" for each method is plotted as the negative value of the detection limit, and is included in the regression analysis.

The theoretical basis for these correlations has not been evaluated, but probably relates to contamination or unknown interferences in the analytical method, as replicate analyses for these methods do not show such large spurious variations. Clearly, further study of this phenomenon is warranted, especially in relation to the analytical sensitivity of the method and its suitability for detecting actual concentrations expected in a given ground water sample.

Similar evaluations of selected analytical methods for other elements yield similar correlations. For example, Figure B3 is a plot of the normalized analytical frequency versus linear concentration for Hg analyses using the CV013 analytical method with a detection limit no lower than 0.0001 mg/L, suggesting the majority of reported Hg analyses are also artifacts. After

discounting for potential artifacts, the remaining chemical analyses are of marginal utility in predicting thermodynamic controls for mercury concentrations in ground waters, and therefore a theoretical interpretation of mercury behavior may be the only recourse for predicting the response of dissolved mercury to elevated partial pressures of CO_2. Figures B4(a) and B4(b) show similar artifacts are operative for lead when less sensitive analytical methods are utilized.

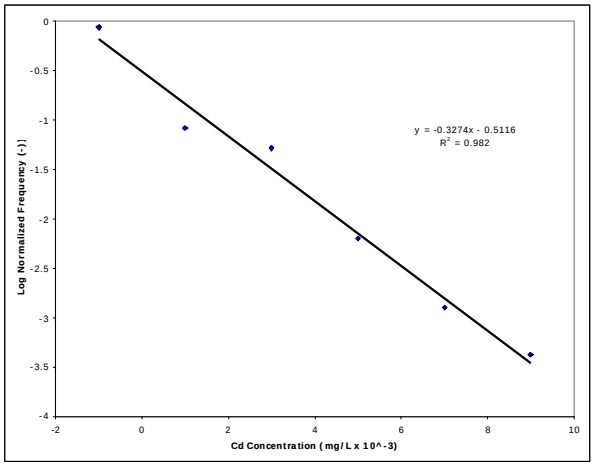

(a)

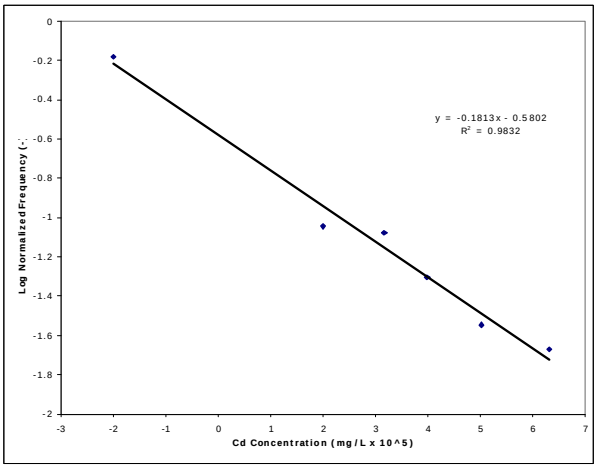

(b)

Fig. B2. Log normalized frequency of chemical analyses as a function of cadmium concentration in ground waters at and above the detection limit for the analytical method. (a) PLA11; (b) PLM43.

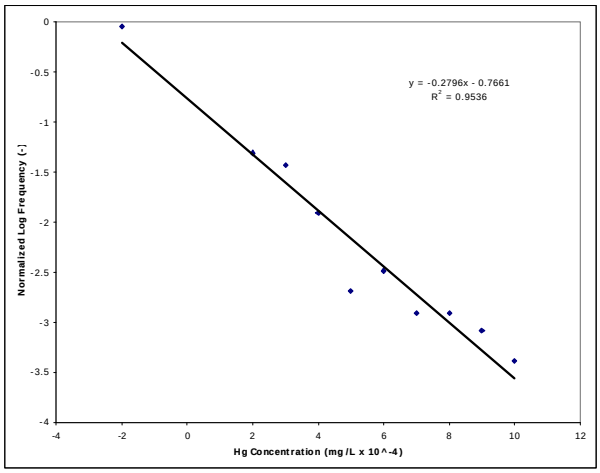

Fig. B3. Log normalized frequency of chemical analyses as a function of mercury concentration in ground waters at and above the detection limit for the CV013 analytical method.

(a)

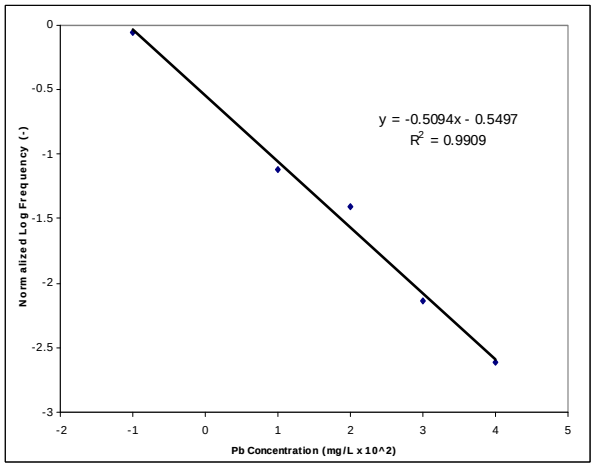

(b)

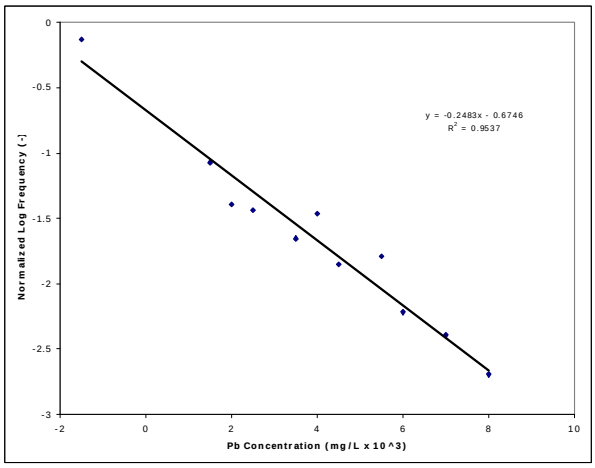

Fig. B4. Log normalized frequency of chemical analyses as a function of lead concentration in ground waters at and above the detection limit for the analytical method. (a) PLA11; (b) CX007.

Appendix C:
Thermodynamic Database Augmentation

C1. Introduction

A substantial augmentation of solubility products of solid phases and dissociation constants of aqueous species is required to adequately model the complex chemistry associated with the behavior of hazardous inorganic constituents in ground waters. The augmentation is not limited merely to those primary minerals and secondary alteration products where the hazardous constituent is an essential component; attention must also be paid to minerals that interact with the hazardous constituents through co-precipitation, ion exchange, and/or adsorption. Furthermore, the database used for EQ3/6 simulations, Data0.dat.YMP, suffers from obsolescence. The solubility products of many common rock-forming minerals listed in the database require revision to more accurately reflect advances since the original compilations used in the database were published.

Appendix C is subdivided into several sections dealing respectively with additional aqueous speciation and minerals for arsenic, lead, antimony and selenium. Corrections are also provided for Fe^{+2} and Fe^{+3} aqueous species, and an expanded database is provided for metastable iron oxides, oxy-hydroxides, and sulfides. Supplementary information for carbonates and chlorite is also included, because of their relevance in participating as pH or Eh buffers. The appendix concludes with a section in which data are presented on minerals that had to be included on a case-by-case basis in order to ensure that the geochemical model reflected reality.

C2. Arsenic

C2.1 Background

The presence of arsenic in groundwater has long been a serious problem in many parts of the world, particularly in the Ganges delta of Bangladesh (Smedley, 2003), where farmers draw drinking water from shallow aquifers that are subject to seasonal oxidation and mobilization of arsenate. In the United States, several areas are also characterized by elevated arsenic concentrations in ground waters, notably in northwestern Nevada, where the municipal water of

the city of Fallon has unacceptably high levels (Smedley, 2003) and the Rio Grande Rift of New Mexico (Bexfield and Plummer, 2003). The city of Albuquerque is forced to treat its water supplies to mitigate excessive concentrations of As. Other regions of the country, such as the Upper Michigan Peninsula and parts of Minnesota (Thornberg and Sahai 2004) and New Hampshire (Utsunomiya et al., 2003), are also affected by high As levels in groundwater. Increasing use of aquifer storage and recovery techniques (ASR) has also lead to arsenic contamination of the recovered water (Arthur et al., 2005). A significant proportion of the sampled more than 38,000 well water samples taken from the NWIS database already possess As levels exceeding current MCLs. The introduction of high pressure CO_2 into aquifers with such elevated ambient As concentrations could aggravate an already marginal water quality in some areas. Therefore, the evaluation of As chemistry in groundwaters is very important, and takes precedence over some other hazardous constituents in relation to the present problem.

The chemistry of As in surficial waters and shallow subsurface groundwaters is extraordinarily complex. As occurs naturally in at least five oxidation states (-3, 0, +2, +3 and +5). Both +3 and +5 states form hydroxy-anions in aqueous solution with varying degrees of protonation. Both are noted for reactions with Fe in both +2 and +3 states. As(V) adsorption onto hydrated ferric oxides (HFO) stabilizes the latter in a metastable or colloidal or nanoparticulate form, which can persist for tens to hundreds of years. In the presence of Ca^{+2}, Ca-As-Fe-OH macro complexes form in solution, which can aggregate to form glassy or amorphous minerals such as pitticite or yukonite. As an added complication, it is well known that the transformation of aqueous As(III) to As(V) and vice versa is sluggish (Cherry et al., 1979). Aqueous As concentrations in ground waters are therefore likely to be dictated not only by the formation of metastable phases and adsorption-stabilized colloids, but also by kinetically hindered redox transformations.

A substantial literature has evolved in which the thermodynamic and kinetic properties of As species have been studied and elucidated, mainly because of the interest in groundwater treatment, and the need to remediate contamination from current and former mining operations. The literature has been searched and thermodynamic data compiled (or in some cases estimated) for 24 aqueous species and complexes, and 15 minerals or potential stabilizing precipitates. Most of these data have been formatted for entry in the EQ3 Data0.dat and TOUGHREACT thermodynamic databases in the form of relevant dissociation constants or solubility products at

25°C. Additional calculations were also conducted using SUPCRT92 (Johnson et al., 1992) to generate solubility and dissociation constant data wherever feasible.

One aspect of As chemistry, which has not been adequately addressed in this report, concerns the substitution of As for S in pyrite. One of the principal causes of As contamination in aquifers occurs through the oxidation of arsenian pyrite. Reich and Becker (2006) have formulated a theoretical solid-solution model quantifying As substitution for S in both pyrite and marcasite. Time constraints prevented the incorporation of this model in the TOUGHREACT simulator. Instead, an empirical correction factor was applied to both arsenopyrite and gudmundite solubility products to account for their dilution from unit activity due to solid solution in pyrite. This was accomplished by reconciling field observations of both As and Sb concentrations in NWIS potable groundwater samples with thermodynamic predictions of their concentrations, as described in Section 3.4.

In the following two sections, methods are described for building an expanded internally consistent database of thermodynamic properties of aqueous As species and solid As phases, respectively, based on an earlier study by Nordstrom and Archer (2003).

C2.2 Aqueous Arsenic Species.

C2.2.1 Calculation of HKF Equation of State Parameters for Aqueous Arsenate and Arsenite Species

The thermodynamic properties of aqueous arsenic species as derived by Nordstrom and Archer (2003) were used as a point of departure. They are summarized in Table C1. Entropy, $\overline{S}^{0}_{P_r,T_r}$, of two species, $HAsO_3^{-2}$, and AsO_3^{-3}, needed to be estimated. This was accomplished through a correlation plot of the entropies of several oxyanion species as listed in Table C2, and illustrated in Figure C1.

Table C1. Thermodynamic properties of Arsenic Solid Phases and Aqueous Species (from Nordstrom and Archer, 2003)

Phase	$\Delta G^0_{f,P_r,T_r}$ cal mol^{-1}	$\Delta H^0_{f,P_r,T_r}$ cal mol^{-1}	$S^0_{P_r,T_r}$ cal mol^{-1} K^{-1}	$C^0_{P_r,T_r}$ cal mol^{-1} K^{-1}
As	0	0	8.516	5.839
S	0	0	7.600	5.402
O_2(g)	0	0	49.003	7.016
H_2(g)	0	0	31.208	6.889
H_2O(l)	-56687	-68315	16.709	17.995
As_2O_3(cub)	-137749	-157091	25.664	23.155
As_2O_3(mon)	-137794	-156709	27.096	23.179
As_2O_5	-185220	-219309	25.201	27.701
S_2(g)	18953	30681	54.510	7.761
AsS(a)	-7481	-7600	15.033	11.233
AsS(b)	-7385	-7409	15.177	11.233
As_2S_3(a)	-20292	-20507	39.149	38.958
As_2S_3(am)	-18356	-15989	47.801	
Phase	$\Delta \overline{G}^0_{f,P_r,T_r}$ cal mol^{-1}	$\Delta \overline{G}^0_{f,P_r,T_r}$ cal mol^{-1}	$\overline{S}^0_{P_r,T_r}$ cal mol^{-1} K^{-1}	$\overline{C}^0_{P_r,T_r}$ cal mol^{-1} K^{-1}
H_2S(aq)	-6661	-9610	28.920	39.914
HS^-(aq)	2880	-4216	15.010	-21.989
$As_3S_4(SH)_2^-$	-30019			
$AsS(OH)(SH)^-$	-58413			
H_3AsO_3(aq)	-152971	-177428	46.804	
$H_2AsO_3^{-1}$	-140454	-170827	26.957	
$HAsO_3^{-2}$	-121272		(-1.839)	
H_3AsO_4(aq)	-183258	-215930	43.755	
H_2AsO_4-	-180127	-217835	26.859	
$HAsO_4^{-2}$	-170586	-217115	-2.729	
AsO_4^{-3}	-154484	-212765	-42.139	
AsO_3^{-3}	-100813		(-46.715)	

Table C2. Standard Partial Molal Entropies, $\overline{S}^0_{P_r,T_r}$, of Selected Oxyanions

Charge	$\overline{S}^0_{P_r,T_r}$, cal mol^{-1} K^{-1}					
	AsO_4^{-3}	AsO_3^{-3}	PO_4^{-3}	PO_3^{-3}	SO_4^{-2}	CH_3COO^-
0	43.755	46.804		43.6		42.7
1	26.859	26.957	21.6	31.7	30	20.6
2	-2.729		-8	4	4.5	
3	-42.139		-53			

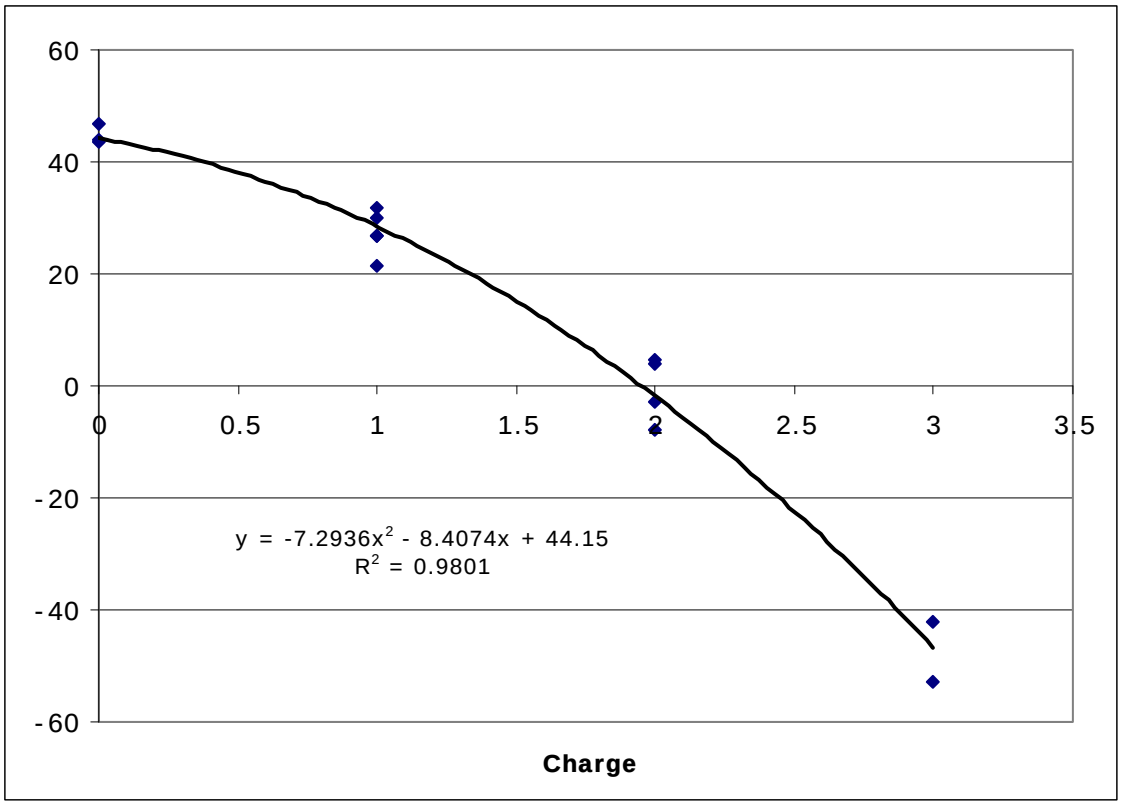

Fig. C1. Regression analysis of standard partial molal entropies, $\overline{S}^0_{P_r,T_r}$, of selected oxyanions as a function of charge.

A regression analysis through all data points yielded the equation listed in Figure C1, with a regression coefficient, R^2, = 0.9801. The calculated values of $\overline{S}^0_{P_r,T_r}$ at Z = -2 and -3 were used as estimates for $HAsO_3^{-2}$ and AsO_3^{-3}. The heat capacities, $\overline{C}^0_{P_r,T_r}$ of all species were then calculated using equations derived by Shock et al. (1997; Table 6), which are for hydrogen bearing anions

$$\overline{C}^0_{P_r,T_r} = 1.65\overline{S}^0_{P_r,T_r} - 46.8$$

and for hydrogen-free anions where $z_j = -3$

$$\overline{C}^0_{P_r,T_r} = 0.60\overline{S}^0_{P_r,T_r} - 92.8$$

Calculation of the HKF equation of state parameters, c_1, c_2 and the Born coefficient, ω_{P_r,T_r}, then follows with application of the following equations (Shock and Helgeson, 1988; Shock et al., 1989). For charged species, the Born coefficient can be calculated from:

$$\omega_{j,P_r,T_r} = \eta Z_j \left[\frac{\eta Z_j}{r_{e,j,P_r,T_r}} - \frac{1}{3.08} \right]$$

where $\eta = \frac{N^0 e^2}{2} = 1.66027 \times 10^5 \overset{0}{A}$ cal mol^{-1}, with N^0 Avogadro's number and e the absolute electronic charge with a value of $4.80298 \times 10^{-10} esu$. r_{e,j,P_r,T_r} is the effective electrostatic radius of the ion

$$r_{e,j,P_r,T_r} = \frac{Z_j^2 \left(\eta Y_{P_r,T_r} - 100 \right)}{\overline{S}^0_{P_r,T_r} - \alpha_z}$$

where Y_{P_r,T_r} has the value $-5.802 \times 10^{-5} K^{-1}$ and refers to the Born function

$$Y = \frac{1}{\varepsilon} \left(\frac{\partial \ln \varepsilon}{\partial T} \right)_P$$

and α_z is a charge dependent correlation parameter

$$\alpha_z = 71.5 \left| Z_j \right|$$

For neutral aqueous inorganic species, the effective Born coefficient is

$$\omega_e = -1514.4 \overline{S}^0_{P_r,T_r} + 0.34 \times 10^5$$

Calculation of c_1 proceeds through the following steps. The heat capacity of an ion is assumed to consist of two components, thus

$$\overline{C}^0_P = \Delta \overline{C}^0_{P,n} + \Delta \overline{C}^0_{P,s}$$

representing respectively the nonsolvation and solvation contributions. The Born coefficient can be used to calculate $\Delta \overline{C}^0_{P,s}$, thus

$$\Delta \overline{C}^0_{P_r,T_r,s} = \omega T X$$

where X is the standard partial molal heat capacity Born Function (Helgeson and Kirkham, 1974)

$$X = \frac{1}{\varepsilon}\left(\left(\frac{\partial^2 \ln\varepsilon}{\partial T^2}\right)_P - \left(\frac{\partial \ln\varepsilon}{\partial T}\right)_P^2\right)$$

which at P_r, T_r has the value of $3.09\,K^{-2} \times 10^{-7}$.

$\Delta\overline{C}^0_{P,n}$ can then be obtained by difference. Furthermore, we have

$$\Delta\overline{C}^0_{P,n} = c_1 + c_2\left(\frac{1}{T-\theta}\right)^2$$

where $c_2 \times 10^{-4} = 0.2037\overline{P}^0_{P_r,T_r} - 3.0346$ and $\theta = 228K$.

The general form of the HKF equation of state is given by

$$\begin{aligned}
\Delta\overline{G}^o = {} & \Delta\overline{G}^o_{f_{\mathrm{Pr},Tr}} - \overline{S}^o_{\mathrm{Pr},Tr}\left(T - T_r\right) - c_1\left(T\ln\left(\frac{T}{T_r}\right) - T + T_r\right) \\
& - c_2\left(\left[\left(\frac{1}{T-\theta}\right) - \left(\frac{1}{T_r-\theta}\right)\right]\left(\frac{\theta - T}{\theta}\right) - \frac{T}{\theta^2}\ln\left[\frac{T_r\left(T-\theta\right)}{T\left(T_r-\theta\right)}\right]\right) \\
& + a_1\left(P - P_r\right) + a_2\ln\left(\frac{\Psi + P}{\Psi + P_r}\right) + a_3\left(\frac{P - P_r}{T-\theta}\right) + a_4\left(\frac{1}{T-\theta}\right)\ln\left(\frac{\Psi + P}{\Psi + P_r}\right) \\
& + \omega_{\mathrm{Pr},Tr}\left[\frac{1}{\varepsilon} - \frac{1}{\varepsilon_{\mathrm{Pr}\,Tr}} + Y_{\mathrm{Pr},Tr}\left(T - T_r\right)\right] + k\left[\omega - \omega_{\mathrm{Pr},Tr}\right]\left(\frac{1}{\varepsilon} - 1\right);
\end{aligned}$$

$$\overline{V}^o = a_1 + a_2\left(\frac{1}{\Psi + P}\right) + \left(a_3 + a_4\left(\frac{1}{\Psi + P}\right)\right)\left(\frac{1}{T-\theta}\right) - \omega Q + \left(\frac{1}{\varepsilon} - 1\right)\left(\frac{\partial\omega}{\partial P}\right)_T;$$

$$\begin{aligned}
\overline{C}^o_P = {} & c_1 + \frac{c_2}{\left(T-\theta\right)^2} - \left(\frac{2T}{\left(T-\theta\right)^3}\right)\left(a_3\left(P - P_r\right) + a_4\ln\left(\frac{\Psi + P}{\Psi + P_r}\right)\right) \\
& + \omega TX + 2TY\left(\frac{\partial\omega}{\partial T}\right)_P - T\left(\frac{1}{\varepsilon} - 1\right)\left(\frac{\partial^2\omega}{\partial T^2}\right)
\end{aligned}$$

where and $[k]$ is a switch function equal to 1 for charged species and 0 for neutral species (Sverjensky et al., 1997), and $[Q]$, $[Y]$, and $[X]$ are given by (Tanger and Helgeson, 1988)

$$Q \equiv -\left(\frac{\partial(1/\varepsilon)}{\partial P}\right)_T = \frac{1}{\varepsilon^2}\left(\frac{\partial \varepsilon}{\partial P}\right)_T;$$

$$Y \equiv -\left(\frac{\partial(1/\varepsilon)}{\partial T}\right)_P = \frac{1}{\varepsilon^2}\left(\frac{\partial \varepsilon}{\partial T}\right)_P;$$

$$X \equiv \left(\frac{\partial Y}{\partial T}\right)_P = \frac{1}{\varepsilon^2}\left(\left(\frac{\partial^2 \varepsilon}{\partial T^2}\right)_P - \frac{2}{\varepsilon}\left(\frac{\partial \varepsilon}{\partial T}\right)_P^2\right)$$

and can be computed from equations expressing the dielectric properties of water to 1000°C and 5 kbar (Johnson and Norton, 1992).

However, the parameters a_1, a_2, a_3 and a_4 relate only to corrections for pressure. Because potable ground waters are obtained from relatively shallow wells, correction of $\Delta\overline{G}^0_{f,j}$ for pressure would be trivial and almost certainly within the uncertainties associated with the derivations under discussion.

C2.2.2 Calculation of HKF Equation of State Parameters for Metal Complexes with Aqueous Arsenate and Arsenite Species

Langmuir et al. (2006) present estimated values of the association constants of a number of metal arsenate complexes. Those complexes relevant to the problem at hand are listed in Table C3.

Table C3. Association Constant and Gibbs Free Energy of Formation of Selected Arsenate Complexes (after Langmuir et al., 2006) and Derived HKF Equation of State Parameters

Complex	$\log K_{assoc}$ at 25°C	$\Delta\overline{G}^0_{f,P_r,T_r}$ cal mol-1	$\overline{S}^0_{P_r,T_r}$ cal mol^{-1} K^{-1}	$\overline{C}^0_{P_r,T_r}$ cal mol^{-1} K^{-1}	c_1 cal mol^{-1} K^{-1}	c_2 cal K mol^{-1} x 10^{-4}	ω_{P_r,T_r} cal mol^{-1} x 10^{-5}	Z
Arsenite Species								
$H_4AsO_3^+$	-0.29	-116510	-81.203					+1
H_3AsO_3(aq)		-152971	46.80	30.43	20.6012	3.1635	-0.3688	0
$H_2AsO_3^-$	-9.17	-140454	26.96	-2.32	15.9835	-3.5072	1.2132	-1
$HAsO_3^{-2}$	-23.27	-121272	-1.84	-49.83	7.0916	-13.1859	3.2706	-2
AsO_3^{-3}	-38.27	-100813	-46.71	-120.83	-13.3179	-27.6474	5.5714	-3
Arsenate Species								
H_3AsO_4(aq)		-183258	43.75	25.40	18.0776	2.1384	-0.3226	0
$H_2AsO_4^-$	-2.30	-180127	26.86	-2.48	15.9024	-3.5402	1.2146	-1
$HAsO_4^{-2}$	-9.29	-170590	-2.73	-51.30	6.3549	-13.4851	3.2840	-2
AsO_4^{-3}	-21.09	-154489	-42.14	-118.08	-12.3472	-27.0882	5.5021	-3
$MgH_2AsO_4^+$	-0.78	-290706	25.86	42.18	32.2896	5.5571	0.1524	1
$MgHAsO_4$(aq)	-6.43	-282997	-19.38	-6.64	8.1099	-4.3879	0.6336	0
$MgAsO_4^-$	-14.75	-271645	-74.45	-73.42	-11.5410	-17.9910	2.7487	-1
$CaH_2AsO_4^+$	-1.24	-313693	45.36	41.23	29.0125	5.3636	-0.1429	1
$CaHAsO_4$(aq)	-6.60	-306380	1.19	-7.59	4.6829	-4.5814	0.3220	0
$CaAsO_4$-	-14.87	-295096	-52.80	-74.37	-15.1173	-18.1845	2.4209	-1
$AlH_2AsO_4^{+2}$	0.77	-300826	-0.73	15.02	25.0924	0.0246	1.0989	2
$AlHAsO_4^+$	-2.00	-297046	-48.43	-33.80	-1.8770	-9.9204	1.2773	1
$AlAsO_4$(aq)	-6.99	-290238	-105.95	-100.58	-34.8667	-23.5235	1.9445	0
$MnHAsO_4$(aq)	-5.54	-230206	-1.66	-5.40	6.3638	-4.1353	0.3651	0
$MnAsO_4^-$	-14.96	-217353	-55.80	-72.18	-13.4157	-17.7384	2.4663	-1
$FeH_2AsO_4^+$	0.38	-205421	33.56	39.62	29.7151	5.0356	0.0358	1
$FeHAsO_4$(aq)	-5.75	-197057	-11.26	-9.20	5.4762	-4.9094	0.5105	0
$FeAsO_4^-$	-14.03	-185759	-65.90	-75.98	-14.2337	-18.5124	2.6193	-1
$FeH_2AsO_4^{+2}$	1.74	-200131	10.05	28.92	31.7358	2.8560	0.9358	2
$FeHAsO_4^+$	0.57	-198535	-37.03	-19.90	4.6789	-7.0890	1.1047	1
FeAsO4(aq)	-2.19	-194769	-93.93	-86.68	-28.3985	-20.6920	1.7624	0
$ZnHAsO_4$(aq)	-6.08	-210169	-12.21	-6.63	7.1149	-4.3859	0.5249	0
$CdHAsO_4$(aq)	-5.58	-194212	-2.93	-4.80	6.8921	-4.0131	0.3843	0
$PbH_2AsO_4^+$	-0.77	-187925	63.06	34.82	22.7867	4.0579	-0.4109	1
PbHAsO4(aq)	-6.25	-180447	19.86	19.86	19.8614	1.0112	0.0392	0

Using the information supplied by Nordstrom and Archer (2003), $\Delta\overline{G}^0_{f,j}$ can be calculated, as also listed in Table C3. A necessary requirement for calculating the HKF equation of state parameters is quantification of $\overline{S}^0_{P_r,T_r}$ and $\overline{C}^0_{P_r,T_r}$, neither of which have been measured or estimated. Calculation of $\overline{S}^0_{P_r,T_r}$ is facilitated by the observation by Sverjensky et al. (1997) that the standard partial molal entropies of association $\Delta\overline{S}^0_{assoc.,P_r,T_r}$ of metal sulfate complexes

$$M^{Z+2} + SO_4^{2-} = MSO_4^Z$$

of a given charge, Z, are essentially identical, as indicated in Figure C2.

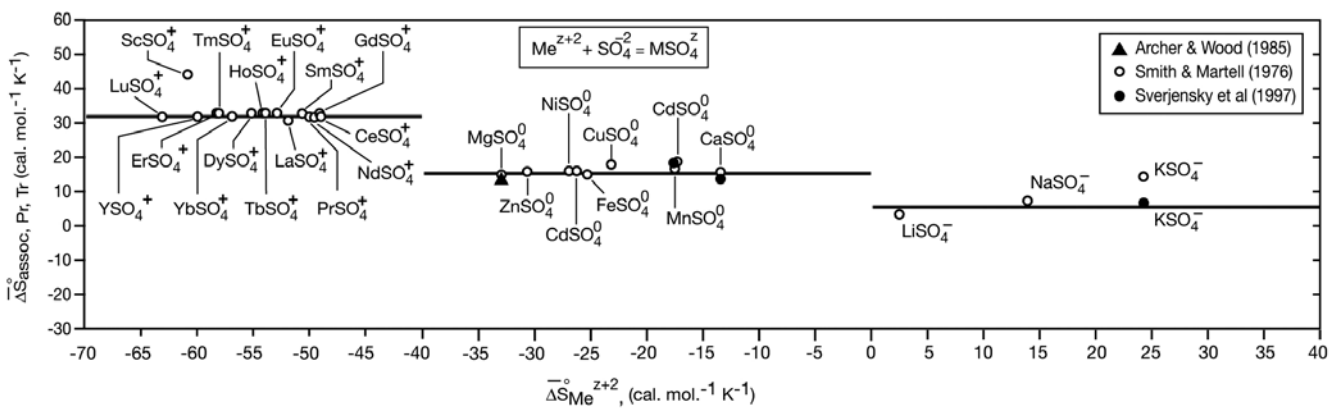

Fig. C2. Standard partial molal entropies of association $\Delta\overline{S}^0_{assoc.,P_r,T_r}$ of metal sulfate complexes (after Sverjensky et al., 1997)

These correlations were summarized by the authors in the form of the following equation:

$$\Delta\overline{S}^0_{assoc.,P_r,T_r,y=1} = \alpha_{Z,SO_4^{2-}}\overline{S}^0_{M^{Z+2}} + \beta_{Z,SO_4^{2-}}$$

where $\alpha_{Z,SO_4^{2-}} = -0.055Z + 0.055$ and $\beta_{Z,SO_4^{2-}} = 13.84Z + 18.16$.

Recognizing that the entropies of oxyanions of identical charge are nearly identical, as shown in Table C2 and Figure C1, above, the assumption was made that $\Delta\overline{S}^0_{assoc.,P_r,T_r}$ for metal arsenate complexes with charges equivalent to those of metal complexes would be equivalent. Thus, for

example, values of $\Delta\overline{S}^0_{assoc.,P_r,T_r}$ for $CaHAsO_4$(aq) are equivalent to $CaSO_4$(aq). The estimated values of $\overline{S}^0_{P_r,T_r}$ all metal complexes listed were calculated using the above equation, and are presented in Table C3.

The estimation of $\overline{C}^0_{P_r,T_r}$ for metal arsenate complexes could not be accomplished by reference to the existing papers describing parameter estimations for the HKF equation of state. The normal procedure is to use correlation plots relating $\overline{C}^0_{P_r,T_r}$ to $\overline{S}^0_{P_r,T_r}$ for given families of ionic or molecular species, e.g., Schock and Helgeson (1988, Eq. 91) and Shock et al. (1989, Eq. 24). However, in this case, no such correlation plots have been developed, and published plots are neither relevant nor adaptable for to arsenate complexes. Perusal of limited $\overline{C}^0_{P_r,T_r}$ data available for metal complexes of oxyanions presented in Sverjensky et al. (1997) indicates that the $\Delta\overline{C}^0_{P,assoc.,P_r,T_r}$ for these species are all of similar magnitude, i.e., circa 50 cal mol^{-1} K, suggesting the formation of outer sphere complexes, as proposed many years ago by Garrels and Christ (1965, Figure 4.4, p. 100). Table C4 presents the results of this analysis. Among those listed complexes is $MnSO_4$(aq). However, Sverjensky et al. (1997), referring to supporting literature, have asserted that the complexation of Fe^{+2} Mn^{+2} and Zn^{+2} involves the release of one or more molecules of water from the inner coordination sphere of central cations in such complexes, and indeed, this may be consistent with the elevated $\Delta\overline{C}^0_{P,assoc.,P_r,T_r}$ values for CH_3COO^- complexes of Fe^{+2} and Zn^{+2}. Compensating for one mol of water would result in a correction of –18.0 cal mol^{-1} K^{-1} to $\Delta\overline{C}^0_{assoc.,P_r,T_r}$ for CH_3COOFe^+ and CH_3COOZn^+ leading to equivalent values of 65 and 67.33 cal mol^{-1} K^{-1}, respectively, which is more in accord with $\Delta\overline{C}^0_{assoc.,P_r,T_r}$ for the oxyanion complexes listed in Table C4. Note, however, that $\Delta\overline{C}^0_{assoc.,P_r,T_r}$ for the reaction between CH3COOH(aq) and either Fe^{+2} or Zn^{+2} is also approximately 50 cal mol^{-1} K^{-1}. Bearing in mind the tentative nature of the analysis, we have made a provisional assumption that $\overline{C}^0_{P_r,T_r}$ for all metal arsenate complexes listed in Table C3 can be estimated assuming that $\Delta\overline{C}^0_{assoc.,P_r,T_r}$ = 50 cal mol^{-1} K^{-1} for all association reactions.

Table C4. A Comparison of Heat Capacities of Dissociation of selected Oxyanions

Reaction	Participating Species	$\overline{C}^0_{P_r,T_r}$	$\Delta\overline{C}^0_{assoc.,P_r,T_r}$
$K^+ + SO_4^{-2} = KSO_4^-$	K^+	-3.0	56.48
	SO_4^{-2}	-64.38	
	KSO_4^-	-10.9	
$K^+ + HSO_4^- = KHSO_4(aq)$	K^+	-3.0	49.42
	HSO_4^-	5.3	
	$KHSO_4(aq)$	57.72	
$Mn^{+2} + SO_4^{-2} = MnSO_4(aq)$	Mn^{+2}	-4.1	47.88
	SO_4^{-2}	-64.38	
	$MnSO_4(aq)$	-20.6	
$Ca^{+2} + CO_3^{-2} = CaCO_3(aq)$	Ca^{+2}	-7.53	47.43
	CO_3^{-2}	-69.5	
	$CaCO_3(aq)$	-29.6	
$Na^+ + HSiO_3^- = NaHSiO_3(aq)$	Na^+	9.06	36.55
	$HSiO_3^-$	-21	
	$NaHSiO_3(aq)$	24.61	
$Ca^{+2} + HSiO_3^- = CaHSiO_3^+$	Ca^{+2}	-7.63	61.5
	$HSiO_3^-$	-21	
	$CaHSiO_3^+$	32.87	
Average Value			49.9
$Fe^{+2} + CH_3COO^- = CH_3COOFe^+$	Fe^{+2}	-7.9	83.0
	CH_3COO^-	6.2	
	CH_3COOFe^+	81.3	
$Zn^{+2} + CH_3COO^- = CH_3COOZn^+$	Zn^{+2}	-5.33	85.33
	CH_3COO^-	6.2	
	CH_3COOZn^+	86.2	
$Fe^{+2} + CH_3COOH = CH_3COOFe^+ + H^+$	Fe^{+2}	-7.9	48.64
	CH_3COOH	40.56	
	CH_3COOFe^+	81.3	
$Zn^{+2} + CH_3COOH = CH_3COOZn^+ + H^+$	Zn^{+2}	-5.33	51.07
	CH_3COOH	40.56	
	CH_3COOFe^+	86.2	

Calculation of the HKF equation of state parameters, c_1, c_2 and the Born coefficient, ω_{P_r,T_r}, follows the procedures outlined above. The respective values are listed in Table C3.

C2.2.3 Derivation of Thermodynamic Properties of Arsenic Solid Phases and Minerals

The following two tables summarize information on arsenic solid phases. Table C5 gives the crystallographic information necessary to calculate molar volumes of the solid phases, which are used in thermodynamic calculations to correct for the effects of pressure, and Table C6 provides

thermodynamic data for the solid phases. This information, in conjunction with the corresponding aqueous basis species information, is used to calculate the solid phase solubility products.

The thermodynamic properties of some of the phases or minerals listed in Table C6 are incomplete. Information available in the literature may be sufficient to estimate preliminary values of $\Delta G^0_{P_r,T_r}$ for the minerals in question, but time constraints prevented further evaluation. In some cases, $\Delta G^0_{P_r,T_r}$ values were taken directly, or calculated from solubility product data reported in the literature, rather than by re-evaluating raw data and using revised thermodynamic data for aqueous species published by Nordstrom and Archer (2003) to recalculate solubility product and $\Delta G^0_{P_r,T_r}$ values. The tabulated data are not entirely consistent internally, and are therefore preliminary. However, the uncertainties introduced by taking this expedient approach are well within the uncertainties of the geochemical model developed in Section 3 of the report, and have no impact on the resulting findings and conclusions.

A very recent paper by Perfetti et al. (2008) gives revised thermodynamic data for arsenopyrite. In this paper, $\Delta G^0_{P_r,T_r}$ for arsenopyrite is given as –32,612 cal/mol, which differs by +1,231 cal/mol from the value reported in Table C6, which was cited from an earlier paper by Pokrovski et al. (2002). Using this revised value for the calculation of solubility products would decrease the extent of undersaturation of arsenopyrite reported in Section 3.4.5.2, Figure 3.34a, by approximately one unit in SI. This change would necessitate a smaller calibration correction (-1.8 vs. –3.0) to match the modeled As concentration in groundwaters in equilibrium with an arsenopyrite solid solution in pyrite, to that actually observed, as presented in Section 3.5.2, Table 3.13. This revised correction appears to be more realistic, although further corroborating evidence is needed.

Table C5. Crystallographic Properties of Arsenic Solid Phases

Name	Formula	Cell Constants							Space Group	Reference
		a_o (Å)	b_o (Å)	c_o (Å)	α	β	γ	Z		
Arsenolite	As_2O_3	11.07343	11.07343	11.07343	90	90	90	16	*Fd3m	Ballirano and Maras (2002)
Claudetite II	As_2O_3	7.99	4.645	9.115	90	78.3	90	4	P2_1/n	Pertlik (1975)
Arsenic	As	3.7597	3.7597	10.4412	90	90	120	6	R3m	Schiferl and Barrett (1969)
Arsenic Oxide	As_2O_5	8.64	8.45	4.62	90	90	90	4	$P2_12_12_1$	Hansen (1977)
Ferrarisite	$Ca_5(AsO_3OH)_2(AsO_4)_2.9H_2O$	8.294	6.722	11.198	106.16	92.94	99.2	1	P-1	Catti et al. (1980)
Guerinite	$Ca_5(AsO_3OH)_2(AsO_4)_2.9H_2O$	17.63	6.734	23.47	90	90.6	90	5	P2_1/n	Catti and Ferraris G (1974)
Haidingerite	$Ca(AsO_3OH).H_2O$	6.904	16.161	7.935	90	90	90	8	Pcnb	Ferraris et al. (1972)
Hornesite	$Mg_3(AsO_4)_2.8H_2O$	10.2573	13.4211	4.7526	90	105.076	90	2	C2/m	Rojo et al. (1996)
Johnbaumite	$Ca_5(AsO_4)_3(OH)$	9.70	-	6.93				2	P 6_3/m or P6_3	Dunn et al. (1980)
Johnbaumite-Pb	$Pb_5(AsO_4)_3(OH)$									
Mimetite	$Pb_5(AsO_4)_3(Cl)$	10.211	-	7.4185				2	P6_3/m	Yonshan et al. (1991)
Pyromorphite	$Pb_5(PO_4)_3(Cl)$	9.9764	-	7.3511				2	P6_3/m	Dai and Hughes (1989)
Orpiment	As_2S_3	11.475	9.577	4.256	90	90.68	90	4	P2_1/n	Mullen and Nowacki (1972)
Pharmacolite	$CaHAsO_4.2H_2O$	5.9745	15.434	6.2797	90	114.83	90	4	Ia	Ferraris et al. (1971)
Pharmacosiderite	$KFe_4(AsO_4)_3(OH)_4.6H_2O$	7.9816	7.9816	7.9816	90	90	90	2	P-43m	Buerger et al. (1967)
Picropharmacolite	$Ca4Mg(HAsO_4)_2(AsO_4)_2.11H_2O$	13.547	13.5	6.71	99.85	96.41	91.6	2	P-1	Cattiet al. (1981)
Pitticite	$Fe_2(AsO_4)(SO_4)(OH).6H_2O$									
Realgar	AsS	9.327	13.563	6.59	90	106.46	90	16	P2_1/n	Kyono et al. (2005)
Pararealgar	AsS	9.909	9.655	9.502	90	97.29	90	16	P2_1/c	Bonazzi et al. (1995)
Scorodite	$FeAsO_4.2H_2O$	8.942	10.075	10.339	90	90	90		Pbca	Xu et al. (2007)
Scorodite	$FeAsO_4.2H_2O$	10.325	8.953	10.038	90	90	90		Pbca	Kitahama et al. (1975)
Symplesite	$Fe_3(AsO_4)_2.8H_2O$	7.97	9.41	4.72	99.917	97.383	105.967	1	P-1	Wolfe (1940)
Talmessite	$Ca_2Mg(AsO_4)_2.2H_2O$	5.874	6.943	5.537	97.3	108.7	108.1	1	P-1	Catti M, et al. (1977)
Tooeleite	$Fe_6(AsO_3)_4(SO_4)(OH)_4.4H_2O$	8.9575	6.4238	9.7912	90	96.032	90	1	C2/m	Morin et al. (2007)
Weilite	$CaHAsO_4$	7.0591	6.8906	7.2006	97.43	103.55	87.75	4	P-1	Ferraris and Chiari (1970)
Yukonite	$Ca_7Fe_{11}(AsO_4)_9O_{10}.24H_2O$									
Arsenopyrite	FeAsS	5.744	5.675	5.785	90	112.28	90	4	P-1	Morimoto and Clark (19610

Table C6. Thermodynamic Properties of Arsenic Solid Phases

Mineral name	Formula	$\Delta G^0_{f,P_r,T_r}$ cal mol^{-1}	Ref	$\Delta H^0_{f,P_r,T_r}$ cal mol^{-1}	Ref	$S^0_{P_r,T_r}$ cal mol^{-1} K^{-1}	Ref	$V^0_{P_r,T_r}$ cm^3 mol^{-1}	Ref	$C^0_{P_r}$ cal mol^{-1} K^{-1}			Ref
										a	$b\times10^3$	$c\times10^{-5}$	
(C3RH2.25)	$Ca_3(AsO_4)_2.2.25H_2O$	-862066								88.361	3.2400	-4.68E+00	5
(C3RH3)	$Ca_3(AsO_4)_2.3H_2O$	-904227								96.911	3.2400	-4.68E+00	5
(C3RH3.67)	$Ca_3(AsO_4)_2.3.67H_2O$	-942878	2							104.549	3.2400	-4.68E+00	5
(C3RH4.25)	$Ca_3(AsO_4)_2.4.25H_2O$	-976338	2							111.161	3.2400	-4.68E+00	5
(C4RH5)	$Ca_4(OH)_2(AsO_4)_2.4H_2O$	-1176881	2							119.981	4.3200	-6.24E+00	5
(F2R1.5SH)	$Fe_4(AsO_4)_3(SO_4)(OH)$									106.309	31.0062	-5.92E+00	5
(FR1.5HX)	$Fe_2(HAsO_4)_3.xH2O$												
(FRX)	$Fe_2(AsO_4)x(HAsO_4)y$												
(R)	As_2O_5	-185220	1	-219309	1	25.201	1	50.781	7	27.701	0.000	0.000	4
Arsenic	As	0	1	0	1	8.516	1	13.049	8	5.137	2.602	-0.089	
Arsenopyrite	FeAsS	-33843	11			16.370	11	26.420	8	18.047	4.780	-7.543	
Arseniosiderite	$Ca_2Fe_3(AsO_4)_3O_2.3H_2O$	-887437				111.33	6	195.618	8	134.327	30.060	-8.450	5
Arsenolite	As_2O_3	-137749	1	-157091	1	25.664	1	50.724	8	8.37	48.6	0.000	4
Ca-arsenate	$Ca_3(AsO_4)_2.xH2O$	-887437				49.761		100.070	8	61.700	13.900	-15.010	
Claudetite	As_2O_3	-137794	1	-156709	1	27.096	1	47.257	8	23.197	9.326	-6.300	
Ferrarisite	$Ca_5(AsO_3OH)_2(AsO_4)_2.9H_2O$	-1866157	2			189.017	6	354.655	8	223.462	5.400	-7.800	5
Guerinite	$Ca_5(AsO_3OH)_2(AsO_4)_2.9H_2O$	-1864962	2			184.458	6	335.580	8	223.462	5.400	-7.800	5
Haidingerite	$Ca(AsO_3OH).H_2O$	-366396	2			35.591	6	66.991	8	40.476	1.080	-1.560	5
Hornesite	$Mg_3(AsO_4)_2.8H_2O$	-887437				114.241	6	190.194	8	149.441	5.220	-4.440	5
Johnbaumite	$Ca_5(AsO_4)_3(OH)$	-1216375	2			94.817	6	170.031		103.457	5.400	-7.800	5
Johnbaumite-Pb	$Pb_5(AsO_4)_3(OH)$	-635516	3			123.721	6	204.215		90.357	32.000	0.000	5
Mimetite	$Pb_5(AsO_4)_3(Cl)$	-630019	10	-713432	10	143.164	10	204.215	8	119.981	4.3200	-6.2400	5
Orpiment	As_2S_3	-20292	1	-20507	1	39.149	1	70.503	8	22.73	13.82	0.605	9
As_2S_3,am	As_2S_3	-18356	1	-15989	1	47.801	1	70.503		22.73	13.82	0.605	9
Pharmacolite	$CaHAsO_4.2H_2O$					43.177	6	79.363	8	51.876	1.080	-1.560	5
Pharmacosiderite	$KFe_4(AsO_4)_3(OH)_4.6H_2O$					162.563	6	306.084	8	184.967	42.605	-9.100	5
Picropharmacolite	$Ca4Mg(HAsO_4)_2(AsO_4)_2.11H_2O$					199.568	6	361.370	8	244.772	10.385	-7.720	5
Pitticite	$Fe_2(AsO_4)(SO_4)(OH).6H_2O$					103.29	6	100.070		123.518	12.406	-2.370	5
Realgar	AsS	-7481	1	-7600	1	15.033	1	29.743	8	12.94	-0.0133	1.396	9
Pararealgar	AsS	-7385	1	-7409	1	15.177	1	30.368	8	12.94	-0.0133	1.396	9
Scorodite	$FeAsO_4.2H_2O$	-306991				49.761		69.117	8	48.396	9.300	-1.780	
Scorodite,am	$FeAsO_4.2H_2O$	-303130				38.313	6	69.117		48.396	9.300	-1.780	5
Symplesite	$Fe_3(AsO_4)_2.8H_2O$	-872736				119.583	6	198.385	8	155.261	6.210	-2.250	5
Talmessite	$Ca_2Mg(AsO_4)_2.2H_2O$					70.333	6	120.084	8	84.021	3.900	-4.600	5
Tooeleite	$Fe_6(AsO_3)_4(SO_4)(OH)_4.4H_2O$					177.878	6	337.409	8	161.252	66.906	-9.470	5
Weillite	$CaHAsO_4$					27.344	6	51.858	8	29.076	1.080	-1.560	5
Yukonite	$Ca_7Fe_{11}(AsO_4)_9O_{10}.24H_2O$			-940771		515.389	6	100.070		609.140	109.860	-30.400	5

Notes: 1. Nordstrom and Archer (2003); 2. Bothe and Brown (1999); Lee and Nriagu (2007); 4. Kelley (1960); 5. Calculated using the summation of oxide components. This work; 6. Calculated using the procedure described by Holland (1989). This work; 7. Jansen (1977); 8. Calculated from cell parameter data. 9. Pokrovski et al. (1996); 10. Flis et al. (2007), $S^0_{P_r,T_r}$ recalculated using elemental data from NIST; 11. Pokrovski et al. (2002).

C3. Lead

C3.1 Introduction

Incorporation of a wider range of lead solid and aqueous species in the ongoing evaluation of groundwater analyses, and in model development, is important for two reasons. First, the ingress of oxygen into aquifers that were formerly reducing, and where lead was presumably immobilized as the sulfide, galena, could induce solubilization of lead exceeding MCLs, even more so than would be induced through pH lowering through the ingress of high-pressure CO_2. It is important to know whether the precipitation of secondary lead salts might restrain lead solubility under those conditions, especially with respect to those ground waters downloaded from the NWIS database, some of which exhibit lead concentrations that are supersaturated with respect to galena. Secondly, the addition of relevant aqueous lead complexes, especially those of carbonate, sulfide and selenide, will aid in a more precise calculations of lead concentrations in solutions saturated with respect to minerals containing lead as an essential component. These additional species might also affect the predicted sorption and ion exchange of lead on aquifer minerals, depending on the nature of the problem at hand. In this appendix, we present thermodynamic properties of lead minerals and other phases where lead is an essential component, and for all aqueous species except for lead sulfide and selenide complexes, which are discussed in Appendices D and E of this report.

C3.2 Aqueous Lead Species

An earlier unpublished compilation of internally consistent thermodynamic properties of a variety of lead carbonates, chlorides and sulfates, and a corresponding compilation relating to lead complexes in solution, was used to calculate their respective solubility products and dissociation constants in the Data0.dat database of EQ3 and the corresponding TOUGHREACT database. All respective constants were calculated using SUPCRT92, in which estimated HKF-equation-of-state parameters for the aqueous species were included. In addition to replacing seven extant aqueous species and eleven solid phases in the database, three additional aqueous species, and thirteen additional solid phases were incorporated. Table C7 lists the thermodynamic properties of aqueous lead species together with their calculated HKF-equation-of-state parameters.

C3.3 Lead Solid Phases and Minerals

The following two tables summarize information on lead solid phases. Table C8 gives the crystallographic information necessary to calculate molar volumes of minerals, which are used in thermodynamic calculations to correct for the effects of pressure, and Table C9 provides thermodynamic data for the solid phase. This information, in conjunction with the corresponding aqueous basis species information is used to calculate the solid phase solubility products. The listed solid phases also include those known to very insoluble. An example is the Pb phosphate, pyromorphite, $Pb_5(PO_4)_3(Cl)$, in the presence of which lead concentrations are known to be depressed to low levels. The application of phosphate compounds as a means of controlling Pb mobility in contaminated soils has been suggested. The corresponding lead arsenate, mimetite, $Pb_5(AsO_4)_3(Cl)$, is also known to be very insoluble, and it is possible that mimetite could limit the saturation concentration of both As and Pb in ground waters. Therefore this mineral is also included as well as the arsenic analogue of apatite, johnbaumite, $Pb_5(PO_4)_3(OH)$.

It should be noted that many of the data compiled in Tables C7, C8, and C9 were evaluated and reconciled over a decade ago. Time did permit only limited retrieval of new information published in the archival literature since that time. A casual perusal of the literature indicates that no substantive changes have occurred since the original work was compiled; rather, the data has been refined and augmented. Therefore, the application of more recent data, where available, would not change the findings of this report in any significant manner, and would be within the limits of geochemical model uncertainty. The advantage in using the current database is that it is internally consistent, and that the solubility product and dissociation constant data have been uniformly treated, as all calculations were performed using SUPCRT (Johnston et al., 1992). However, a complete review of the data in the light of more recent published data is definitely recommended.

C3.4 Acknowledgements

We would like to acknowledge the contributions of Mr. Motomi Oshika, a guest scientist at the Berkeley Lab during 1992-3, who assisted in the evaluation of the thermodynamic properties of lead minerals, under a FY 1992 allocation of Exploratory R&D Funds to one of the authors (John Apps) for the project “Synthesizing Optical $PbSO_4$ for Advanced Scintillation Applications”.

Table C7. Thermodynamic Properties of Lead Aqueous Species

Aqueous Species	$\Delta G^0_{f,P_r,T_r}$	$\Delta H^0_{f,P_r,T_r}$	$\overline{S}^o$	$\overline{C}p^{o\,bf}$	$\overline{V}^{oCg}$	$a_1^{uaa}\ x10$	$a_2^{uaa}\ x10^{-2}$	$a_3 v.aa$	$a_4^{w.aa}\ 10^{-4}$	c_1^{baa}	$c_2^{waa} \times 10^{-4}$	$w^{az} \times 10^{-5}$	Charge
H^+	0	0	0	0	0	0	0	0	0	0	0	0	+1
HCO_3^-	-140282[l]	-164898[m]	23.53[m]	-8.46	24.6	7.5621	1.1505	1.2346	-2.8266	12.93965	-4.7579	1.2733	-1
CO_3^{-2}	-126191[m]	-161385[m]	-11.95[m]	-69.5[n]	-5.02	2.8524	-.39844	6.4142	-2.6143	-3.3206	-17.1917	3.3914	-2
Pb^{+2}	-5710[h]	220[e]	4.2[e]	-12.74	-15.6	-0.0051	-7.7939	8.8134	-2.4568	8.6624	-5.6216	1.0788	2
$Pb(OH)^+$	-52089	-57652[*]	21.34	4.54	7.029	2.804	-0.9348	6.1174	-2.7404	10.9315	-2.1098	0.2284	1
$Pb(OH)_2(aq)$	-95060	-111214[*]	41.57	33	48.127	8.4485	12.8476	.07206	-3.3101	22.8390	3.6875	-0.2895	0
$Pb(OH)_3^-$	-137641	-166209[*]	40.06	15.1792	40.06	7.5921	10.7680	1.4938	-3.2241	24.4800	0.0574	1.0223	-1
$PbCO_3(aq)$	-141819	-156632[*]	40.72	29	46.880	8.2735	12.3922	0.9392	-3.2913	20.6134	2.8727	-0.2767	0
$Pb(CO_3)_2^{-2}$	-272746	-301163[*]	70.01	-14.492	83.41	13.906	26.173	-4.5397	-3.8610	17.5025	-5.9866	2.1523	-2
$PbCl^+$	-39046	-43260[*]	28.0		3.400[*]	2.2870	-2.9703	8.5760	-2.6502	21.8	1.8542	0.16800	1
$PbCl_2$	-71190	-78281[*]	45.0		22.400[*]	4.7542	3.9456	3.9447	-2.9421	22.2616	3.2801	-0.2550	0
$PbCl_3^-$	-102147	-115066[*]	52.1		41.400[*]	7.7573	12.3640	-1.6927	-3.2901	39.698	5.521	0.9679	-1
$PbCl_4^{-2}$	-133254	-153342[*]	54.7		60.399[*]	10.7757	20.8252	-7.3588	-3.6399	57.0825	7.5985	2.2060	-2
Cl^-	-31379[h]	-39933[e]	13.56	-29.44[d]	17.79[d]	4.0320	4.8010	5.5630	-2.847	-4.40	-5.714	1.4560	-1
OH-	-3.7595[h]	-54977[e]	-2.56[e]	-32.79[d]	-4.18[d]	1.2527	0.0738	1.8423	-2.7821	4.15	-10.346	1.7246	-1
SO_4^{-2}	-177930[h]	-217400e	4.50[e]	-64.38[d]	13.88[d]	8.3014	-1.9846	-6.2122	-2.6970	1.64	-17.998	3.1463	-2
HSO_4^-	-180630[r]	-212500[r]	30.0[r]	5.3	35.2	6.9788	9.2590	2.1108	-3.1618	20.0961	-1.9550	1.1748	-1

Notes a: cal mol^{-1}; b: cal $mol^{-1}K^{-1}$; c:cm^3mol^{-1}; d: Tanger and Helgeson; e: CODATA(1978); *: supcrt; f: from electrolytes in Table 10 unless otherwise indicated; h: calculated from $\Delta\overline{H}\,\overset{o}{S}PT$ and $\overline{S^O}$ shown using standard entropiues of the elements from CODATA (1978); g: From electrolytes in Table 9 unless otherwise indicated; l: Helgeson, Kirkham, and Flowers (1981); m: Berg and Vanderzee (1978); r: consistent with log KrPT, Δ HrPt AND Δ Srpt from dissociation reaction; u: Cal $Mol^{-1}xbar^{-1}$; v: cal K $mol^{-1}xbar^{-1}$; w: cal K mol^{-1}; z: from Table 1, 2, and 3; aa: calculated in a manner consistent with table 8 unless otherwise indicated

Table C8. Crystallographic Properties of Lead Solid Phases

Mineral Name	Formula	Unit	Cell Parameters						Z	Space Group	Reference
			a_o	b_o	c_o	α	β	γ	4		
Cotunnite	$PbCl_2$	Kx Å	7.67 7.68	9.15 9.17	4.5 4.51	90	90	90	 4	Pnam	Palache et al. (1951)
Laurionite	PbOHCl	Å Kx	9.72 9.7	4.06 4.05	7.11 7.1	90	90	90		Pcmn	Palache et al. (1951)
	$3PbO.PbCl_2.nH_2O$	Å	9.57	-	-	90	90	90			
Lorettoite	$Pb_7O_6Cl_2$								4		Palache et al. (1951)
Mendipite	$Pb_3O_2Cl_2$	Kx Å	9.50 9.52	11.87 11.89	5.87 5.88	90	90	90	 4	Pnma $P2_12_12_1$	Palache et al. (1951)
Paralaurionite	Pb(OH)Cl	Kx Å	10.77 10.79	3.97 3.98	7.18 7.19	90	117.22	13/60		$C2_1/m$	Palache et al. (1951)
Penfieldite	Pb_2OHCl_3	Å	11.28	x	48.65				4	P6/m	Cesbron and Schubnel (1968);
Fieldlerite	$Pb_3(OH)_2Cl_4$	Kx Å	16.59 16.62	8.00 8.02	7.19 7.20	90	102.20	90	 4	$P2_1/a$	Palache et al. (1951)
Anglesite	$PbSO_4$	Kx Å	8.45 8.47	5.38 5.39	6.93 6.94	90	90	90	 4	Pnma	Palache et al. (1951)
Lanarkite	$Pb_2(SO_4)O$	Kx Å	13.73 13.76	5.68 5.69	7.07 7.08	90	116.22	90	 2	C_2/m	
Sulfate Dibasque (Second Source)	$2PbO.PbSO_4$	Å Å	7.814 8.06	5.803 5.79	8.035 7.17	90	102.64 103	90	2	$P2_1$ or $P2_1/m$	Boivin et al. (1968)
	$3PbO.PbSO_4$	Å	10.30	6.37	7.45	87.2	75.0	79.2	4	P1 or p1	
Lanarkite	$PbO.PbSO_4$	Å	13.751	5.6969	7.0699	–	115.82	-	2	P	
	$3PbO.PbSO_4.H_2O$	Å	10.30	6.37	7.45	87.2	75.0	79.2	4	P1 or p1	Boivin et al. (1968)
2nd Source	$4PbO.PbSO_4$	Å	11.5234 11.443	11.7138 11.666	7.3152 7.316	90 90	91.04 90.82	90 90		$P2_1/a$	Boivin et al. (1968)
Hydrocerussite											
Plumbonacrite											
Matlockite											
Lead											
Litharge											
Massicot											

Notes a. Palache et al. (1951); b. Did not calculate; c. Cesbron and Schubnel (1968); d. Boivin et al. (1968), Tridot et al. (1969); e. Kuzel (1973).

Table C9. Thermodynamic Properties of Lead Solid Phases

Mineral Name	Formula	G.F.W. g. .mol^{-1}	$\Delta G^0_{f,P_r,T_r}$ cal.mol^{-1}	Ref.	$\Delta H^0_{f,P_r,T_r}$ kcal.mol^{-1}	Ref.	$S^0_{P_r,T_r}$ cal.mol^{-1}.k^{-1}	Ref.	$V^0_{P_r,T_r}$ cm^3.mol^{-1}	Ref.	$C^0_{P_r}$ Coefficients, cal.mol^{-1}.k^{-1}			Ref.
											a	b x 10^3	c x 10^{-5}	
Lead	Pb	207.2	0.0		0.0		15.484		18.153		5.290 7.77	2.80 -0.72	0.23 0.00	
Litharge	PbO	223.199	-45244		-52440		16.214		23.983		10.385 10.794	4.77 4.0	-0.610 0.00	
Massicot	PbO	223.199	-44910	8,9,11	-51940		16.42		23.983	23	9.05	6.40	0.00	14
Lead Hydroxide	$Pb(OH)_2$	241.215	-108100	8,9,11,12	-123300	8,9,11	26.69	26	41.2	26	17.71	12.24	0.00	26
Cotunnite	$PbCl_2$	278.106	-75050		-85800	20	32.50		47.84		15.96	8.00	0.00	14
Anglesite	$PbSO_4$	303.258	-194353		-219870		35.51		47.95		10.96	31.0	4.2	
Cerussite	$PbCO_3$	267.209	-150370		-168000		31.3		40.747		12.39	28.60	0.00	
-	$(PbO)_2.Pb(OH)_2$	687.613					58.9	26	90.33	15	38.91	20.24	0.00	26
Matlockite	$PbO.PbCl_2$	501.305	-126557	26	-144700	8,9	47.93	26	68.89		26.56	12.0	0.00	26
Lorretoite	$Pb_7O_6Cl_2$													
Mendipite	$(PbO)_2.PbCl_2$	724.505	-176860	6	-199800	8,9	65.79		100.305		37.16	16.0	0.00	26
-	$(PbO)_3.PbCl_2$	947.704			-253400	8,9					47.76	20.0	0.00	26
Lanarkite	$PbO.PbSO_4$	526.457	-246700	8,9,12	-276658		53.374		75.1		21.778	33.87	3.473	3
-	$(PbO)_2.PbSO_4$	749.656	-294000	9	-328189		70.326		107.1	26	34.830	39.28	2.940	3
-	$PbO.(PbCO_3)_2$	757.618	-351600		-395342	26	74.097		79.469		35.165	61.970	-0.621	
Laurionite	PbClOH	259.660	-93470	9	-109402	26	28.83		42.26		16.835	10.12	0.00	26
Paralaurionite	PbOHCl	259.660	-92340		-108361	26	28.53	26	41.36	26	16.835	10.12	0.00	26
Penfieldite	Pb_2OHCl_3	537.766					61.22		89.71		32.795	18.12	0.00	26
Fieldlerite	$Pb_3(OH)_2Cl_4$	797.427					93.22	26	141.285	26	49.63	28.24	0.00	26
-	$(Pb(OH)_2)_3.PbCl_2$	1001.770									69.09	44.72	0.00	26
Hydrocerussite	$Pb(OH)_2.(PbCO_3)_2$	775.633	-408328		-456000	21	86.083		112.894		45.735	61.970	-0.621	
-	$(PbO)_3.PbSO_4$	990.871	-341200	8	-388800	8,9	81.4	8,9	139.7	26	42.74	43	4.2	26
Plumbonacrite	$Pb_{10}O(OH)_6(CO_3)_6$	2550.098	-1270767		-1448776	26	272.629		357.584		144.590	190.680	-2.448	

Notes 1. Solans-Huguet and Font-Altaba (1967); 2. Derriche and Perrot (1976); 3. Kellogg (1989). 4. Esdaile (1967). 5. Kellogg and Basu (1960) Abdul-Samad et al. (1982). 6. Humphreys et. al. (1980). 7. Loza et. al. (1984). 8. Wagman et al. (1968); 9. Wagman et. al. (1982); 10. Chase et. al. (1985); 11. Weast et al. (1984); 12. Dekock (1986). 14. Kelley (1960); 15. Tolkachev et. al. (1958). 16. Brasseur (1940); 17. Toptygina et. al. (1984). 18. Kuzel (1973) 19. Cesbron and Schubnel (1968). 20. Shelton (1970). 21. Ball and Casson (1977). 22. Taylor and Lopata (1984). 23. Hill (1985). 24. Howie and Moser (1968), density referred to Clark and Tyler (1939). 25. SUPCRT. 26. This work.

C4. Antimony and Selenium

C4.1 Aqueous Antimony and Selenium Species

Table C10 gives the thermodynamic properties for aqueous species of Sb(III). Sb(V) species, SbO_2^+ and $Sb(OH)_6^-$, were also included in the geochemical model using extant data in the EQ3 Data0.dat database. The relevant selenite and selenate complexes included in the model were also extant data in the EQ3 Data0.dat database. The properties of selenide species used or derived in this study are discussed in Appendix E.

C4.2 Antimony and Selenium Solid Phases and Minerals.

Trace concentrations of selenides of heavy metals can play an important role in defining the solubility of hazardous constituents selected for study in this report. In Table C11, the crystallographic properties of selected selenides and antimony minerals are summarized with the purpose of calculating their molar volumes, which are given, together with other thermodynamic properties in Table C12.

Table C10. Thermodynamic Properties of Antimony Aqueous Species

Aqueous Species	$\Delta\overline{G}^0_{f,P_r,T_r}$ cal mol^{-1}	$\overline{S}^0_{P_r,T_r}$ cal mol^{-1} K^{-1}	$\overline{C}^0_{P_r,T_r}$ cal mol^{-1} K^{-1}	$\overline{V}^0_{P_r,T_r}$ cm^3 mol^{-1}	a_1[d] x 10 cal mol^{-1} bar^{-1}	a_2[a] x 10^{-2} cal mol^{-1}	a_3[e] cal K mol^{-1} bar^{-1}	a_4[f] x 10^{-4} cal K mol^{-1}	c_1 cal mol^{-1} K^{-1}	c_2 x 10^{-4} cal K mol^{-1}	ω_{P_r,T_r} cal mol^{-1}
$Sb(OH)_3(aq)$	-154010	49.43	39.09	54	9.1415	14.5397	0.0630	-3.3801	28.6838	4.9284	-0.038
$Sb(OH)_4^{-1}$	-195038	42.28	22.96	44.58	8.1966	12.2325	0.9671	-3.2847	28.6515	1.6426	0.9815
$H_2Sb_2S_4(aq)$	-35488	69.36	71.3	70.7	11.4268	20.1196	-2.1236	-3.6107	47.5025	11.4892	-0.038
$HSb_2S_4^{-1}$	-28583	50.70	32.56	50.7	8.9913	14.1728	0.2068	-3.3649	33.0864	3.5984	0.8540
$Sb_2S_4^{-2}$	-15622	42.38	-30.48	44.66	8.7546	13.5948	0.4332	-3.3410	12.3553	-9.2424	2.6016

Note: Data after Akinfiniev et al. (1994) and Bessinger (2000)

Table C11. Crystallographic Properties of Antimony and Selenium Minerals

Name	Formula	Cell Constants							Space Group	Reference
		a_o (Å)	b_o (Å)	c_o (Å)	α	β	γ	Z		
Naumannite	Ag_2Se	4.333	7.062	7.764	90	90	90	4	*P2_12_12_1	Wiegers (1971)
Berzelianite	Cu_2Se	5.765	5.765	5.765	90	90	90	4	Fm3m	Heyding and Murray (1976)
Antimonselite	Sb_2Se_3	11.794	3.986	11.648	90	90	90	4	Pnma	Caracas and Gonze (2005)
Clausthalite	PbSe	6.1243	6.1243	6.1243	90	90	90	4	Fm3m	Wyckoff (1963)
Tiemannite	HgSe	6.084	6.084	6.084	90	90	90	4	F-43m	Earley (1950)
Ferroselite	$FeSe_2$	4.804	5.784	3.586	90	90	90	2	Pnnm	Pickardt et al. (1975)
Stibnite	Sb_2S_3	11.3107	3.8363	11.2285	90	90	90	4	Pnma	Bayliss and Nowacki (1972)
Antimony	Sb	4.50661	4.50661	4.50661	57.108	57.108	57.108	20	R-3m	Wyckoff (1963)
Senarmonite	Sb_2O_3	11.1519	11.1519	11.1519	90	90	90	16	Fd-3m	Svensson (1975)
Valentinite	Sb_2O_3	4.911	12.464	5.412	90	90	90	4	Pccn	Svensson (1974)
Berthierite	$FeSb_2S_4$	11.401	14.148	3.758	90	90	90	4	Pnam	Lemoine et al. (1991)
Gudmundite	FeSbS	6.02	5.93	6.02	90	67.87	90	4	P1_1/c	Buerger (1939)
Kermesite	Sb_2S_2O	8.147	10.709	5.785	102.78	110.63	101.00	4	P-1	Bonazzi et al. (1987)

Table C12. Thermodynamic Properties of Selenides and Antimony Minerals

Mineral name	Formula	$\Delta G^0_{f,P_r,T_r}$ cal mol^{-1}	Ref	$\Delta H^0_{f,P_r,T_r}$ cal mol^{-1}	Ref	$S^0_{P_r,T_r}$ cal mol^{-1} K^{-1}	Ref	$V^0_{P_r,T_r}$ cm^3 mol^{-1}	Ref	$C^0_{P_r}$ cal mol^{-1} K^{-1}			Ref
										a	$b\times10^3$	$c\times10^{-5}$	
Naumannite	Ag_2Se	-11998		-10397		35.813		35.768		19.479	-	-	
Berzelianite	Cu_2Se	-17089		-15607		30.914		28.846		19.460	-	-	
Cadmoselite	CdSe	-33830		-34600		19.900		33.727		11.190	2.23	-	3
Clausthalite	PbSe	-23566		-24092		23.827		34.583		11.29	2.39	-	3
Tiemannite	HgSe	-9130		-10397		23.995		33.905		11.70	3.70	-	3
Ferroselite	$FeSe_2$	-19598		-21511		13.011		30.003		16.871	-	-	
Kullerudite	$NiSe_2$	-25096		-26052		24.138		32.206		18.028	-	-	
Antimony	Sb	0.		0.		10.773		18.188	6	2.490	5.930	1.880	
Senarmonite	Sb_2O_3	-151400				27.370		52.220	6	22.530	12.030	-3.179	
Valentinite	Sb_2O_3	-149600				29.430		49.874	6	24.840	10.300	-3.197	
Stibnite	Sb_2S_3	-35846				43.499		73.352	6	28.750	3.927	-1.264	
Antimonselite	Sb_2Se_3	-30019		-30497		48.911		82.441	6	28.38	5.00	-	3
Gudmundite	FeSbS	-109433	5	-109060	5	106.000	5	29.971	6	126	-	-	5
Berthierite	$FeSb_2S_4$	-61176				58.560		91.261	6	46.590	0.2630	-3.860	
Kermesite	Sb_2S_2O		8		8		8	66.282	6				

Notes 1. Zotov et al. (2003); 2. Xiong (2003); 3. Mills (1974); 4. Robie (1967); 5. Williams Jones and Normand (1997); 6. Calculated from cell parameters. See text; 7. Bonazzi et al. (1987); 8. Thermodynamic properties for kermesite require calculation based on data reported by Williams Jones and Normand (1997), which was in turn based on earlier work by Babcan (1976) and used in this study to calculate Log K(kermesite) directly.

C5. Iron

C5.1 Revision of Fe^{2+} and Fe^{3+}

Uncertainties relating to the thermodynamic properties of the ferrous and ferric ions in aqueous solution have bedeviled precise modeling of geochemical systems involving these species for some time, e.g. see Nordstrom (1984) and Reardon and Beckie (1987). Recent work on the solubility of siderite (Preis and Gamsjager, 2002) provides support for the validity of the properties of Fe^{2+} in the survey by Parker and Khodakovskii (1995). We therefore incorporated revised properties of Fe^{2+} and Fe^{3+} in SUPCRT92 and recalculated the solubility products of all participating minerals whose thermodynamic properties were derived from calorimetry. These included chlorite, daphnite, pyrite, goethite and hematite, as well as appropriate corrections to the solubility products of siderite and ankerite.

Calculations for generating the HKF EoS parameters for Fe^{2+} and Fe^{3+} were conducted with the aid of an Excel spreadsheet. In order to independently check the correctness of the transcribed equations, calculations were repeated for both species using the $\overline{C}^0_{P_r,T_r}$ and $\overline{S}^0_{P_r,T_r}$ cited by Shock et al. (1997). The derived values for the Born coefficient, ω_{P_r,T_r}, and c_1, which depends on the value of , did not match closely with those cited by Shock et al. (1997). Agreement was obtained only if r_{e,j,P_r,T_r} for each species was assumed to have a discrete value of 2.64 and 3.56 $\overset{o}{A}$, respectively. Furthermore, instead of using

$$\alpha_z = 71.5\left|Z_j\right|,$$

the original intercepts were used for the regressed data for $\Delta\overline{S}^o_{n,j} - Z_j\Delta\overline{S}^o_{s,H^+abs}$ (cal mol^{-1} K^{-1}) for aqueous species with Z_j = 1, 2 or 3 against $Z_j^2/r_{e,j}$ ($\overset{o}{A}$), where α_z = 72, 141 and 211 cal mol^{-1} K^{-1}, respectively. After appropriate substitution, close agreement was obtained, as shown in Table C13.

Table C13. Comparison of HKF EoS Parameters for Fe^{2+} and Fe^{3+}

Parameter	Shock et al. (1997)		This Work	
	Fe^{2+}	Fe^{3+}	Fe^{2+}	Fe^{3+}
c_1, cal mol^{-1} K^{-1}	14.7860	19.0459	14.7863	19.0462
c_2, cal K mol^{-1} x 10^{-4}	-4.6437	-6.8233	-4.6438	-6.8234
ω_{P_r,T_r}, cal mol^{-1} x 10^{-5}	1.4382	2.5812	1.4382	2.5812

In the present study, the calculated values for r_{e,j,P_r,T_r} given in Shock and Helgeson (1988) were used in the calculation of ω_{P_r,T_r} and c1. The a1 through a4 HKF equation of state parameters for Fe2+ and Fe3+ (Shock et al., 1997) were retained. The thermodynamic properties for both species are summarized in Table C14.

Table C14. Thermodynamic Parameters for Fe^{2+} and Fe^{3+}

Parameter	Fe^{2+}	Fe^{3+}
$\Delta\overline{G}^0_{f,P_r,T_r}$, cal mol^{-1}	-21637	-3891
$\Delta\overline{H}^0_{f,P_r,T_r}$, cal mol^{-1}	-21511	-11711
$S^0_{P_r,T_r}$, cal mol^{-1} K^{-1}	-24.283	-66.539
$\overline{C}^0_{P_r,T_r}$, cal mol^{-1} K^{-1}	-7.37	-18.85
$\overline{V}^o$, cm^3 mol^{-1}	-22.2	-37.0
a_1, cal mol^{-1}xbar^{-1}	-0.7867	-2.4256
a_2, cal mol^{-1}	-9.6869	-13.6961
a_3, cal K mol^{-1}xbar^{-1}	9.5479	11.1141
a_4, cal K mol^{-1}	-2.3780	-2.2127
c_1, cal mol^{-1} K^{-1}	15.2738	20.0173
c_2, cal K mol^{-1} x 10^{-4}	-4.5359	-6.8743
ω_{P_r,T_r}, cal mol^{-1} x 10^{-5}	1.4574	2.6358

C5.2 Iron Minerals

Iron minerals are a particularly important factor in modeling the behavior of hazardous constituents in shallow groundwaters. Not only do they participate in buffering the redox potential of the system, but also by virtue of their adsorptive properties and their commonly very large specific surface areas (i.e., very fine crystallinity), they can be a significant reservoir of adsorbed hazardous constituents. Iron minerals of interest to the problem at hand consist of three broad classes: (1) Ferric/ferrous oxides and oxy-hydroxides, (2) silicates containing ferrous iron, particularly phyllites, and (3) sulfides. The recent literature was reviewed, and crystallographic

and thermodynamic data compiled, for a number of pertinent minerals, and the resulting information is summarized in Tables C15 and C16.

Because the point of zero charge (PZC) of ferric oxides/hydroxides lies in the pH range of circa 8.5, these minerals are generally positively charged over the pH range of the majority of shallow potable groundwaters, and would remain so upon intrusion of high-pressure CO_2. The net positive charge attracts and adsorbs anionic species from solution. They are therefore likely to adsorb oxy-anionic species of As(III), As(V), Sb(III), Sb(V) and Se(II), Se(IV) and Se(VI). Other potential adsorbents include negatively charged sulfide and selenide complexes of heavy metals (Appendix D and Appendix E), although it is quite likely that sulfide and selenide species could be destabilized through oxidation of S(-II) and Se(-II) to higher oxidation states, depending on the overall equilibrium state.

Two of the minerals listed are of particular interest: ferrihydrite and green rust. Ferrihydrite, a nanocrystalline or amorphous hydroxide, traditionally given the formula, $Fe(OH)_3$, is commonly used in laboratory studies to quantify adsorption of charged or molecular species from solution, e.g., see the classic text on surface complexation modeling by Dzomback and Morel (1990). Until very recently, the structure of ferrihydrite was unknown. Indeed, it was commonly believed that ferrihydrite might consist of two separate phases (on the basis of X-ray diffraction studies) and thus referred to as “2-line” and “6-line” ferrihydrite. All this changed in 2007, when Michel and his co-workers (Michel et al., 2007a, 2007b; Penn, 2007), using advanced X-ray diffraction techniques and sophisticated methods of interpretation, were able to resolve the structure unambiguously as being isostructural with akdalaite, $Al_{10}O_{14}(OH)_2$, more commonly known as tohdite (Shpanov et al., 1970; Tilley and Eggleton, 1994). With ferrihydrite now known to possess the stoichiometry, $Al_{10}O_{14}(OH)_2$, calorimetric data for a series of ferrihydrites with differing specific surface areas and quantities of adsorbed water, (Majzlan et al., 2004) could be re-evaluated, and the enthalpy of formation, $\Delta H^0_{f,P_r,T_r}$, for coarsely crystalline ferrihydrite calculated. Figure C3 shows a plot of measured $\Delta H^0_{f,P_r,T_r}$, vs. excess water, extrapolated to zero excess water, the value at the intersection of the regression trendline with the y-axis being $\Delta H^0_{f,P_r,T_r}$ reported in Table C16.

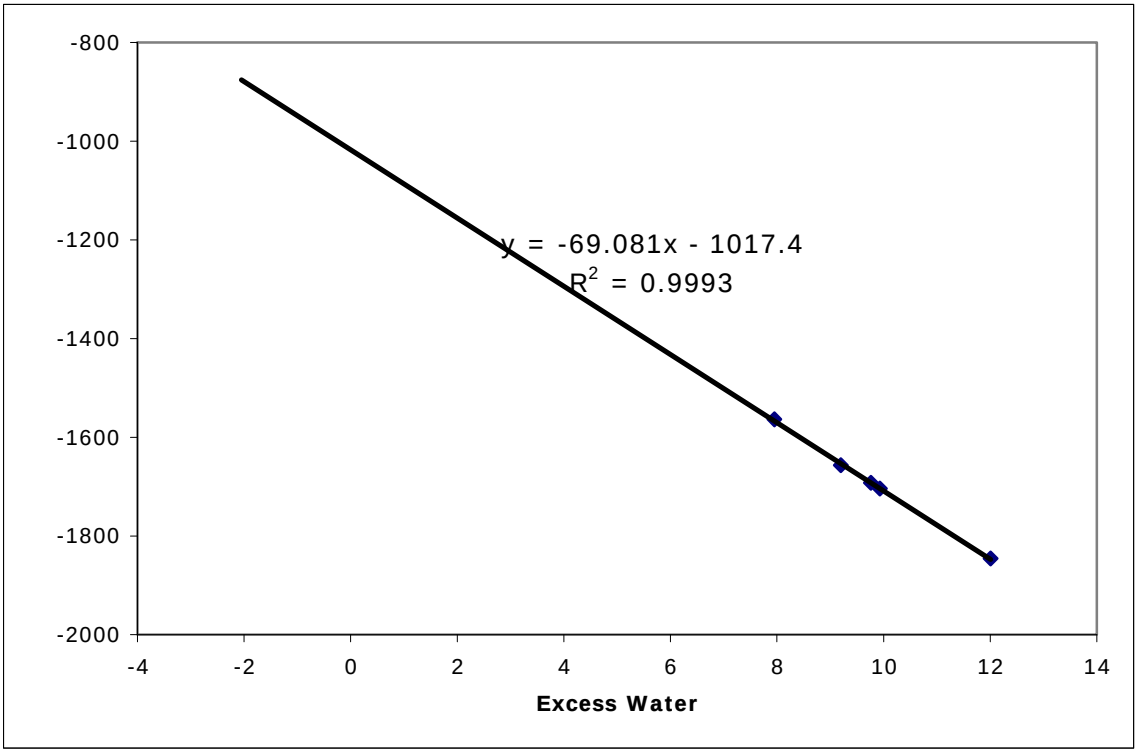

Fig. C3. Correlation of calorimetrically determined enthalpy of formation of ferrihydrite samples in relation to their content of excess water. Data from Majzlan et al. (2004)

Green rust is a mineral consisting of stacked layers separated by coordinated water molecules of Fe(II) tri-octahedral sheets, one of the basic building blocks of phyllosilicates or clay minerals. The octahedral sheet can be either of the gibbsite type, $Al_2(OH)_6$, or of the brucite type $Mg_3(OH)_6$, representing di- and tri-octahedral sheets, respectively. Partial *in situ* oxidation of the Fe(II) to Fe(III) in a tri-octahedral sheet causes the octahedral sheet to develop a net positive charge, which is satisfied through the uptake of anionic species in the inter-layer sites. The charge-balancing anion is commonly SO4-2, but any of the oxy-anionic species of As(III), As(V), Sb(III), Sb(V), Se(II), Se(IV) and Se(VI), as well as HCO3- or CO3-2 can also occupy sites. Because of their structural similarity to clays, such phases are sometimes referred to as "anionic" clays in distinction to regular "cationic" clays. In Tables C15 and C16, the properties of a typical idealized anionic clay, green rust, is given, where the stoichiometry of the waters of hydration were adjusted to fully saturate the interlayer positions.

Table C15. Crystallographic Properties of Iron Minerals, excluding those containing Arsenic

Name	Formula	Cell Constants							Space Group	Reference
		a_o (Å)	b_o (Å)	c_o (Å)	α	β	γ	Z		
Goethite	FeO(OH)	4.5979	9.9510	3.0178	90	90	90	4	Pbnm	Yang et al. (2006)
Lepidocrocite	FeO(OH)	12.4	3.87	3.06	90	90	90	4	Bbmm	Wyckoff (1963)
Hematite2	Fe_2O_3	5.038		13.772				6	R-3c	Blake et al. (1966)
Maghemite	Fe_2O_3	8.33			90	90	90	12	Fd3m	Pecharroman et al. (1995)
E-Fe_2O_3	Fe_2O_3	5.095	8.789	9.437	90	90	90	8	$Pna2_1$	Tronc et al. (1998)
Marcasite	FeS_2	4.4446	5.4246	3.3864	90	90	90	2	Pnnm	Rieder et al. (2007)
Pyrite	FeS_2	5.4166			90	90	90	4	Pa3	Bayliss (1977)
Ferrihydrite	$Fe_{10}O_{14}(OH)_2$	~5.95		~9.06	90	90	90	1	$P6_3mc$	Michel et al. (2007)
Mackinawite	FeS	3.6735		5.0328	90	90	90	2	P4/nmm	Lennie et al. (1995)
Greigite	Fe_3S_4	9.876			90	90	90	8	Fd3m	Skinner et al. (1964)
Schwertmannite	$Fe(III)_{16}O_{16}(OH)_{12}(SO_4)_2$	10.66(4)		6.04(1)	90	90	90	1	P4/m (?)	Bigham et al. (1994)
Green Rust	$Fe(II)_4Fe(III)_2(OH)(SO_4).8H_2O$	5.524		11.011				0.5	$P\bar{3}m1$	Simon et al. (2003)

Table C16. Thermodynamic Properties of Iron Phases (Excluding those containing Arsenic and Carbon)

Mineral name	Formula	$\Delta G^0_{f,P_r,T_r}$ cal mol^{-1}	Ref	$\Delta H^0_{f,P_r,T_r}$ cal mol^{-1}	Ref	$S^0_{P_r,T_r}$ cal mol^{-1} K^{-1}	Ref	$V^0_{P_r,T_r}$ cm^3 mol^{-1}	Ref	$C^0_{P_r}$ cal mol^{-1} K^{-1}			Ref
										a	$b\times10^3$	$c\times10^{-5}$	
Goethite	FeO(OH)	-117065	5			14.269	4	19.866	9	0.289	55.736	0.750	4
Lepidocrocite	FeO(OH)	-114747	5			15.559	4	22.108	10	14.283	14.465	-1.847	4
Hematite	Fe_2O_3	178155	20	-197720		20.940	20	30.384	11	23.490	18.600	-3.550	20
Maghemite	Fe_2O_3	-173972	5			22.228	4	29.007	12	25.526	15.557	-4.508	4
E-Fe_2O_3	Fe_2O_3	-171558	6	-190727	6	22.228	6	31.811	13	25.526	15.557	-4.508	21
Marcasite	FeS_2	-37859	23	-40511	23	12.882	23	24.584	26	17.880	1.320	-3.050	25
Pyrite	FeS_2	-38293	20	-41000	20	12.650	20	23.926	14	17.880	1.320	-3.050	20
Ferrihydrite	$Fe_{10}O_{14}(OH)_2$	-799730	6,7	-1017400		101.800	3	167.280	15	124.560	93.000	-17.800	2
Mackinawite	FeS	-22300	22	-21900	24	15.4	24	20.450	16	12.000	-	-	24
FeS,am	FeS	-21300	22	-20900	24	15.4	24			12.000	-	-	24
Greigite	Fe_3S_4	-69400	22	-70300	24	47.1	24	72.511	17	42.000	-	-	24
Schwertmannite	$Fe(III)_{16}O_{16}(OH)_{12}(SO_4)_2.12H_2O$	-2661124	6,8	-		254.950	3	413.335	18	395.855	136.399	-26.000	2
Green Rust	$Fe(II)_4Fe(III)_2(OH)(SO_4).8H_2O$	-1330280	1	-		192.870	3	350.466	19	220.065	20.6806	-5.370	2

Notes 1. Hansen et al. (1994), modified to account for $8H_2O$ of water; 2. Calculated using the summation of oxide components; 3. Calculated using the procedure described by Holland (1989). This work. 4. Majzlan et al. (2003a); 5. Majzlan et al. (2003b); 6. Majzlan et al. (2004); 7. Data reinterpreted. See text; 8. Modified to account for $12H_2O$ of water; 9. Yang et al. (2006); 10. Wyckoff (1963); 11. Blake et al. (1966); 12. Pecharroman et al. (1995); 13. Tronc et al. (1998); 14. Bayliss (1977); 15. Michel et al. (2007); 16. Lennie et al. (1995); 17. Skinner et al. (1964); 18. Bigham et al. (1994); 19. Simon et al. (2003); 20. As reported by Helgeson et al. (1978); 21. Assumed the same as for maghemite, in conformity with assumption for $S^0_{P_r,T_r}$ by Majzlan et al. (2004); 22. Berner (1967); 23. Robie and Hemingway (1995); 24. Estimates provided by Anderko and Shuler (1998); 25. Assumed to be equivalent to pyrite; 26. Rieder et al. (2007)

C6. Carbonates

An essential requirement for reactive transport simulations involving CO_2 sequestration is the need for accurate thermodynamic data of participating carbonate phases. Recent studies have revealed respectively the possible existence of substantial errors in the Gibbs free energy of formation of magnesite and dolomite (Rock et al., 2001). Furthermore, the experimental consistency of siderite solubility data (Preis and Gamsjager, 2002) has been recently established, and by inference, validated the thermodynamic data for ferrous and ferric ions recommended by Parker and Khodakovskii (1995). These modifications also require a redetermination of the thermodynamic properties of the ankerite solid solution utilized in earlier work (Xu et al., 2003).

The thermodynamic properties of dolomite and magnesite were calculated, using the Gibbs free energy values determined by Rock et al. (2001), together with the respective entropies provided by Robie and Hemingway (1995). These, together with entropy data for end-member ankerite, $CaFe(CO3)_2$, from Holland and Powell (1998), and the properties of siderite from Preis and Gamsjager (2002) as well as calcite from the SUPCRT92 database, were used to calculate the properties of end-member ankerite and the ankerite ideal binary solid solution with the limiting composition: $CaMg_{0.3}Fe_{0.7}CO_3)_2$, using the lattice energy calculations reported by Chai and Navrotsky (1996). The thermodynamic data for carbonates, either calculated as described above or utilized in the present study, are summarized in Table C17.

Table C17. Thermodynamic Properties of Selected Carbonate Minerals

Mineral name	Formula	$\Delta G^0_{f,P_r,T_r}$ cal mol^{-1}	Ref	$\Delta H^0_{f,P_r,T_r}$ cal mol^{-1}	Ref	$S^0_{P_r,T_r}$ cal mol^{-1} K^{-1}	Ref	$V^0_{P_r,T_r}$ cm^3 mol^{-1}	Ref	$C^0_{P_r}$ cal mol^{-1} K^{-1}			Ref
										a	$b\times10^3$	$c\times10^{-5}$	
Calcite	$CaCO_3$	-269880	1,2	-288552	1,2	22.150	1	36.934	1	24.980	5.240	-6.200	1
Magnesite	$MgCO_3$	-240791	4	-260816	6	15.557	3	28.018	1	19.731	12.539	-4.748	1
Siderite	$FeCO_3$	-162261	5	-179732	5	22.818	5	29.378	1	11.630	26.800	0.000	1
Dolomite	$CaMg(CO_3)_2$	-513341	4	-552250	6	37.089	3	64.365	1	41.557	23.952	-9.884	1
Ankerite	$Ca(Mg_{0.3}Fe_{0.7})(CO_3)_2$	-457553	6	-494243	6	43.627	6	65.594	6	46.070	18.011	-10.437	6

Notes 1. Helgeson et al. (1978); 2. Helgeson (1990), Gibbs free energies calculated from solubility data reported by Plummer and Busenberg (1982) [Enthalpies adjusted for the correction in the Gibbs free energy]; 3. Robie and Hemingway (1995); 4. Rock et al. (2001); 5. Preis and Gamsjager (2002); 6. This work. See text.

C7. Chlorite

In prior simulations (Xu et al., 2002), chlorite was represented as a 1:1 mixture of clinochlore and daphnite. The solubility products used were those derived originally from the thermodynamic evaluation of phase equilibria by Helgeson et al. (1987). More recent and comprehensive evaluations, e.g., those conducted by Holland and Powell (1998), indicate that a revision in the solubility products of clinochlore and daphnite is called for. Although clinochlore and daphnite are only minor components in most sedimentary arenaceous rocks, a revision is justified because they compete with secondary carbonates for magnesium and ferrous iron, and they can buffer the redox potential when coexisting with pyrite.

The calculated thermodynamic properties for clinochlore and daphnite were taken from Holland and Powell (1998). The thermodynamic properties of chlorite, $Mg_{2.5}Fe_{2.5}Al_2[Si_3O_{10}](OH)_8$, were calculated assuming ideal solid solution between the end members. These properties were entered into the SUPCRT92 database, and the chlorite solubility products were calculated. The thermodynamic data used in the current study are given in Table C18.

Table C18. Thermodynamic Parameters for Chlorite Minerals

Parameter	Units	Clinochlore $Mg_5Al_2[Si_3O_{10}](OH)_8$	Ref.	Daphnite $Fe_5Al_2[Si_3O_{10}](OH)_8$	Ref.	Chlorite $Mg_{2.5}Fe_{2.5}Al_2[Si_3O_{10}](OH)_8$	Ref.
$\Delta G^0_{f,P_r,T_r}$	cal mol^{-1}	-1975051	4	-1562107	4	-1768992	4
$\Delta H^0_{f,P_r,T_r}$	cal mol^{-1}	-2134288	1	-1709845	1	-1922066	4
$S^0_{P_r,T_r}$,	cal mol^{-1} K^{-1}	98.112	1	130.258	1	115.562	4
$V^0_{P_r,T_r}$,	cm^3 mol^{-1}	207.110	1	213.420	1	210.260	4
$C^0_{P_r}$ Coefficients							
a	cal mol^{-1} K^{-1}	166.500	2	176.210	2	171.355	3
$b\times10^3$		42.100	2	43.760	2	42.930	3
$c\times10^{-5}$		-37.470	2	-33.820	2	-35.645	3

Notes 1. Holland and Powell (1998); 2. Helgeson et al. (1978); 3. Interpolated between clinochlore and daphnite; 4. This work.

C8. Miscellaneous

The mineral hemimorphite proved to be an important thermodynamic control on the concentration of dissolved zinc in oxidized groundwaters, and might also control in part the

concentration in reducing groundwaters containing sphalerite. Thermodynamic data are extremely limited, essentially confined to preliminary study by McPhail et al. (2006), who measured the solubility at 50 and 80ºC and computed the solubility product at the same temperatures. In Figure C4, a linear extrapolation of Log K(hemimorphite) is made as a function of reciprocal temperature to 25ºC. The resulting value, Log K = 23.981, incorporated in the EQ3/6 and TOUGHREACT thermodynamic databases.

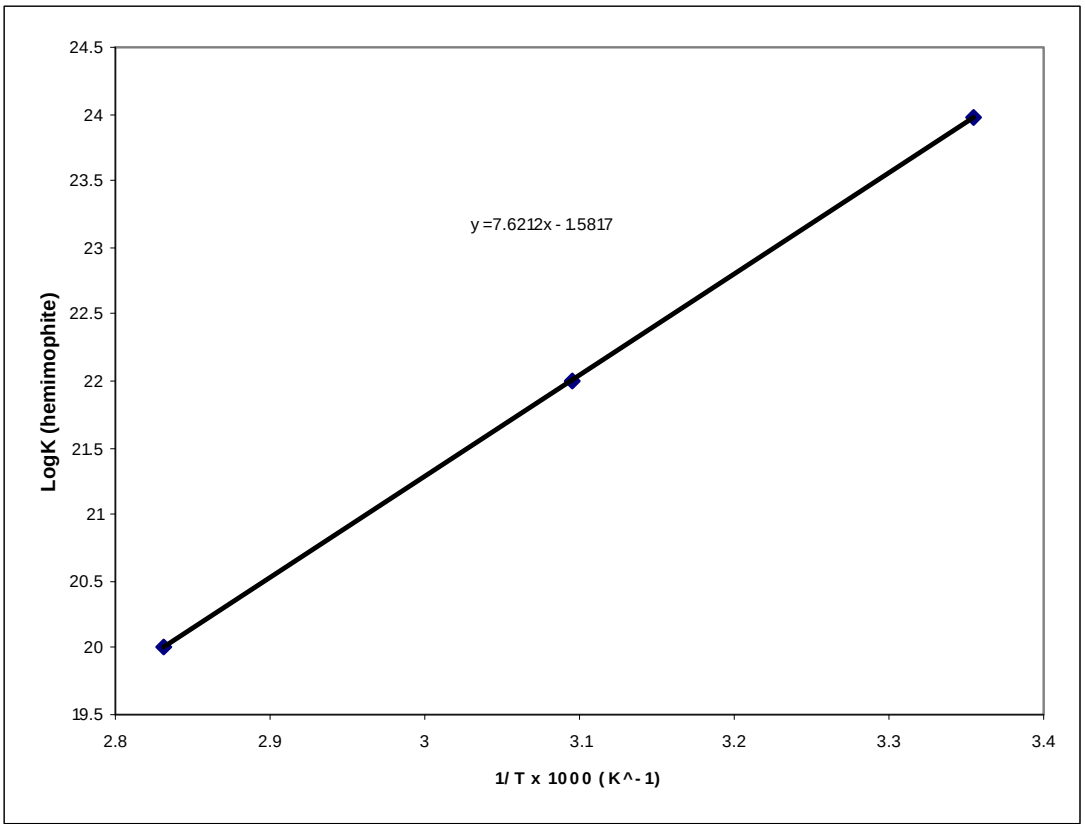

Fig. C4. A linear extrapolation of the solubility product of hemimorphite to 25ºC with reciprocal temperature, 1/K. Data from McPhail et al. (2006).

Appendix D:
Solubilities of Sulfides of Cadmium, Mercury, Lead and Zinc at 25°C

D1. Background

The present study requires the calculation of the solubilities of minerals containing hazardous inorganic constituents as essential components under conditions that might occur in shallow potable water aquifers. The majority of the more than 38,000 groundwaters downloaded from the NWIS database and evaluated during the course of the present investigation appear to be reducing, and it is probable that pyrite or some other iron sulfide is present. Under such conditions, log P_{H2S} (bar) ranges from approximately –8 to –10, and among the minerals potentially controlling the solubility of Zn, Cd, Hg and Pb in solution are the corresponding sulfides sphalerite, greenockite, cinnabar and galena. The divalent cations of these four elements can also complex with sulfide species (HS^- and H_2S) and selenide species (HSe^- and H_2Se) in solution, potentially enhancing both sulfide and selenide mineral solubilities.

Among the sulfide and presumably selenide complexes in solution at equilibrium with the respective sulfides and selenide minerals are a series of neutral species of undefined stoichiometry, but circumstantial evidence suggests that they may be oligomers possessing formulas Me_xS_x, where x = 1,2,3,4… Experimental evidence also suggests that these species are predominant under equilibrium conditions with the metal sulfide mineral, and thus must be taken into account if thermochemical data pertaining to sulfide mineral equilibria with respect to the aqueous phase are to be reconciled and mineral sulfide equilibria are to be modeled realistically. For this reason, both the identities of sulfide complexes of the cations of and their respective dissociation constants needed to be incorporated in the thermodynamic databases of both EQ3/6 and TOUGHREACT codes. Without such data, simulations of reactive chemical transport of these metals in the presence of elevated P_{CO2} would not be representative.

In this appendix, we review the issues concerning identification of the relevant sulfide complexes, and how their dissociation constants, K_{diss}, relate to the solubility products, K_s, of the

corresponding sulfide minerals, using galena (PbS) as an example. In the companion Appendix E, we review issues relating to the corresponding selenide complexes. Then, on the basis of a literature review, we choose and describe internally consistent data sets of sulfide and selenide species dissociation constants and associated solubility products for incorporation in the EQ3/6 and TOUGHREACT databases.

The procedure followed was first to generate a correlation plot for Log $K(MeS)_s$ and Log $K(MeS)_{aq}$ for sulfide species (Me = metal). A correlation plot was also generated comparing solid phase sulfide and selenide species, together with Hg sulfide and selenide species (Appendix E). The latter plot then allowed prediction of unknown neutral and charged selenide complexes of the relevant heavy metals based upon the identities and literature values of aqueous sulfide complexes of Cd, Hg Pb and Zn, and neutral sulfide complexes estimated from the first correlation plot. The resulting data were then incorporated in the EQ3/6 database and EQ3 run using a representative groundwater composition, based on the distribution of heavy metal concentrations observed in NWIS groundwaters, taking into account possible analytical artifacts. Alternative hypotheses were tested until a satisfactory reconciliation of all parameters was achieved, and the calculated saturation indices for those heavy metal sulfides and selenides expected to be present, based on observed modes of occurrence, fell close to 0, i.e., within ± 2 units. The interdependence of all parameters tightly restricted the ranges over which each parameter could be varied independently. Therefore, although the results presented in this appendix and the following Appendix E leave room for refinement, it is expected that such refinements would not alter substantially the findings presented in this report.

D2. Issues

In both the EQ3/6 and TOUGHREACT codes, mineral solubility is defined in terms of a dissolution equation relating the mineral to the "basis" species in solution, e.g., for galena, the reaction is:

$$PbS + H^+ = Pb^{+2} + HS^- \qquad \text{(D1)}$$

where Pb^{+2} and HS^- are the basis species in this case, and the solubility product is defined as

$$K_s = \frac{[Pb^{+2}][HS^-]}{[PbS][H^+]} \tag{D2}$$

with [ ] denoting thermodynamic activities. The activity of the solid phase is unity for a pure substance. In addition, knowledge of the potential complexes of the basis species in solution is required. In the example given, these complexes modify the total aqueous concentrations of both Pb^{+2} and HS^-. Elsewhere in this report (Section 3.5), we show that apart from sulfide and selenide complexes, other significant aqueous species affecting the saturation concentration of Pb in shallow potable aquifers include $PbCO_3$(aq), $PbOH^+$, $Pb(CO_3)_2^{-2}$ and $PbCl^+$ in addition to Pb^{+2}. The corresponding dissociation constants for these complexes are also defined in terms of the basis species. At higher sulfide concentrations, not normally encountered in potable water aquifers, significant quantities of sulfide complexes with Pb^{+2} might also form, e.g., $Pb(HS)_2$(aq) and $Pb(HS)_3^-$, as shown by Hemley (1953) and Giordano and Barnes (1979). It is under such conditions that experiments are sometimes conducted, either to measure mineral sulfide solubilities, or to characterize the dissociation constants of relevant sulfide complexes in solution, where the saturated mineral is used as a thermodynamic control.

The solubility product, defined by Eqn. (D2) can also be calculated from independent knowledge of the Gibbs free energies, $\Delta G^0_{f,P_r,T_r}$, of the participating species, just as the measured solubility can be used to calculate $\Delta G^0_{f,P_r,T_r}$ of the solid phase. $\Delta G^0_{f,P_r,T_r}$ of the solid phase or mineral can be obtained from calorimetric, thermo- or electro-chemical, or phase equilibrium studies. For example, $\Delta G^0_{f,P_r,T_r}$(galena) has been determined from electrochemical (galvanic cell) measurements (Kiukkola and Wagner, 1957), thermochemical measurements (Stubbles and Birchenall, 1959), and by high-temperature oxide-melt solution calorimetry (Deore and Navrotsky, 2006). In Table D1, the solubility products of four sulfide phases are cross-compared with the corresponding values of $\Delta G^0_{f,P_r,T_r}$ derived from various property measurements.

Table D1. Gibbs Free Energy of Formation and Solubility Products of Selected Trace Metal Sulfides

Source	Notes	ZnS (sphalerite)		CdS (greenockite)		HgS (cinnabar)		PbS (galena)	
		$\Delta G^0_{f,P_r,T_r}$ kcal mol^{-1}	$\log K_s$ at 25°C	$\Delta G^0_{f,P_r,T_r}$ kcal mol^{-1}	$\log K_s$ at 25°C	$\Delta G^0_{f,P_r,T_r}$ kcal mol^{-1}	$\log K_s$ at 25°C	$\Delta G^0_{f,P_r,T_r}$ kcal mol^{-1}	$\log K_s$ at 25°C
Robie and Hemingway (1995)		**-47.71±0.36**	-11.27±0.26	**-34.92±0.31**	-14.09±0.23	**-9.73±0.65**	-38.08±0.48	**-23.14±0.48**	-14.87±0.35
Deore and Navrotsky (2006)		**-48.29±0.96**	-11.69±0.70	**-34.73±0.99**	-13.95±0.73			**-23.09±1.04**	-14.84±0.76
Dyrssen and Kremling (1990)		-47.25±0.93 -44.55±0.44	**-10.93±0.68** **-8.95±0.32** (wurtzite)	-33.97±0.93	**-13.39±0.68**	-10.85±0.55 -11.67±0.55	**-38.9±0.4** (black) **-39.5±0.4** (red)	-21.91±0.78	**-13.97±0.57**
Daskalakis and Helz (1993)		-48.005	**-11.482**						
Shea and Helz (1989)								-20.29	**-12.78**
Daskalakis and Helz (1992)				-33.93±0.35	**-13.36±0.26**				
Paquette and Helz (1995)						-7.85	**-36.7**		

Notes:

1. Bold face values are given or derived directly from the source reference.
2. $\log K_s$ is in reference to the dissolution reaction: MS(s) + H^+ = M^{+2} + HS^-. Where M is Zn, Cd, Hg or Pb.
3. $\Delta G^0_{f,P_r,T_r}$ values referenced to Deore and Navrotsky (2006) were calculated from $\Delta H^0_{f,P_r,T_r}$ assuming that $T\Delta S^0_{f,P_r}$ corresponds to that assumed by Robie and Hemingway (1995)
4. Uncertainties in derived values are calculated assuming no uncertainty in values of the aqueous species, and are therefore minimum values.
5. $\Delta G^0_{f,P_r,T_r}$ values given by Robie and Hemingway (1995) are from Schaefer and Gokcen (1982) for sphalerite; Adami and King (1964) for greenockite; Pankratz and King (1987) for cinnabar; Stubbles and Birchenall (1959) and Kiukkola and Wagner (1957) for galena.

Most $\Delta G^0_{f,P_r,T_r}$ values calculated from solubility measurements in Table D1 are less negative than those determined using other methods. However, the thermochemical determinations summarized by Robie and Hemingway (1995) agree with the calorimetric determinations by Deore and Navrotsky (2006) within experimental error. Thus, it appears that solubility measurements may not adequately describe the speciation or thermodynamic behavior of the system. Tossell (1999), in his paper advocating *ab initio* quantum mechanical methods to calculate the stabilities of Hg complexes in solution, summarized the serious limitations of corresponding experimental methods:

(1) "The speciation models are often ambiguous, with different researchers obtaining apparently different sets of species and formation constants."
(2) "… chemical components[,] whose activities or concentrations cannot be varied experimentally[,] are indeterminable, e.g., the participation of water in such species cannot be determined in aqueous solution. Spectral studies could, in principle, determine which species were present, as well as their concentrations if relative spectral intensities for the different species could be assessed. However, in many cases the species concentrations are so low that no usable spectra can be obtained."

Tossell, in particular, singled out Hg sulfide speciation as a case in point, but such problems also extend to the other metal sulfide species considered in this appendix. In a more recent review, Rickard and Luther (2006) reiterate the limitations of current experimental methods, noting that "One of the astonishing things the uninitiated reader will discover… is the large number of sulfide complexes that have been proposed and even modeled with little or no evidence to support their existence in the first place." Given the current uncertainties in the literature, it is prudent to regard the following analysis with caution, even though the results presented are sufficiently robust to allow their use in the evaluation of thermodynamic controls on heavy metal solubilities in potable groundwaters.

Explanations for the mismatch between the calculated and measured aqueous solubilities of chalcogenides in general has been accommodated by postulating equilibrium with a neutral species in solution, possessing the same stoichiometry as that of the solid phase, thus:

$$\text{MeS(s)} = \text{MeS(aq)} \qquad \text{(D3)}$$

where [MeS(aq)]/[MeS(s)] = K_{int}, the intrinsic solubility product (Dyrssen, 1985, 1988; Dyrssen and Wedborg, 1989, 1991; Benoit et al., 1999; Rickard, 2006). The precise nature of the complex is unknown. Dyrssen and Wedborg (1991) argue convincingly that it could not be a monomer. They point out that HgS(aq) is equivalent to the hydrated species, Hg(OH)(SH)(aq), and one cannot be distinguished from the other using conventional speciation studies (Tossell, 1999; *vide supra*), i.e.,

$$HgS(aq) + H_2O = Hg(OH)(SH)(aq);\ \text{Log K is undetermined.} \qquad (D4)$$

Although the two stoichiometries cannot be distinguished in solubility studies, it is reasonable to assume that the complex is composed of $(OH)^-$ and SH^- rather than S^{-2} and H_2O. Dyrssen and Wedborg (1991) showed, using correspondence plots for Hg stability constants, and theory relating to calculation of mixed ligand complexes (Anfalt et al., 1968), that the calculated dissociation constant for the latter species is

$$Hg(OH)(SH)(aq) + H^+ = HgSH^+ + H_2O;\ \text{Log K} = +3.4. \qquad (D5)$$

This dissociation constant is comparable with those of other hydrolytic reactions, e.g.,

$$Hg(OH)2(aq) + H^+ = HgOH^+ + H_2O;\ \text{Log K} = +2.6 \qquad (D6)$$

$$HgCl(OH)(aq) + H^+ = HgCl^+ + H_2O;\ \text{Log K} = +3.1 \qquad (D7)$$

However, the measured dissociation constant for

$$HgS(aq) + H^+ = HgSH^+;\ \text{Log K} \approx -8.9 \qquad (D8)$$

differs by approximately 12 log units. Similar incompatibilities were also recognized in computing the intrinsic solubility products for ZnS and CdS, based respectively on the work by Gubeli and Ste-Marie (1967) and by Ste-Marie et al. (1964).

More recently, Rickard (2006), in studying the solubility of mackinawite (FeS), also identified and determined experimentally the intrinsic solubility product for this mineral

$$FeS(\text{mackinawite}) = FeS(aq) \qquad (D9)$$

He concluded that the FeS(aq) complex was an oligomer, citing earlier electrochemical studies by Buffle et al. (1988) and Theberge and Luther (1997) of FeS(aq) in equilibrium with amorphous FeS. The exact stoichiometry of FeS(aq) is uncertain. Theberge and Luther (1997) concluded that polymerization occurred as a two-step process, in which the octahedrally coordinated hex-aquo Fe^{+2} ion reacted with HS^-, thus,

$$Fe(H_2O)_6^{+2} + HS^- = Fe(H_2O)_5(HS)^+ + H_2O \qquad \text{(D10)}$$

followed by polymerization to form a trimer

$$3Fe(H_2O)_5(HS)^+ + 3HS^- = Fe_3S_3(H_2O)_6(aq) + 3H_2S + 9H_2O \qquad \text{(D11)}$$

Implicit in this reaction is a transformation from octahedral to tetrahedral coordination in the ferrous ion, and formation of a closed six-member ring representing a basic building block in both cubic FeS and in mackinawite (where Fe(II) is tetrahedrally coordinated in both). However, it should be noted that the probability of the simultaneous reaction of six aqueous entities is extremely unlikely. Therefore Eqn. D11 must be considered merely a summary reaction that incorporates a series of intermediate steps, including the formation of a precursor dimer, and that it is probable that equilibria between the postulated trimer and its precursors is established at saturation with respect to the solid phase.

A further comparison can be made with sulfide complexes of As and Sb, which form ionizing oligomeric complexes $H_3As_3S_6(aq)$ and $H_2Sb_2S_4(aq)$, respectively. These complexes apparently form to the exclusion of simpler monomeric species. Although both As and Sb are present in these complexes in the (III) state, a parallelism with the formation of postulated analogous oligomers with divalent (II) metals is suggested by the limited experimental evidence regarding the formation of $Fe_3S_3(H_2O)_6(aq)$.

Similar arguments could be advanced in defining polymer formation with respect to Zn and Cd sulfide complexes, where both Zn and Cd are tetrahedrally coordinated in both isostructural polymorphs, i.e., cubic sphalerite and hawleyite, and hexagonal wurtzite and greenockite, respectively. Hg(II) is tetrahedrally coordinated in cubic met cinnabar, but in cinnabar it is octahedrally coordinated. A similar coordination change is also noted in the sulfides of manganese (MnS). For example, in alabandite, Mn is octahedrally coordinated, whereas in

ramsbergite, it is tetrahedrally coordinated in an anti-wurtzite structure. Thus, it is unclear whether Hg(II) aqueous sulfide complexes are octahedrally or tetrahedrally coordinated. Because metacinnabar is less stable than cinnabar, it is more likely that Hg(II) is octahedrally coordinated in sulfide complexes. With octahedral coordination, as also occurs with respect to Pb in galena, it would be logical to infer that the aqueous complexes are dimers, $Me_2S_2(H_2O)_x(aq)$, or tetramers, $Me_4S_4(H_2O)_y(aq)$ (where Me is either Hg or Pb), forming single or double four-member rings respectively. However, Rozen et al. (2003), on the basis of mass spectrometry of freeze dried aqueous samples, indicated that the species had the formula Pb_3S_3.

D3. Estimation of the Dissociation Constants of Neutral Sulfide Complexes

If a comparison is made between the sulfide solubility products and the dissociation constants of the neutral oligomeric sulfide complexes for the four metals for which data are available (Fe(II), Zn(II), Cd(II) and Hg(II)), conventionally written as

$$MeS(s) + H^+ = Me^{+2} + HS^- \qquad \text{(D12)}$$

and

$$1/x[Me_xS_x(aq) + xH^+ = xMe^{+2} + xHS^-]$$

i.e.,

$$MeS(aq) + H^+ = Me^{+2} + HS^- \qquad \text{(D13)}$$

where x is probably 2, 3 or 4 (depending on the nature of the metal ligand), a surprisingly good correlation between the two is obtained, as shown by regression trendline (a) in Figure D1.

Table D2. A Comparison between the Solubility Product of a Sulfide Mineral, and the Apparent Dissociation Constant of the Corresponding Neutral Species in Solution at 25°C

Mineral	**Composition**	**Log K $(MeS)_s$**	**Source**	**Log K $(MeS)_{aq}$**	**Source**
Mackinawite	FeS	-3.50	1	+2.20	1
Sphalerite	ZnS	-11.27	2	-5.63	3
Greenockite	CdS	-14.09	2	-7.24	3
Cinnabar	HgS	-38.08	2	-28.08	4
Galena	PbS	-14.87	2	-8.06	5

Notes:

1. Rickard (2006)
2. Derived from thermochemical data provided by Robie and Hemingway (1995)
3. Dyrssen and Wedborg (1991) from data reported by Gubeli and Ste-Marie (1967) and Ste-Marie et al. (1964)
4. Dyrssen and Wedborg (1989)
5. This work.

However, despite the impressive correlation between Log $K(MeS)_s$ and Log $K(MeS)_{aq}$, incorporation of the dissociation constants of neutral sulfide and corresponding selenide complexes in the database did not satisfactorily resolve the unrealistic predictions of sulfide and selenide mineral saturation indices in NWIS potable waters.

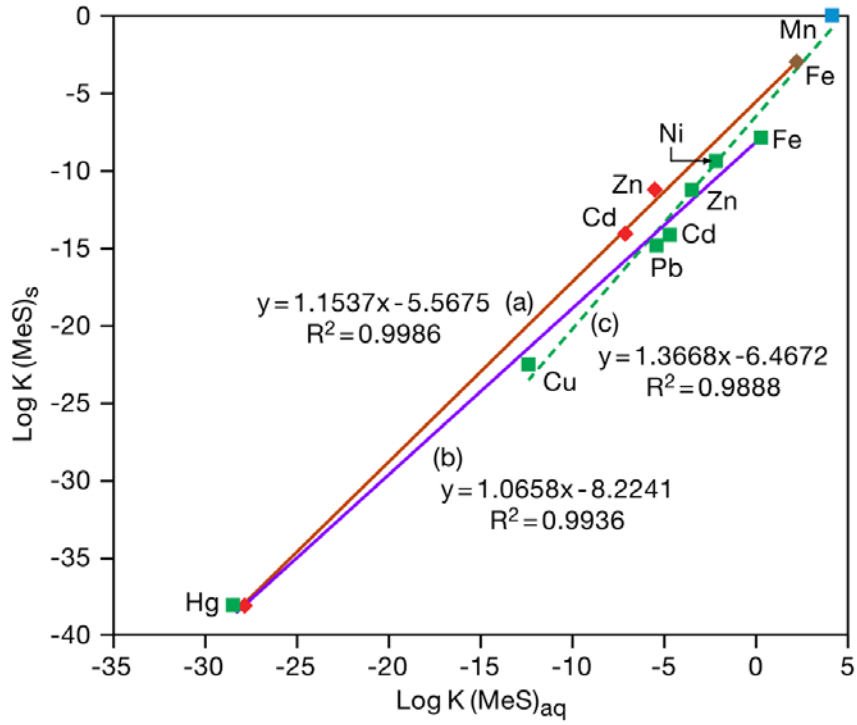

Fig. D1. Correlation between the solubility product of a sulfide mineral, and the apparent dissociation constant of the corresponding neutral species in solution at 25°C.

An alternative approach at estimating the correlation between the solid and aqueous sulfides and selenide species was then examined. Dyrssen (1988), citing earlier work (Dyrssen, 1985), attempted to correlate the stability constants for sulfide complexes of a range of heavy and transition metals with the corresponding aqueous extraction constants, K_{ex}, for dithizone dissolved in carbon tetrachloride:

$$Me^{n+} + n\ H_2Dz(org) = Me(Hdz)_n(org) + n\ H^+ \qquad \text{(D14)}$$

He used studies by Ste-Marie et al. (1964) and Gubeli and Ste-Marie (1967) on Cd and Zn sulfide complexes, respectively, to calibrate the correlation equation:

$$\log K(MeS)_{aq} = -0.95 \log K_{ex} - A \qquad \text{(D15)}$$

where $\log K(MeS)_{aq}$ represents Eq. (D13), and $A = 3.02$. Table D3 summarizes the respective parameters cited in Dyrssen (1988, 1989) together with other data used in the current analysis. When the data given in Table D3 are plotted, both Pb and Zn deviated significantly from the

observed trend, although the data for Cd and Hg yielded satisfactory results for both sulfides and selenides (greenockite and cadmoselite, and cinnabar and tiemannite, respectively). Arbitrary revisions of the values of $\log K(MeS)_{aq}$ to –5.5 and –3.5 for Pb and Zn, respectively, not only achieved better coherence with $\log K(MeS)_{aq}$ values for other metals, but also yielded satisfactory saturation indices for galena, clausthalite, and sphalerite for the representative NWIS potable waters. The resulting regression trendline (b) is shown in Figure D1. For the purposes of this study, the $\log K(MeS)_{aq}$ values for Cd, Pb and Zn summarized in Table D3 with the noted corrections for Pb and Zn are provisionally accepted for use in the databases for EQ3/6 and TOUGHREACT, and applied for the prediction of neutral selenide complexes of Cd, Pb and Zn. With respect to Hg, the value for $\log K(MeS)_{aq}$ is chosen that was used in the construction of regression trendline (a) in Figure D1. This value is based on the intrinsic solubility product for HgS estimated by Dyrssen and Wedborg (1991), $\log K_{\text{int}} - 10$. This value gave somewhat better agreement with postulated saturation with respect to cinnabar in NWIS potable waters.

Table D3. Estimated Values of Neutral Sulfide Stability Constants, $K(MeS)_{aq}$, based on the Corresponding Dithizone Extraction Constants, K_{ex}, compared with Sulfide Solubility Products, $K(MeS)_S$

Metal	$\log K_{ex}$ [1]	$\log K(MeS)_{aq}$ [4]	$K(MeS)_S$
Mn(II)	-5.4	+2.1	-0.02
Fe(II)	-3.4	+0.2	-7.90[3]
Ni(II)	-0.8	-2.3	-9.50[3]
Cu(II)	10.0	-12.5	-22.50[3]
Zn(II)	2.0	-4.9[2]	-11.27
Cd(II)	1.9	-4.8	-14.09
Hg(II)	26.8	-28.5	-38.08
Pb(II)	0.4	-3.4[2]	-14.87

Notes:

1. As cited by Dyrssen (1988) from Irving (1977)
2. Adjusted to -3.5, -5.5 respectively for Zn and Pb. See text.
3. Values cited by Dyrssen (1989). All other values for Log K(MeS), as given in Table D1.
4. As cited by Dyrssen (1989)

Despite the satisfactory agreement achieved through the correlation of $\log K(MeS)_{aq}$ with $\log K_{ex}$ proposed and used by Dyrssen in several of his papers, agreement is poor with respect to FeS from the more recent work of Rickard (2006). Furthermore, if $\log K(MeS)_{aq}$ for Mn is correlated with $\log K(MeS)_s$ using $\Delta G^0_{f,P_r,T_r}$ by Robie and Hemingway (1995), correlation of Mn(II) with

the rest of the data set is also poor. Arbitrary correction of $\log K(MnS)_{aq}$ to account for the relative difference between $\log K_{ex}$ for Fe(II) and Mn(II) does, however, restore a more restricted correlation, if the outlier for Hg is excluded and the values obtained by Rickard (2006) replace those given by Dyrssen (1989), as indicated for regression trendline (c) in Figure D1. Clearly, such speculations do little to improve the rigor of the analysis and are included merely to suggest further lines of inquiry.

In the following paragraphs, we briefly describe the data sets for sulfide complexes of Zn, Cd, Hg and Pb with reference to the compilations in Tables D1 and D2, and to selected speciation models for each metal in the published literature.

D4. Greenockite (CdS)

The data for $\Delta G^0_{f,P_r,T_r}$ for greenockite indicates ≈ 1.00 kcal/mol discrepancy between those values obtained by calorimetry or thermochemical measurements, and those derived from solubility measurements. Davies-Colley et al. (1985), in comparing measured Cd^{+2} concentrations in relatively high p(HS^-) anaerobic estuarine sediments with those based on the assumed presence of greenockite precipitate, found that greenockite solubility was exceeded by about one log unit. The basis for their calculations was $\Delta G^0_{f,P_r,T_r}$(greenockite) = -34.8 kcal/mol from an earlier publication by Robie et al (1978), which is similar to that given by Robie and Hemingway (1995). The sulfide speciation used in their calculations also differs from that given by Daskalakis and Helz (1992). Davies-Colley et al. (1985) attribute the discrepancy to the possible presence of polysulfide complexes, or that the solubility-controlling sulfide was a poorly ordered CdS phase. Given the inherent uncertainties in the interpretation of field data, and lack of knowledge as to the nature of immobile Cd^{+2} in the sediments, i.e., whether as a discrete solid phase, or in solid solution with sphalerite, or whether adsorbed on thiol groups on organic material, it is perhaps surprising that such good agreement was obtained. Table D4 presents the internally consistent data set for Cd sulfide complexes from the study by Daskalakis and Helz (1993). The Log K value for the dissociation of CdS(aq) is derived from data presented by Dyrssen and Wedborg (1991) as summarized in Table D4, and the solubility product is based on thermochemical data given by Robie and Hemingway (1995).

Table D4. Complexes of HS- with Cd+2 after data by Daskalakis and Helz (1993), CdS(aq) after Dyrssen and Wedborg (1991) and Greenockite Solubility Product derived from Thermochemical Data given by Robie and Hemingway (1995), all at 25°C

Reaction	**Log K**
$Cd(HS)_3^- = Cd^{+2} + 3\ HS^-$	-16.44
$Cd(HS)_4^{-2} = Cd^{+2} + 4\ HS^-$	-17.89
$Cd(OH)_2(HS)^- + 2\ H^+ = Cd^{+2} + 3\ HS^- + 2\ H_2O$	+2.47
$CdS(aq) + H^+ = Cd^{+2} + HS^-$	-4.8
$CdS(greenockite) + H^+ = Cd^{+2} + HS^-$	-14.09

D5. Cinnabar (HgS)

Discrepancies in derived values of $\Delta G^0_{f,P_r,T_r}$(cinnabar) are substantial, ranging over almost 4 kcal/mol, and the corresponding values of log K_s show a range of approximately 3 units (Table D1). The uncertainty is aggravated by questions concerning the identification of Hg sulfide species in solution and the magnitudes of their dissociation constants, *c.f.* Tossell (1999). We have identified and calculated the relevant dissociation constants using the results presented by Schwarzenbach and Widmer (1963) and modified by Paquette and Helz (1997) on the solubility of red cinnabar in buffered 0.7 M KCl solution at 25°C. In order to retrieve the dissociation constants from their data, a solubility product for cinnabar must be assumed, and the first dissociation constant for H_2S(aq) specified. The solubility product derived from $\Delta G^0_{f,P_r,T_r}$(cinnabar), given by Robie and Hemingway (1995) (Log K = -38.08), and the dissociation constant for H_2S(aq) specified by Bessinger (2000) (Log K = -6.980) were used in the calculation. Corrections to zero ionic strength standard state conditions were not applied, as activity coefficient corrections are self compensating for two of the three species, and correction for the third would not be very accurate given the limited amount of available data. Results of the calculations are presented in Table D5.

Table D5. Complexes of HS- with Hg+2 after data by Schwartzenbach and Widmer (1963) and modified by Paquette and Helz (1997), HgS(aq) after Dyrssen and Wedborg (1989) and Cinnabar Solubility Product derived from Thermochemical Data given by Robie and Hemingway (1995), all at 25°C

Reaction	**Log K**
$Hg(HS)_2(aq) = Hg^{+2} + 2\ HS^-$	-39.65
$HgS(HS)^- + H^+ = Hg^{+2} + 2\ HS^-$	-32.67
$HgS_2^{-2} + 2\ H^+ = Hg^{+2} + 2\ HS^-$	-23.91
$HgS(aq) + H^+ = Hg^{+2} + HS^-$	-28.08
$HgS(cinnabar) + H^+ = Hg^{+2} + HS^-$	-38.08

Incorporation of the neutral HgS(aq) complex in the analysis is essential, as use of the cited solubility product for cinnabar and the dissociation constants of the Hg sulfide aqueous species alone would predict unrealistically low Hg concentrations in groundwaters. This difficulty was also recognized by Benoit et al. (1999), who incorporated HgS(aq) in their study of dissolved mercury behavior in sediments from the Florida Everglades and the Patuxent River Estuary of Maryland. Our value for Log K = -28.08 can be compared with their value of –26.5 and their assumed Log solubility product of cinnabar of –37.0 instead of –38.08 used here. Correction for the higher solubility product would yield a value of –27.6, which is in substantial agreement with our own value for this parameter.

It should be noted that Benoit et al. (1999) did not assume that dissolved mercury had at any time equilibrated with cinnabar as a discrete solid phase in the sediments under study. Rather, they considered cinnabar as a potential solid solution component in a matrix of iron monosulfide or pyrite. Their treatment was analogous to their assumption that Hg^{+2} complexes with a "solid solution" of thiol groups on organic material. However, although saturation with respect to cinnabar was never observed, their model predicted quite well the variability of Hg concentration in sediment pore waters with dissolved sulfide concentration, and was independently correlated with expected methyl mercury speciation. Their model could therefore be considered a reasonable paradigm for testing the correlation of aqueous Hg concentrations with cinnabar saturation, even extrapolated to the much lower dissolved sulfide concentrations expected in potable groundwaters.

D6. Galena (PbS)

Issues relating to the solubility of galena in groundwaters are discussed at somewhat greater length than in previous sections for other sulfide minerals, because of its relevance in this project. Reported values for the solubility product of galena (PbS), as defined by the dissolution equation

$$PbS + H^{+} = Pb^{+2} + HS^{-} \qquad \text{(D16)}$$

vary over two orders of magnitude, as shown in Table D1. The value utilized by Wang and Jaffe (2004) in their simulations of galena dissolution in shallow potable water aquifers was taken from a database compiled for the MINTEQ code (Felmy et al., 1984; Hydrogeologic and Allison Geoscience Consultants, 1999), but also used by the PHREEQ-C code (Parkhurst and Appelo, 1999). This database (minteq.v4.dat 85 2005-02-02 16:13:00Z dlpark), gives a $\log K_s$ value of -13.97 at 25°C for the above reaction. The source of this value can be traced to Dyrssen and Kremling (1990), who in a study of trace metal behavior in anoxic Baltic waters attempted to derive Log K_s values for a number of metal sulfides. The values presented are based on the product of two reaction constants, K_1, and K_{sO}, representing respectively the reactions:

$$H^{+} + S^{2-} = HS^{-} \qquad \text{(D17)}$$

and

$$M_aS_b(s) = aM^{n+} + bS^{2-} \qquad \text{(D18)}$$

where M represents the metal with charge +2 (n=2, a=b=1) or +1 (n=1, a=2, b=1). Because of the high degree of uncertainty in K_2 (published values of $\text{Log}K_1$ vary between 12 and 18.51±0.56), the authors utilized published values of K_{sO} together with corresponding values for K_1 from the original sources to calculate the product (K_1 K_{sO}) for the reaction:

$$M_aS_b(s) + bH^{+} = aM^{n+} + bHS^{-} \qquad \text{(D19)}$$

which for galena is represented by the reaction described in Eq. (D1).

The PHREEQ-C code is also capable of using another database used by the WATEQ code (wateq4f.dat 431 2005-08-23 17:29:36Z dlpark). This database gives a $\log K_s = -12.780$ at 25°C for the reaction in Eq. (D1), which is 1.2 log units higher than the value cited by Dyrssen and Kremling (1990). The cited value is a correction by Shea and Helz (1989) for Pb complexation by chloride ion based on results from an earlier experimental study by Uhler and Helz (1984). The latter investigators enhanced the solubility of galena through Pb^{+2} complexing with ethylene diamine acetic acid (EDTA) in a solution of disodium EDTA and 0.1 M NaCl. The technique overcomes a serious difficulty in analyzing solution compositions where one or more of the principal chemical components are at or below the detection limits of available analytical methods, yet introduces additional complexity and uncertainty associated with the thermodynamic parameters needed to interpret the behavior of the chelating agents used in the study. The technique is also dependent on knowledge of the identities and thermodynamic properties of lead sulfide complexes in solution. Finally, derivation of K_s depends on appropriate ionic strength corrections to permit extrapolation to standard state conditions. Despite much progress in making such corrections, current techniques still leave room for improvement.

The EQ3/6 code (Wolery et al., 1992) used in this study utilizes another thermodynamic database data0.ymp.R4 (downloaded N.S. 3/3/05 DTN: SN0410T0510404.002), which was qualified for use under the Yucca Mountain Project and supported by the U.S. Department of Energy. The database gives a $\log K_s = -14.8544$ at 25°C for the reaction in Eq. (1), which is 0.95 log units lower than the value cited by Dyrssen and Kremling (1990). This value was calculated from the thermodynamic properties for galena reported in Helgeson et al. (1978), who in turn cited Mills (1974). The reported value for $\Delta G^0_{f,P_r,T_r}$, -23.12 kcal/mol, is close to the -23.14 kcal/mol reported by Robie and Hemingway (1995), which is in turn based on thermochemical measurements by Stubbles and Birchenall (1959). Stubbles and Birchenall (1959) conducted thermochemical measurements on lead/lead sulfide equilibria between 585 and 920ºC, necessitating a substantial extrapolation to the 25ºC reference temperature. Uhler and Helz (1984), in referring to the same work, note further that, apart from the magnitude of the extrapolation, additional uncertainties arise from phase changes in both elemental lead and sulfur between 585 and 25ºC, contributing

to an overall uncertainty in excess of 2 kcal/mol in $\Delta G^0_{f,P_r,T_r}$ (galena), or > ±1.5 units in $LogK_s$. However, this uncertainty is much larger than that estimated by Robie and Hemingway (1995) for the same data (Table D1).

Barrett and Anderson (1982, 1988) measured the solubility of both galena and sphalerite (ZnS) at temperatures between ≈25 and 95ºC in sodium chloride brines ranging between 3 and 5 M. These investigators then independently calculated the solubilities of galena and sphalerite to 300ºC in sodium chloride brines between 1 and 5 M at pH = 4 and $m_{s(r)}$ = 0.001. They also compared their measured solubilities with the independently calculated values, and obtained a reasonable match (calculated values were between 0.3 and 0.7 log units too low). Their calculations were based on $logK_s$(galena) cited in Bowers et al. (1985), which appears to have been derived from the sources cited by Helgeson et al. (1976). The calculations took into account Pb chloride complexing quantified by Seward (1984) and Ruaya and Seward (1986), and activity coefficient (γ_i) corrections were based on the b-dot method described by Helgeson (1969). Barrett and Anderson (1988) contrasted their results using the $logK_s$(galena) cited in Bowers et al. (1985) with those obtained by Uhler and Helz (1984), noting the almost two order of magnitude discrepancy, and pointing out that using the latter would result in calculated solubilities much greater than their measured values. However, they also note that their own experimental measurements are subject to errors arising from inadequate corrections for liquid junction potentials in their measurements of pH. Furthermore, their calculated solubilities are subject to the same uncertainties associated with corrections for chloride and sulfide complexing by Pb^{+2}. Inadequate corrections for activity coefficients of the ionic species in high-ionic strength sodium chloride brines are also of concern to the derived results of Uhler and Helz (1984), as noted above.

In conclusion, the discrepancies between K_s(galena) derived from solubility measurements and those based on thermochemical measurements are so significant that meaningful predictions of galena solubility in shallow potable groundwaters at ambient temperatures are not possible unless the conflict is resolved. This conflict appears to be caused by failure to account for the presence of the oligomeric complex PbS(aq), by analogy with the resolved discrepancies between measured and calculated sphalerite, greenockite and cinnabar solubilities, given in the preceding sections. We therefore adopted the strategy described in the introduction of this

Appendix, i.e., Log K_s(galena) would be based on thermochemical data, and the dissociation constant of PbS(aq) would be estimated based on the regression analysis between Log $K(MeS)_s$ and $\log K(MeS)_{aq}$ illustrated in Figure D1. The value chosen for Log (PbS)aq, -5.5, is consistent, within the overall uncertainty of the analysis, with independent measurements by Rozan et al. (2003), who give a value for $LogK_{THERM} = 16.83 \pm 0.33$ for PbS(aq), 36.38±0.47 for Pb_2S_2(aq), 62.49±0.61 for Pb_3S_3, and 135.6±0.8 for Pb_6S_6, respectively, for the reaction

$$xPb^{+2} + xS^{-2} = Pb_xS_x(aq) \tag{D20}$$

Normalizing these $LogK_{THERM}$ values to unit stoichiometry, as well as recasting the reaction in terms of HS^- and as a dissociation yields $LogK(PbS)(aq)$ = +0.31, -1.67, -4.46 and -6.08, respectively. Bearing in mind that Rozan et al. (2003), on the basis of mass spectrometry determinations of freeze-dried samples, found that the species Pb_3S_3(aq) appeared to predominate, it can be seen that there is reasonable agreement between the normalized log K value for that species, -4.46, and the value of –5.5 provisionally accepted for the average of all oligomeric PbS(aq) species. Note, however, that the foregoing calculation assumed $LogK_{THERM} = 16.83 \pm 0.33$ for the reaction

$$S^{-2} + H^+ = HS^- \tag{D21}$$

Values ranging from 18.51 ± 0.56 (Schoonen and Barnes, 1988) to ≈ 14.0 have been reported in the literature (Dyrssen, 1989). Therefore the uncertainties in the derived values for $LogK(PbS)(aq)$ from Rozan et al. (2003) are substantial.

The dissociation constants for other Pb sulfide species in solution are derived from the association constants reported by Giordano and Barnes (1979) at 30°C, which are essentially identical to earlier work by Hemley (1953) at 25°C, and were treated analogously to those for Hg sulfide complexes using solubility products derived from $\Delta G^0_{f,P_r,T_r}$ (galena), given by Robie and Hemingway (1995) (Log K = -14.870), and the dissociation constant for H_2S(aq) specified by Bessinger (2000) (Log K = -6.98). The relevant data are given in Table D6.

Table D6. Complexes of HS- with Pb^{+2} after data by Giordano and Barnes (1979), PbS(aq) computed in this Appendix, and Galena Solubility Product derived from Thermochemical Data given by Robie and Hemingway (1995), all at 25°C

Reaction	Log K
$Pb(HS)_2(aq) = Pb^{+2} + 2\ HS^-$	-14.058
$Pb(HS)_3^- = Pb^{+2} + 3\ HS^-$	-15.258
$PbS(aq) + H^+ = Pb^{+2} + HS^-$	-5.5
$PbS(galena) + H^+ = Pb^{+2} + HS^-$	-14.870

D7. Sphalerite (ZnS)

Excellent agreement is obtained for the calculated values of $\Delta G^0_{f,P_r,T_r}$ for sphalerite derived from the data by Daskalakis and Helz (1993), Deore and Navrotsky (2006), and Schaefer and Gokcen (1982). The value of $\Delta G^0_{f,P_r,T_r}$ derived from data by Dyrssen and Kremling (1990) is somewhat higher, but otherwise in reasonable agreement. Barrett and Anderson (1988), using a value of Log K_s for sphalerite of –11.40, found that the measured solubility at 25°C was 0.4 log units higher in 3 *M* NaCl brine, i.e., Log Ks ≈ –11.00, consistent with that of –10.93 reported by Dyrssen and Kremling (1990). Bearing in mind that Barrett and Anderson's measured solubility measurements are difficult to interpret, as noted further in Section D5 of this appendix, the consistency of their results with other solubility measurements, and with thermochemical determinations of $\Delta G^0_{f,P_r,T_r}$ suggests that reasonable confidence can be attached to the internally consistent dataset for sulfide speciation and log K_s for sphalerite, obtained by Daskalakis and Helz (1992), and presented in Table D7, below. An uncertainty of about ± 1 log unit is expected in predictions of sphalerite saturation indices. The Log K value for the dissociation of ZnS(aq) is derived from data presented by Dyrssen and Wedborg (1991) as summarized in Table D7, and the solubility product is based on thermochemical data given by Robie and Hemingway (1995).

Table D7. Complexes of HS- with Zn+2 after data by Daskalakis and Helz (1992), ZnS(aq) after Dyrssen and Wedborg (1991) and Sphalerite Solubility Product derived from Thermochemical Data given by Robie and Hemingway (1995), all at 25°C

Reaction	Log K
$Zn(HS)_4^{-2} = Zn^{+2} + 4\ HS-$	-14.640
$ZnS(HS)^- + H^+ = Zn^{+2} + 2\ HS^-$	-6.842
$ZnS(HS)_2^{-2} + H^+ = Zn^{+2} + 3\ HS^-$	-6.152
$ZnS(aq) + H^+ = Zn^{+2} + HS^-$	-3.5
$ZnS(sphalerite) + H^+ = Zn^{+2} + HS$	-11.27

D8. Recommendations for Further Refinement of Thermodynamic Data Pertinent to Sulfide and Selenide Solubilities

A pragmatic approach was taken in the foregoing analysis to reconcile thermochemical data for solid sulfide and selenide minerals with measured aqueous solubilities, and further reconcile field measurements of heavy metal concentrations in potable groundwaters with postulated saturation indices for the sulfide and selenide minerals. For reasons of time, an in-depth analysis was not conducted.

In their review of metal sulfide complexes and clusters, Rickard and Luther (2006) cite studies suggesting the existence of several other charged and uncharged oligomeric metal clusters of Fe, Cu, Zn, Cd, Ag, Au, Pb and Hg. Supporting evidence is for the most part equivocal, and further definitive studies are needed to resolve current ambiguities regarding cluster stoichiometries and stabilities. The same authors also cite recent work by Zhang and Millero (1994), Al-Farawati and van den Berg (1999), and Rozan et al. (2003) all of whom used various voltammetric techniques to identify sulfide speciation in marine waters for a range of elements, including those of interest in this report. Unfortunately, time did not permit evaluation of their findings in relation to the work presented here. However, some preliminary checks indicate consistency with the results presented in this appendix. Further analysis of the data presented in these and other papers cited by Rickard and Luther (2006), as well as the work of ongoing investigations must be conducted as part of a broader strategy to refine the geochemical model for potable waters.

The following are aspects of the problem that were insufficiently addressed.

(1) The aqueous species MeS(aq) represents a distribution of oligomeric complexes, which would vary depending on both intensive and extensive variables in the system. Molecular dynamic modeling and/or spectroscopic studies will be required to establish the identities of species and their thermodynamic relations. Recent studies of sulfide complexation in marine waters using voltammetric methods (*vide supra*) must be reviewed and compared with earlier work cited in this appendix and account taken of oligomeric species where their thermodynamic properties have been quantified.

(2) Experimental measurements of sulfide and selenide mineral solubilities were conducted in a variety of supporting electrolytes. Ionic strength corrections to the activities of species were not uniformly treated or evaluated.

(3) Corrections to mineral solubilities by assuming the presence of neutral sulfide complexes were made without a re-evaluation of the raw data. Consequently, corrections to the distributions between species such as MeS(aq) and species such as $Me(HS)_2$(aq) were accounted for in a consistent manner.

(4) Improved correlation plots between sulfide and selenide species might be achieved by consideration of experimental work on selenide complexes of Mn and Ag by Mehra and Gubeli (1970a and 1970c).

(5) Changes in the distributions of sulfide and selenide minerals as a function of heavy metal abundances and redox potential in natural systems should be examined further to establish the phase relations of selenide minerals in relation to corresponding sulfide minerals in potable water aquifers.

(6) In making tests of the validity of calculated saturation indices of sulfides and selenides in potable groundwaters, the effect of temperature was ignored. Potable groundwater temperatures could range down to as low as 5ºC, which could shift the calculated saturation index by as much as one log unit. In situ temperatures of the studied NWIS potable waters should be retrieved and temperature corrections made for the dissociation constants of all participating aqueous species and all participating mineral solubility products.

(7) The stability constants of mixed sulfide/selenide complexes should be estimated and incorporated in the thermodynamic database used in the evaluation of saturation indices of sulfide and selenide minerals in potable groundwaters.

Appendix E:
Dissociation Constants for Selenides of Arsenic, Cadmium, Mercury, Lead and Antimony

E1. Background

During the course of the current investigation, it became apparent that the concentrations of several hazardous inorganic constituents in groundwaters could be controlled by their selenides, rather than their corresponding sulfides. This supposition is reinforced by field evidence for the existence of clausthalite (PbSe) occurring in over 50% of coals in the Appalachian Basin and 10% outside the Basin (Finkelman, 1981), and the occasional occurrence of tiemannite (HgSe) in coal (Tewalt et al., 2001). Furthermore, both cadmoselite (CdSe) and antimonselite (Sb_2Se_3) have been observed in sedimentary formations under conditions that might suggest their presence in potable groundwater aquifers.

Preliminary calculations of the saturation indices for metal (Me) selenides, using solubility products based on thermodynamic data in reported in the published literature, for the reaction:

$$Me_aSe_b(s) + bH^+ = aMe^{n+} + bHSe^- \qquad \text{(E1)}$$

also indicated that all of the cited selenides would be extremely supersaturated in those groundwaters from the NWIS database reporting Se together with Cd, Hg, Pb or Sb. In fact, the calculated saturation indices were so unrealistically high (≈ +5 to +10), that it was clear that that the thermodynamic database used in the EQ3/6 code for the evaluation was seriously deficient and failed to represent the behavior of selenide mineral solubilities. this deficiency would compromise the objective of the study to correctly identify and quantify the thermodynamic controls governing the concentrations of the cited constituents in potable groundwaters.

An obvious omission in the Data0.dat database were the selenide complex dissociation constants corresponding to those of sulfide complexes with As^{+3}, Cd^{+2}, Hg^{+2}, Pb^{+2}, Sb^{+3}, Zn^{+2} and Fe^{+2}, which were incorporated on the basis of a review of their dissociation constants given in Appendix D. A perusal of the literature lead to the discovery of two reviews regarding the solubilities of selenium phases and selenium speciation in solution, Cowan (1988) and Seby et al.

(2001). Both reviews cited the same sources regarding selenide complexation with metal ions, which were limited to studies by Mehra and Gubeli (1970a,b, 1971) concerning Ag, Mn and Hg selenide complexation. No other studies relating to selenide complexation with metals in aqueous solution appear to have been published since date of the latest review. Only the information by Mehra and Gubeli (1971) concerning Hg selenide complexing is relevant to the current study. In the following paragraphs, we discuss how the available data were adapted to account for selenide complexation with As^{+3}, Cd^{+2}, Hg^{+2}, Pb^{+3}, Sb^{+3}, Zn^{+2} and Fe^{+2}.

E2. Hg Selenide Complexes in Aqueous Solution

Mehra and Gubeli (1971) independently determined the Log solubility product of HgSe, according to the reaction

$$HgSe(s) = Hg^{+2} + Se^{-2} \quad \text{(E2)}$$

to be –56.6±0.2. Assuming Log K for the reaction

$$HSe- = H^{+} + Se^{-2} \quad \text{(E3)}$$

is –14.0±1.0 (Seby et al., 2001), it follows that Log K(tiemannite) for the reaction

$$HgSe(s) + H^{+} = Hg^{+2} + HSe^{-} \quad \text{(E4)}$$

is –42.6. This value is comparable with the value, -43.27, calculated from thermochemical data reported by Vaughan and Craig (1978), and the same as that reported by Mills (1974), which has been incorporated in the EQ3/6 Data0.dat, V4.2.YMP, and accepted in this report.

The data presented by Mehra and Gubeli (1971) also allows calculation of the intrinsic solubility of HgS (tiemannite) under acid conditions (i.e., at pH < 3.8), as their measurements were conducted in 1 Normal $NaClO_4$ solution assumed to be in equilibrium with solid HgSe. Assuming the reaction

$$HgSe(s) = HgSe(aq) \quad \text{(E5)}$$

is in equilibrium with a total log concentration of Hg = -7.83, as reported by Mehra and Gubeli (1971), then $LogK_{\text{int}} = -7.83$. Given that Log K(tiemannite) for the reaction (E2) is –43.27, the dissociation constant for the reaction

$$\text{HgSe(aq)} + \text{H}^{+} = \text{Hg}^{+2} + \text{HSe}^{-} \qquad \text{(E6)}$$

is $LogKHgSe(aq) = -35.43$.

Instead of postulating the existence of HgSe(aq) as a proxy for oligomeric species in solution, Mehra and Gubeli (1971) assumed the existence of a complex of the form Hg(HSe)(OH)(aq), which, through subtraction of one H_2O, assumes the same form as HgSe(aq). The two species are therefore equivalent, and it would be impossible to discriminate between the two on the basis of the experimental results alone.

Mehra and Gubeli (1971) also postulated the existence of two other species in solution, $Hg(HSe)_2(OH)^-$ and $Hg(HSe)_2(OH)_2^{-2}$, which are equivalent to $HgSe(HSe)^-$ and $HgSe_2^{-2}$, respectively.

Association constants for each were defined thus:

$$\beta_{21} = \frac{\left[Hg(HSe)_2(OH)^-\right]}{\left[Hg^{+2}\right]\left[HSe^-\right]^2\left[OH^-\right]} = \frac{\left[Hg_{complex}\right]K_2^2}{K_{sp} \bullet K_W\left[H^+\right]\left[Se^{-2}\right]} \qquad \text{(E7)}$$

where $Log\beta_{21} = 52.8 \pm 0.3$, and

$$\beta_{22} = \frac{\left[Hg(HSe)_2(OH)_2^{-2}\right]}{\left[Hg^{+2}\right]\left[HSe^-\right]^2\left[OH^-\right]^2} = \frac{\left[Hg_{tot}\right]K_2^2}{K_{sp} \bullet K_W{}^2\left[Se^{-2}\right]} \qquad \text{(E8)}$$

where $Log\beta_{22} = 61.0 \pm 0.3$. The value of the second ionization constant, $LogK_2 = -11.6$, had been determined earlier by Mehra and Gubeli (1970a). $LogK_{sp} = 56.6 \pm 0.2$ is the solubility product of HgSe, tacitly assumed to be tiemannite. It was also calculated from the value reported for the reaction

$$\text{HgSe} = \text{Hg}^{+2} + \text{Se}^{-2} \qquad \text{(E9)}$$

Log K_w is the dissociation constant for water, which was not specified. The log K_2 value is inconsistent with that recommended by Seby et al. (2001) (log K_2 = -14.0 ±1.0), the elevated value being possibly caused by inadvertent contamination by polyselenides generated through oxidation of HSe^- by traces of oxygen (Wood, 1958), even though the study was conducted under an inert atmosphere of nitrogen. Because a 1 M $NaClO_4$ solution was used as the supporting electrolyte, a more realistic value for log K_W is –13.7, a value used by Dyrssen (1988) in correcting for the ionic strength of seawater. Finally, $LogK_{sp}$ differs from that calculated from thermochemical data by approximately 0.7 log unit, which might be due to a finer crystallinity of the material used in their solubility determinations. Because this discrepancy is within the overall uncertainty of the calculations, no correction was applied to account for this difference. Application of appropriate corrections yields revised values for the dissociation constants, which are presented in Table E1.

Table E1. Dissociation Constants of Complexes of HSe- with Hg+2 and the Tiemannite Solubility Product in 1 M NaClO4 Solution at 25ºC (after data by Mehra and Gubeli, 1971).

Reaction	**Log K**
$HgSe(aq) + H^+ = Hg^{+2} + HSe^-$	-35.43
$HgSe(HSe)^- + H^+ = Hg^{+2} + 2\ HSe^-$	-39.10
$HgSe_2^{-2} + 2\ H^+ = Hg^{+2} + 2\ HSe^-$	-28.80
$HgSe(s) + H^+ = Hg^{+2} + HSe^-$	-43.27

Corrections were inconsistently applied to the reported dissociation constants for $HgSe(HSe)^-$ and $HgSe_2^{-2}$. The corrected value for Log K($HgSe(HSe)^-$) should have been –34.30. However, had this value been used instead of that cited in Table E1, the calculated Log K values of selenide complexes given in this appendix would have differed very little from those actually calculated and used in subsequent calculations in this report. With respect specifically to Hg selenide complexation, the differences are also inconsequential, and well within the overall uncertainty of the model results, as the $HgSe(HSe)^-$ species is always less than 10^{-6} % of the total Hg in groundwaters. It should also be noted that the corrections are preliminary, and that a more careful re-evaluation of the findings by Mehra and Gubeli (1971) is required. Furthermore, it is very probable that both $HgSe(HSe)^-$ and $HgSe_2^{-2}$ species are oligomeric, and this should also be taken into account in re-interpreting the data.

E3. Estimated Dissociation Constants of Selenide Complexes of As^{+3}, Cd^{+2}, Pb^{+3}, Sb^{+3}, Zn^{+2} and Fe^{+2} in Aqueous Solution

In the absence of any information pertaining to selenide complexes for Cd^{+2}, Pb^{+3}, Sb^{+3}, Zn^{+2} and Fe^{+2}, values of their dissociation constants were estimated from those of the corresponding sulfide complexes using a linear correlation equation in which were plotted solubility product pairs for metal sulfide and selenide minerals, offset values of the dissociation constant pairs for H_2S(aq) and H_2Se(aq), and HS^- and HSe^-, respectively, and dissociation constants for Hg sulfide and selenide aqueous complex pairs. The respective sulfide and selenide solubility products are calculated from thermochemical, electrochemical or calorimetric data, but not solubility measurements. The data used in this plot and the sources of information are given in Table E2. Note that metacinnabar and marcasite solubility products are used in place of those for cinnabar and pyrite, respectively, in order to compare sulfide and selenide minerals with identical crystal structures.

The initial regression was conducted on all species together, correcting H_2Se(aq) and HSe^- species values by an identical amount sufficient to bring them into colinearity with the trend of the solid phases. The aqueous species were then restored to the original values, and then the value for the dissociation constant for HSe^- adjusted to ensure that the slopes of the two lines were identical. This entailed adjustment from Log K(HSe^-) = -14.0 ±1.0 to –14.67, which is well within the uncertainty of value assigned by (Seby et al., 2001). The reason for the offset is not known, but might be ascribed to the effects of solvation and electrostriction in the aqueous phase acting on these molecular and ionic species, e.g., see Shock and Helgeson (1988). The analysis and interpretation is quite speculative, and may be modified upon more comprehensive review.

Table E2. Log K Values of Sulfide and Selenide Aqueous Complex and Mineral Pairs used to generate a Correlation Plot to Estimate the Dissociation Constants of Unknown Metal Selenide Complexes and Effective Solubility Products of Metal Selenides

Sulfide			Selenide		
Species	**Log K**	**Source**	**Species**	**Log K**	**Source**
Aqueous					
HS^-	-16.52	1	HSe^-	-14.67	4
$H_2S(aq)$	-6.99	2	$H_2Se(aq)$	-3.81	5
HgS(aq)	-28.08	3	HgSe(aq)	-35.43	4
$HgS(HS)^-$	-32.67	3	$HgSe(HSe)^-$	-39.10	4
HgS_2^{-2}	-23.91	3	$HgSe_2^{-2}$	-28.80	4
Mineral					
CdS (greenockite)	-14.09	6	Cadmoselite	-18.89	7
Meta-cinnabar	-37.78	6	Tiemannite	-43.27	7
Galena	-14.87	6	Clausthalite	-20.78	7
Marcasite	-49.87	7	Ferroselite	-55.45	7

Notes:

1. Dyrssen (1988); 2. Bessinger (2000); 3. Paquette and Helz (1997); 4. this appendix; 5. Seby et al. (2001); 6. Appendix D; 7. EQ3/6 Data0.ymp.R4 database (see Appendix D)

The data summarized in Table E2 and results from the regression analysis are shown in Figure E1. The linear regression of the data is good ($R^2 = 0.993$). The regression equation was used to estimate the dissociation constants for the corresponding selenide analogues of sulfide complexes of As(III), Cd(II), Pb(II), Sb(III), Zn(II) and Fe(II), which are presented in Table E3. These estimated values were incorporated in the thermodynamic databases of EQ3/6 and TOUGHREACT, and used to calculate saturation indices of selenide minerals in those NWIS groundwaters that were analyzed for Se.

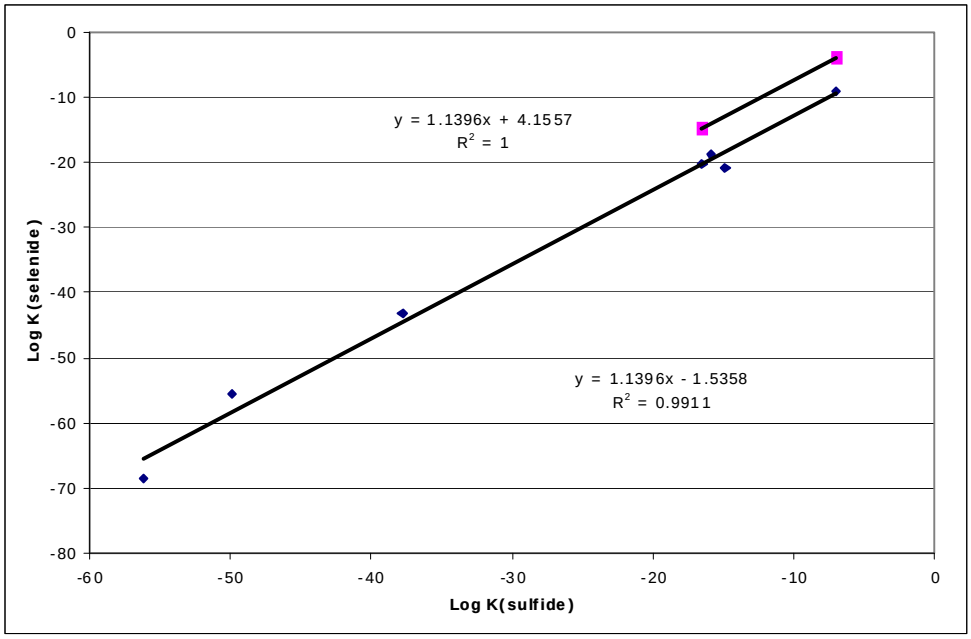

Fig. E1. Linear regression of dissociation constants of Hg sulfide and selenide complex pairs, and solubility product pairs for metal selenides and sulfides. "aq." refers to aqueous species.

Table E3. Estimated Log K Values of Selenide Aqueous Complexes of As+3, Cd+2, Pb+3, Sb+3, Zn+2 and Fe+

Reaction	**Log K**
Arsenic	
$H_3As_3Se_6(aq) + 1.5O_2(g) + 9H_2O = 3H_2AsO_4^- + 6HSe^- + 9H^+$	-23.96
$H_2As_3Se_6^- + 1.5O_2(g) + 9H_2O = 3H_2AsO_4^- + 6HSe^- + 8H^+$	-19.63
$HAs_3Se_6^{-2} + 1.5O_2(g) + 9H_2O = 3H_2AsO_4^- + 6HSe^- + 7H^+$	-10.64
$AsSe(OH)(SeH)^- + 0.5O_2(g) + 2H_2O = H_2AsO_4^- + 2HSe^- + 2H^+$	-6.91
Cadmium	
$CdSe(aq) + H^+ = Cd^{+2} + HSe$	-10.24
$Cd(HSe)_3^- = Cd^{+2} + 3HSe^-$	-23.47
$Cd(HSe)_4^{-2} = Cd^{+2} + 4HSe^-$	-25.12
$Cd(OH)_2(HSe)^- + 2H^+ = Cd^{+2} + 3HSe^- + 2H_2O$	-1.98
Lead	
$PbSe(aq) + H^+ = Pb^{+2} + HSe^-$	-11.04
$Pb(HSe)_2(aq) = Pb^{+2} + 2HSe^-$	-20.76
$Pb(HSe)_3^- = Pb^{+2} + 3HSe^-$	-22.15
Antimony	
$H_2Sb_2Se_4(aq) + 6H_2O = 2Sb(OH)_3 + 4HSe^- + 4H^+$	-70.63
$HSb_2Se_4^- + 6H_2O = 2Sb(OH)_3 + 4HSe^- + 3H^+$	-64.88
$Sb_2Se_4^{-2} + 6H_2O = 2Sb(OH)_3 + 4HSe^- + 2H^+$	-54.08
Zinc	
$ZnSe(aq) + H^+ = Pb^{+2} + HSe^-$	-8.76
$Zn(HSe)_4^{-2} = Zn^{+2} + 4HSe^-$	-21.42
$ZnSe(HSe)^- + H^+ = Zn^{+2} + 2HSe^-$	-12.56
$ZnSe(HSe)_2^{-2} + H^+ = Zn^{+2} + 3HSe^-$	-11.78
Iron	
$FeSe(aq) + H^+ = Fe^{+2} + HSe^-$	-2.28

Appendix F:
Improved Adsorption Models in TOUGHREACT

F1. Introduction

Many minerals such as metal oxides, hydroxides and layered silicates (Al_2O_3, TiO_2, FeOOH, SiO_2, kaolinite, etc.) exhibit electrically charged surfaces in the presence of natural waters. These surfaces contain ionizable functional groups (e.g., silanol groups in hydrated silica, Si-OH) being responsible for chemical reactions at the surface. Adsorption via surface complexation has been widely studied (Dzombak and Morel, 1990; Lutzenkirchen, 2006) and is a key process with respect to the fate and transport of heavy metals (e.g., Bradl, 2004) or other hazardous constituents such as arsenic (Goldberg, 2002; Goldberg et al., 2005; Manning and Goldberg, 1997). We have therefore incorporated into TOUGHREACT a model considering adsorption via surface complexation, using different surface complexation models such as the non-electrostatic model, the double layer model, and the constant capacity model (Dzombak and Morel, 1990). The surface complexation models implemented in TOUGHREACT were verified by comparison with other codes such as PHREEQC (Parkhurst and Appelo, 1999) and CRUNCH (Steefel, 2001). This Appendix includes two main parts. In the first part, we described the mathematical formulation and numerical implementation of surface complexation adopted in TOUGHREACT, while in the second part, we review the surface complexation reactions and their thermodynamic data used in the reactive transport simulations conducted in Section 4.

F2. Surface Complexation Models

F2.1 Surface Electric Potential Model

The sorption of solutes on solid surfaces can be described as a chemical reaction between the aqueous species and the specific surface sites (surface complexation). These surface reactions include proton exchange, cation binding and anion binding via ligand exchange at surface

hydroxil sites (represented here as XOH to avoid confusion with other chemical species). For example, the sorption of a metal could be represented as:

$$XOH + M^{z+} = XOM^{z+-1} + H^{+} \tag{F1}$$

At equilibrium, the sorption reactions can be described by the mass law equation:

$$K_{app} = \frac{\left[XOM^{z_{+}^{-1}}\right] a_{H^{+}}}{\left[XOM\right] a_{M^{z+}}} \tag{F2}$$

where K^{app} is referred to as the apparent equilibrium constant, because it includes surface charge effects and hence is dependent on the extent of surface ionization (Dzombak and Morel, 1990), *a* is the thermodynamic activity of the aqueous species, and the terms in brackets represent the concentration of surface complexes (mol/kg).

In aqueous complexation reactions, the electric charge is assumed to be homogeneously distributed in the solution. However, surface reactions take place on a fixed charged surface which creates an electrostatic field. An additional energetic term accounting for the work needed for the aqueous species to travel across the surface electric field is required:

$$\Delta G_{ads} = \Delta G_{intr} + \Delta G_{coul} = \Delta G_{intr} + (\Delta G_{\psi=0} - \Delta G_{\psi=\psi_0}) = \Delta G_{intr} - zF\psi_0 \tag{F3}$$

where ΔG_{ads} is the free enthalpy change of the overall adsorption reaction, ΔG_{intr} and ΔG_{coul} are the free enthalpy change due to chemical bonding and to the electrostatic work, respectively, z is the charge of the surface species, F the Faraday's constant (96485 C/mol), and ψ_0 is the mean surface potential (V). Since

$$\Delta G = -RTlnK\ , \tag{F4}$$

Equation (F3) can be rewritten as:

$$K_{app} = K_{int}\, e^{\frac{zF\psi_0}{RT}}\ , \tag{F5}$$

where R is the gas constant (8.314 J/mol/K), T is the absolute temperature (K), and K_{int} is the intrinsic equilibrium constant which does not depend on the surface charge.

F2.2 Diffuse Layer Model

The diffuse layer model has been described in great detail by Dzombak and Morel (1990) and was applied to adsorption of metals on iron oxide surfaces. In the diffuse layer model, the solid-water interface is composed of two layers: a layer of surface-bound complexes and a diffuse layer of counter ions in solution. The surface charge is calculated from the total surface species adsorbed on the layer:

$$\sigma_p = \frac{F}{A}\sum_{k=1}^{N_s} z_k y_k \tag{F6}$$

According to the Gouy-Chapman theory, the surface charge density σ_p (c/m^2) is related to the potential at the surface (volt) by:

$$\sigma_d = (8RT\varepsilon\varepsilon_0 I \times 10^3)^{1/2} \sinh(zF\psi_0/2RT), \tag{F7}$$

where R is the molar gas constant (8.314 J mol^{-1} K^{-1}), T is the absolute temperature (K), ε is the relative dielectric constant of water (ε = 78.5 at 25 ^{o}C), ε_0 is the permittivity of free space (8.854×10^{-12} C V^{-1} m^{-1} or 8.854×10^{-12} C^2 J^{-1} m^{-1}), and c is the molar electrolyte concentration (M). Equation (F7) is only valid for a symmetrical electrolyte (Z=ionic charge).

It is common to use the linearized version of Equation (F7) for low values of the potential:

$$\sigma_p = \varepsilon\varepsilon_0\kappa\psi_0, \tag{F8}$$

where $1/\kappa$ (m) is the double-layer thickness defined as:

$$\frac{1}{\kappa} = \left(\frac{\varepsilon\varepsilon_0 RT}{2F^2 \cdot 1000I}\right)^{1/2} \tag{F9}$$

Equations (F7) can be simplified by rewritten $(8RT\varepsilon\varepsilon_0 I \times 10^3)^{1/2}$ for 25 ^{o}C :

$$\sigma_p = 0.1174 I^{1/2} \sinh(zF\psi_d/2RT) \tag{F10}$$

Therefore, in the diffuse-layer model, the value of the capacitance C relating the surface charge and the potential can be calculated based on theoretical considerations (Equation (F8)) instead of being an experimental fitting parameter.

F2.3 Constant Capacitance Model

Similar to the diffused-layer, the constant capacitance model is based on the assumption that all the species are adsorbed in the same layer and a diffuse layer of counterions constitutes the transition to homogenous solution. However, differently from the diffuse-layer model, the relationship between the surface charge and the potential is assumed to be linear:

$$\sigma = C\psi \tag{F11}$$

where C is a constant value to be obtained from fitting experimental data.

F2.4 Mathematical Formulation of Adsorption Reactions

Lets us consider the following surface desorption reaction:

$$XOM^{z_+-1} = XOH + M^{z_+} - H^+$$

with the equilibrium constant of the reaction given as:

$$K_{\text{int}} = \frac{[XOH]a_M}{[XOM]a_{H^+}} e^{\left(\frac{-zF\psi_0}{RT}\right)} \tag{F12}$$

Usually, the neutral surface complex XOH is included in the N_C aqueous primary species. The new unknown is the potential term

$$\tilde{\psi} = \frac{-F\psi_0}{RT} \tag{F13}$$

The concentration of a surface complex, y_j, (mol/m^3), can be expressed in terms of the concentration of the primary species and the potential term:

$$y_j = K_j^{-1} \prod_{i=1}^{N_C} c_i^{\nu_{ji}^y} \gamma_i^{\nu_{ji}^y} e^{z_j \tilde{\psi}} \qquad j = 1 \ldots N_Y \tag{F14}$$

where K_j is the intrinsic equilibrium constant of the desorption reaction.

In order to solve for the potential term, an additional equilibrium equation is needed. For the double diffuse layer model, we obtain Equation (F15), if the Guy-Chapman double-layer theory is used to relate surface charge and the potential (Equation (F7)). If the linearized Equation (F8) is used, we obtain Equation (F16). If a constant capacity model is used, we obtain Equation (F17).

$$(8RT\varepsilon\varepsilon_0 I \times 10^3)^{1/2} \sinh(-\tilde{\psi}/2) - \frac{F}{A} \sum_{k=1}^{N_s} z_k y_k = 0 \tag{F15}$$

$$\frac{F^2}{A\varepsilon\varepsilon_0 \kappa RT} \sum_{k=1}^{N_s} z_k y_k + \tilde{\psi} = 0 \tag{F16}$$

$$\frac{F^2}{ACRT} \sum_{k=1}^{N_s} z_k y_k + \tilde{\psi} = 0 \tag{F17}$$

F2.5 Implementation in TOUGHREACT

When surface complexation is considered, the total concentration of the primary species j at time zero (initial conditions) is assumed to be known, given by:

$$T_j^0 = c_j^0 + \sum_{k=1}^{N_x} \nu_{kj} c_k^0 + \sum_{m=1}^{N_p} \nu_{mj} c_m^0 + \sum_{n=1}^{N_q} \nu_{nj} c_n^0 + \sum_{s=1}^{N_s} \nu_{sj} c_s^0 \qquad j = 1 \ldots N_C \tag{F18}$$

where superscript 0 represents time zero; c denotes concentration; subscripts j, k, m, n and s are the indices of the primary species, aqueous complexes, minerals at equilibrium, minerals under kinetic constraints, and surface complexes, respectively; N_c, N_x, N_p, N_q and N_s are the number of corresponding species and minerals; and ν_{kj}, ν_{mj}, ν_{nj} and ν_{sj} are stoichiometric coefficients of the primary species in the aqueous complexes, equilibrium, kinetic minerals, and surface complexes, respectively.

After a time step Δt, the total concentration of primary species j (T_j) is given by

$$T_j = c_j + \sum_{k=1}^{N_x} \nu_{kj} c_k + \sum_{m=1}^{N_p} \nu_{mj} c_m + \sum_{n=1}^{N_q} \nu_{nj} \left(c_n^0 - r_n \Delta t \right) + \sum_{s=1}^{N_s} \nu_{sj} c_s \qquad j = 1 \ldots N_C \tag{F19}$$

where r_n is the kinetic rate of mineral dissolution (negative for precipitation, units used here are mole per kilogram of water per time), for which a general multi-mechanism rate law can be used (Xu et al., 2006). T_j^0 and T_j are related through generation of j among primary species as follows

$$T_j - T_j^0 = \sum_{l=1}^{N_a} \nu_{lj} r_l \Delta t \qquad \mathrm{j} = 1, \ldots \mathrm{N_C} \tag{F20}$$

where l is the aqueous kinetic reaction (including biodegradation) index, N_a is total number of kinetic reactions among primary species, and r_l is the kinetic rate which is in terms of one mole of product species.

By substituting Equations (F18) and (F19) into Equation (F20), and denoting residuals as F_j^c (which are zero in the limit of convergence), we have

$$\begin{aligned}
F_j^c \;=\; & (c_j - c_j^0) && \text{Primary species} \\
& + \sum_{k=1}^{N_x} \nu_{kj} (c_k - c_k^0) && \text{equilibrium aqueous complexes} \\
& + \sum_{m=1}^{N_p} \nu_{mj} (c_m - c_m^0) && \text{equilibrium minerals} \\
& - \sum_{n=1}^{N_q} \nu_{nj} r_n \Delta t && \text{kinetic minerals} \\
& - \sum_{l=1}^{N_a} \nu_{lj} r_l \Delta t && \text{kinetics among primary species} \\
& + \sum_{s=1}^{N_s} \nu_{sj} (c_s - c_s^0) && \text{surface complexes} \\
= \; & 0 \qquad j = 1 \ldots N_C
\end{aligned} \tag{F21}$$

According to mass-action equations, the concentrations of aqueous complexes c_k can be expressed as functions of concentrations of the primary species c_j. Kinetic rates r_n and r_l are functions of c_j. The expression for r_n is given in Xu et al. (2006), and r_l will be presented later.

No explicit expressions relate equilibrium mineral concentrations c_m to c_j. Therefore, N_P additional mass-action equations (one per mineral) are needed. Surface complexes are expressed as the product of primary species and an additional potential term $\tilde{\psi}$. Additional equilibrium equations (Equation (F16) or (F17) depending on the surface complexation model) have to be solved together with Equation (F21) and the N_p mass-action equations for equilibrium minerals.

The final Jacobian matrix has $Nc+Np+N_\psi$ rows and $Nc+Np+N_\psi$ columns, as follows:

$$\begin{array}{cccc} & Nc & Np & N\psi \\ Nc & \dfrac{\partial F_j^c}{\partial c_i} & \dfrac{\partial F_j^c}{\partial p_i} & \dfrac{\partial F_j^c}{\partial \tilde{\psi}} \\ Np & \dfrac{\partial F_j^p}{\partial c_i} & \dfrac{\partial F_j^p}{\partial p_i} & \dfrac{\partial F_j^p}{\partial \tilde{\psi}} \\ N\psi & \dfrac{\partial F^{\tilde{\psi}}}{\partial c_i} & \dfrac{\partial F^{\tilde{\psi}}}{\partial p_i} & \dfrac{\partial F^{\tilde{\psi}}}{\partial \tilde{\psi}} \end{array} \tag{F22}$$

$$J^{cc} = \frac{\partial F_j^c}{\partial c_i} = \delta_{ji} + \sum_{k=1}^{N_x} \nu_{kj}\nu_{ik}\frac{c_k}{c_i} + \sum_{n=1}^{Nq} \nu_{nj}\nu_{in}\frac{k_n A_n \Omega_n}{c_i} + \sum_{s=1}^{Ns} \nu_{sj}\nu_{is}\frac{c_s}{c_i} \tag{F23}$$

$$J^{c\tilde{\psi}} = \frac{\partial F_j^c}{\partial \tilde{\psi}} = \sum_{s=1}^{Ns} \nu_{sj} z_s c_s \tag{F24}$$

$$J^{\tilde{\psi}c} = \frac{\partial F^{\tilde{\psi}}}{\partial c_i} = -\sum_{s=1}^{N_s} z_s \nu_{is}\frac{c_s}{c_i} \tag{F25}$$

or

$$J^{\tilde{\psi}c} = \frac{\partial F^{\tilde{\psi}}}{\partial c_i} = \frac{F^2}{A\varepsilon\varepsilon_0\kappa RT}\sum_{s=1}^{N_s} z_s \nu_{is}\frac{c_s}{c_i} \tag{F26}$$

or

$$J^{\tilde{\psi}c} = \frac{\partial F^{\tilde{\psi}}}{\partial c_i} = \frac{F^2}{ACRT}\sum_{s=1}^{N_s} z_s \nu_{is}\frac{c_s}{c_i} \tag{F27}$$

$$J^{\tilde{\psi}\tilde{\psi}} = \frac{\partial F^{\tilde{\psi}}}{\partial \tilde{\psi}} = -\tfrac{1}{2}(8RT\varepsilon\varepsilon_0 I \times 10^3)^{1/2}\cosh(-\tilde{\psi}/2) - \frac{F}{A}\sum_{k=1}^{N_s} z_k z_k y_k \tag{F28}$$

or

$$J^{\tilde{\psi}\tilde{\psi}} = \frac{\partial F^{\tilde{\psi}}}{\partial \tilde{\psi}} = \frac{F^2}{A\varepsilon\varepsilon_0 \kappa RT} \sum_{s=1}^{N_s} z_s z_s c_s + 1 \tag{F29}$$

or

$$J^{\tilde{\psi}\tilde{\psi}} = \frac{\partial F^{\tilde{\psi}}}{\partial \tilde{\psi}} = \frac{F^2}{ACRT} \sum_{s=1}^{N_s} z_s z_s c_s + 1 \tag{F30}$$

F2.6 Verification in Comparison with Other Codes

The surface complexation calculation by TOUGHREACT has been verified against other codes such as PHREEQC (Parkhurst and Appelo, 1999) and CRUNCH (Steefel, 2001). The example of zinc sorption at low site density presented by Dzombak and Morel (1990) has been used by PHREEQC and CRUNCH to verify their surface complexation calculation. Zinc sorption on hydrous ferric oxide is simulated assuming two types of sites, weak and strong. Protons and zinc ions compete for the two types of binding sites, and equilibrium is described by mass-action equations. The double layer model is used to calculate the speciation of Zn^{2+} in aqueous and surface complexes. The example considers the variation in sorption of zinc on hydrous ferric oxides as a function of pH for low zinc concentration (10^{-7} M) and high zinc concentrations (10^{-4} M) in 0.1 M sodium nitrate electrolyte.

Figure F1 shows the calculation results of Dzombak and Morel (1990). Table 1 compares the calculated equilibrium speciation of Zn^{2+} calculated by TOUGHREACT and CRUNCH. Both simulators arrive at almost identical results. Figures F2 shows the calculated equilibrium speciation of Zn^{2+} as a function of pH calculated by TOUGHREACT.

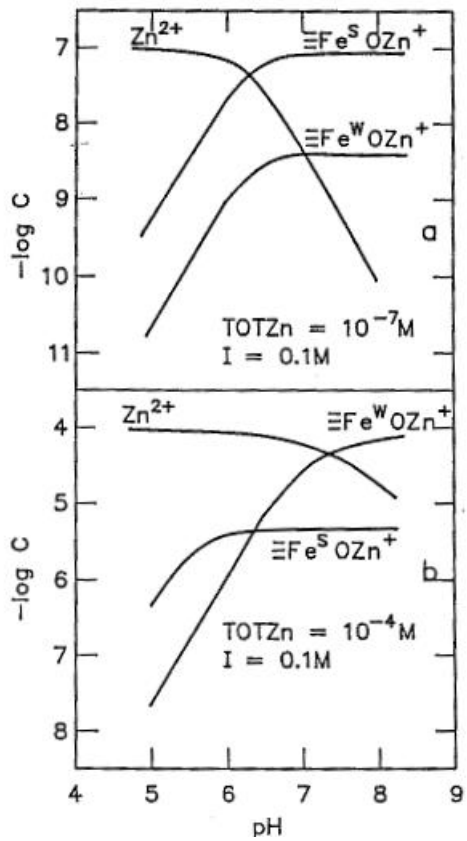

Fig. F1. Calculated equilibrium speciation as a function of pH for zinc in a 90-mg/L HFO suspension: The top figure shows results for Total Zn=10^{-7} M, I = 0.1 M; the bottom figure shows results for Total Zn = 10^{-4} M, I = 0.1 M (Dzombak and Morel, 1990).

Table F1. Calculated equilibrium speciation for zinc by TOUGHREACT and by CRUNCH

pH	Zn^{2+}		$Fe^{s}OZn^{+}$		$Fe^{w}OZn^{+}$	
	TOUGHREACT	CRUNCH	TOUGHREACT	CRUNCH	TOUGHREACT	CRUNCH
5	9.94E-08	9.94E-08	5.51E-10	6.03E-10	2.31E-11	2.52E-11
6	6.48E-08	6.28E-08	3.38E-08	3.57E-08	1.43E-09	1.51E-09
7	2.60E-09	2.61E-09	9.34E-08	9.34E-08	3.99E-09	3.99E-09
8.062	1.40E-10	1.38E-10	9.58E-08	9.58E-08	4.09E-09	4.09E-09

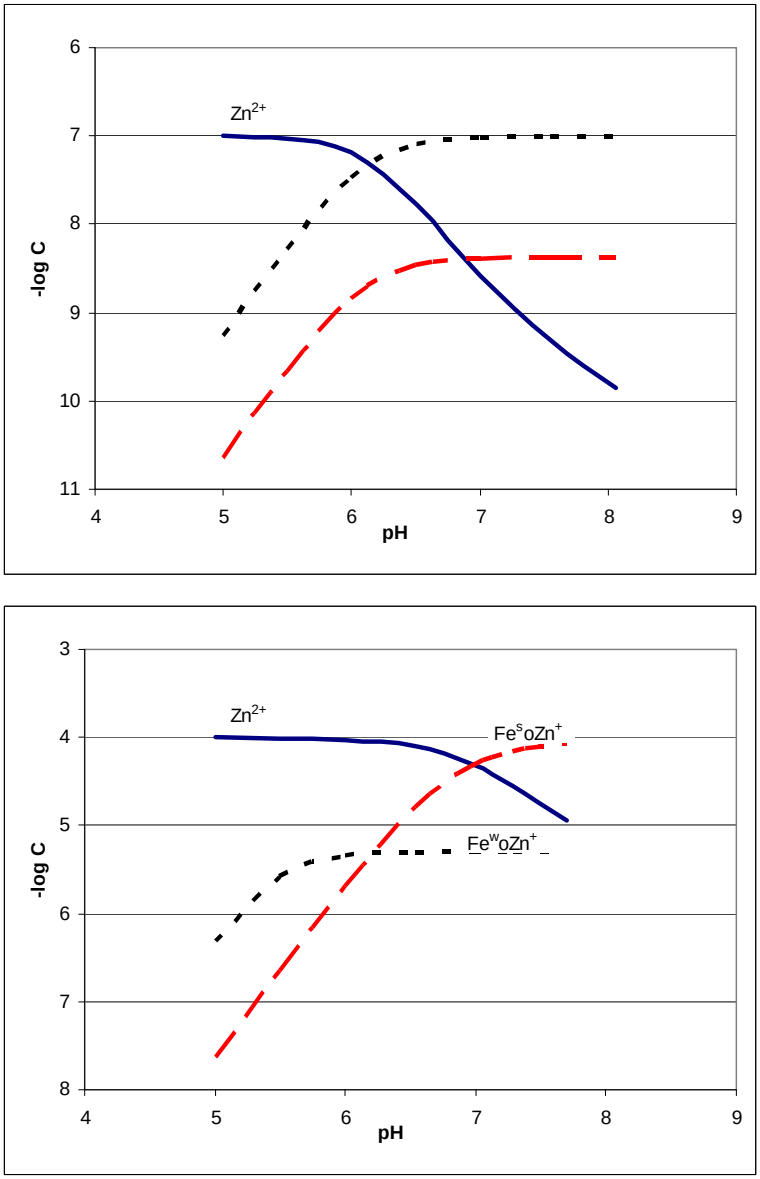

Fig. F2. Calculated equilibrium speciation as a function of pH for zinc. The top figure shows results for Total Zn=10^{-4} M, I = 0.1 M; the bottom figure shows results for Total Zn=10^{-7} M, I = 0.1 M.

F3. Surface Complexation Reactions and Parameters Used in Section 4

The adsorption of heavy metal (and arsenic) ions on minerals is influenced by a variety of factors, the most important being pH, type and speciation of metal ion involved, as well as heavy metal competition (Bradl, 2004). In this study, we consider goethite, illite, kaolinite, and smectite as principal adsorbents, mainly because these minerals have strong adsorption capacity, and we focus on lead and arsenic as relevant hazardous constituents**.** A literature analysis was conducted to determine the relevant surface complexation reactions and their thermodynamic constants for these cations and minerals, as summarized below.

Adsorption of Pb(II) on goethite was investigated under varying conditions. Kovacevic et al. (2000) experimentally studied the adsorption of lead species on goethite. Experiments were carried out for total Pb species concentrations of 2.5×10^{-4} mol/L, ph of 3–6, and ionic strength of 2×10^{-3} mol/L. The calculated surface complexation constant (logK) is -0.9 for a reaction expressed in the following form:

$$SOPb^{+} + H^{+} \rightleftharpoons Pb^{+2} + SOH \qquad \text{(F31)}$$

where *S* indicates surface, and $SOPb^{+}$ and SOH are surface complexes.

Muller and Sigg (1991) investigated the adsorption of Pb(II) on goethite in dilute (i.e., 2.41×10^{-7} mol/L) Pb (II) solutions over a pH range 6.6–8.2. Their published surface complexation constant (logK) is 0.52 for the monodentate surface complex (Equation F31) and 6.27 for the bidentate surface complex. Published surface complexation constants by Muller and Sigg (1991) are adopted in our simulations here, since they were obtained under conditions similar to the simulation setup in terms of Pb(II) concentration and pH. Since PbCO3(aq) is used as the primary species in our simulation instead of Pb(II), the reaction described in Equation (F31) occurs together with the following reaction between PbCO3(aq) and Pb(II):

$$Pb^{+2} + HCO_3^{-} \rightleftharpoons H^{+} + PbCO_3(aq) \qquad \log K = -3.06 \qquad \text{(F32)}$$

Note that the log*K* value of Equation (F32) was taken from the EQ3/6 V7.2b data base (Wolery, 1993).

Combining Equations (F31) and (F32), we obtain the surface complexation reaction shown in Table F2, where log*K* is -2.56. Note that the surface complex is expressed as Goe_OPb^{+} instead of $SOPb^{+}$, in order to distinguish it from other surface complexes of Pb(II).

Hizal and Apak (2006) studied lead(II) adsorption individually on kaolinite-based clay minerals. They performed experiments on three samples and calculated surface complexation constants and site densities. In our study, the surface complexation constant is taken to be the average of the value for these three samples, which is -1.87 for Equation (F31). Combining Equations (F31) and (F32), the log*K* value is -4.95.

Using batch adsorption experiments, Gu and Evans (2007) investigated the adsorption of Pb(II) onto illite as a function of pH and ionic strength. (Surface complexation of Pb on illite in a 0.01 mol/L $NaNO_3$ electrolyte is considered in our model because the majority of the potable groundwaters recorded in the NWIS database (USGS, 2008) have an ionic strength around 0.01M.) The investigators provided surface complexation constants for complexes on both edge and basal sites. Here, we refer to these as constants for strong sites ($Ill^{s}_OPb^{+}$) and weak sites ($Ill^{w}_OPb^{+}$), respectively (see Table F2).

Bradbury and Baeyens (2005) summarized surface complexation constants on smectite for more than ten metals. They presented linear free energy relationships (LFER) for strong and weak sites. The LFER correlated the surface complexation constants with aqueous complexation constants of the corresponding aqueous complexes. The calculated surface complexation constants for Pb(II) on montmorillonite, a member of the smectite group, for strong and weak sites using the LFERs (see Table 6 in Bradbury and Baeyens, (2005) are adopted in our simulation (see Table F2).

All the surface complexation reactions for lead used in the present simulation are listed in Table F2, while Table F3 summarizes these reactions using Pb^{+2} as primary species.

Adsorption of arsenite species on minerals can be described by three surface complexation reactions:

$$SH_2AsO_3 + H_2O \rightleftharpoons SOH + H_3AsO_3 \qquad \text{(F33)}$$

$$SHAsO_3^- + H_2O + H^+ \rightleftharpoons SOH + H_3AsO_3 \tag{F34}$$

$$SHAsO_3^{-2} + H_2O + 2H^+ \rightleftharpoons SOH + H_3AsO_3 \tag{F35}$$

where *S* denotes the surface of any mineral.

Surface complexation constants (see Table F3) for adsorption of arsenite on goethite are taken from Dixit and Hering (2003) by combining two reactions:

$$Goe_OH_2AsO_3 + H_2O \rightleftharpoons Goe_OH + AsO_3^{-3} + 3H^+ \qquad \log K = -39.93 \tag{F36}$$

$$AsO_3^{-3} + 3H^+ \rightleftharpoons H_3AsO_3 \qquad \log K = 34.74 \tag{F37}$$

Goldberg (2002) published the surface complexation constants (log*K*) for Equations (F36) and (37), which are -4.68 and 2.27, respectively. These constants are similar to those reported by Dixit and Hering (2003).

Goldberg (2002) also presented the surface complexation constants for the adsorption of arsenite on illite, kaolinite, and smectite. However, Manning and Goldberg (1997) gave a more complete description for adsorption of arsenite on these three minerals. In our study, we use the published surface complexation constants for Equations (F33), (F34) and (F35) from Manning and Goldberg (1997) (see Table F4). Table F4 summarizes the surface complexation reactions of As used in Section 4.

Specific surface area and site density are the other two important parameters affecting adsorption. Table F5 summarizes some published values for specific surface area and site density, while Table F6 lists those values used in the base model.

Table F2. Surface complexation of Pb on different minerals using PbCO3(aq) as primary species

Adsorbent	Surface Complexes	Reactions	Log k_{int}	Reference
goethite	Goe_OPb+	Goe _OPb$^+$ + HCO_3^- $\rightleftharpoons$ Goe_OH + $PbCO_3$(aq)	-2.56	(Muller and Sigg, 1991)
goethite	(Goe _O)$_2$Pb	(Goe _O)$_2$Pb + H^+ + HCO_3^- $\rightleftharpoons$ 2Goe_OH + $PbCO_3$(aq)	3.18	
kaolinite	Kao_OPb+	Kao_OPb$^+$ + HCO3$^-$ $\rightleftharpoons$ Kao_OH + PbCO3(aq)	-4.95	(Hizal and Apak, 2006)
illite	Ill^s_OPb+	Ill^s_OPb$^+$ + HCO3$^-$ $\rightleftharpoons$ Ill^s_OH + PbCO3(aq)	-4.43	(Gu and Evans, 2007)
illite	Ill^w_OPb+	Ill^w_OPb$^+$ + HCO3$^-$ $\rightleftharpoons$ Ill^w_OH + PbCO3(aq)	0.78	
smectite	Sme^s_OPb+	Sme^s_OPb$^+$ + HCO3$^-$ $\rightleftharpoons$ Sme^s_OH + PbCO3(aq)	-4.18	(Bradbury and Baeyens, 2005)
smectite	Sme^w_OPb+	Sme^w_OPb$^+$ + HCO3$^-$ $\rightleftharpoons$ Sme^w_OH + PbCO3(aq)	-1.78	
glauconite	Gla_OPb$^+$	Gla_OPb$^+$ + HCO_3^- $\rightleftharpoons$ Gla _OH + $PbCO_3$(aq)	-6.4	(Smith et al., 1996)

Table F3. Surface complexation of Pb on different minerals using Pb^{+2} as primary species.

Adsorbent	Surface Complexes	Reactions	Log k_{int}	Reference
goethite	Goe_OPb+	Goe _OPb$^+$ + H^+ $\rightleftharpoons$ Goe_OH + Pb^{+2}	0.5	(Muller and Sigg, 1991)
goethite	(Goe _O)$_2$Pb	(Goe _O)$_2$Pb+2H^+ $\rightleftharpoons$ 2Goe_OH + Pb^{+2}	6.24	
kaolinite	Kao_OPb+	Kao_OPb$^+$ + H^+ $\rightleftharpoons$ Kao_OH + Pb^{+2}	-1.89	(Hizal and Apak, 2006)
illite	Ill^s_OPb+	Ill^s_OPb$^+$ + H^+ $\rightleftharpoons$ Ill^s_OH + Pb^{+2}	-1.37	(Gu and Evans, 2007)
illite	Ill^w_OPb+	Illw_OPb$^+$ + H^+ $\rightleftharpoons$ Illw_OH + Pb^{+2}	3.84	
smectite	Sme^s_OPb+	Sme^s_OPb$^+$ + H^+ $\rightleftharpoons$ Sme^s_OH + Pb^{+2}	-1.12	(Bradbury and Baeyens, 2005)
smectite	Sme^w_OPb+	Sme^w_OPb$^+$ + H^+ $\rightleftharpoons$ Sme^w_OH + Pb^{+2}	1.28	
glauconite	Gla_OPb$^+$	Gla_OPb$^+$ + H^+ $\rightleftharpoons$ Gla _OH + Pb^{+2}	-3.34	(Smith et al., 1996)

Table F4. Surface complexation of H_3AsO_3 on different minerals

Adsorbent	Surface Complexes	Reactions	Log k_{int}	Reference
goethite	Goe _H_2AsO_3	Goe _H_2AsO_3 + H_2O $\rightleftharpoons$ Goe _OH + H_3AsO_3	-5.19	(Dixit and Hering, 2003)
goethite	Goe _$HAsO_3^-$	Goe _$HAsO_3^-$ + H_2O + H^+ $\rightleftharpoons$ Goe_OH + H_3AsO_3	2.34	
kaolinite	Kao_H_2AsO_3	Kao _H_2AsO_3 + H_2O $\rightleftharpoons$ Kao _OH + H_3AsO_3	-8.23	(Manning and Goldberg, 1997)
kaolinite	Kao _$HAsO_3^-$	Kao_$HAsO_3^-$ + H_2O + H^+ $\rightleftharpoons$ Kao _OH + H_3AsO_3	0.664	
kaolinite	Kao _$OAsO_3^{2-}$	Kao_AsO_3^{2-} + H_2O + $2H^+$ $\rightleftharpoons$ Kao _OH + H_3AsO_3	13.67	
illite	Ill_H_2AsO_3	Ill _H_2AsO_3 + H_2O $\rightleftharpoons$ Ill_OH + H_3AsO_3	-9.07	(Manning and Goldberg, 1997)
illite	Ill _$HAsO_3^-$	Ill _$HAsO_3^-$ + H_2O + H^+ $\rightleftharpoons$ Ill _OH + H_3AsO_3	-3.000	
illite	Ill_AsO_3^{2-}	Ill_AsO_3^{2-} + H_2O + $2H^+$ $\rightleftharpoons$ Ill_OH + H_3AsO_3	10.3	
smectite	Sme _H_2AsO_3	Sme _H_2AsO_3 + H_2O $\rightleftharpoons$ Sme _OH + H_3AsO_3	-8.89	(Manning and Goldberg, 1997)
smectite	Sme _$HAsO_3^-$	Sme _$HAsO_3^-$ + H_2O + H^+ $\rightleftharpoons$ Sme _OH + H_3AsO_3	4.650	
smectite	Sme _AsO_3^{2-}	Sme _AsO_3^{2-} + H_2O + $2H^+$ $\rightleftharpoons$ Sme _OH + H_3AsO_3	13.700	
albite~low	Alb _OH_2AsO_3	Alb _H_2AsO_3 + H_2O $\rightleftharpoons$ Alb _OH + H_3AsO_3	-7.58	(Manning and Goldberg, 1997)
albite~low	Alb _$OHAsO_3^-$	Alb _$OHAsO_3^-$ + H_2O + H^+ $\rightleftharpoons$ Alb _OH + H_3AsO_3	2.43	
albite~low	Alb _$OAsO_3^{2-}$	Alb _$OAsO_3^{2-}$ + H_2O + $2H^+$ $\rightleftharpoons$ Alb _OH + H_3AsO_3	14.8	

Table F5. Summary of published specific surface area and site densities

Absorbent	Specific surface area (m^2/g)	Site density (mol/m^2)		Reference
		Strong site	Weak site	
hematite	5.4	0.00219	0.219	Dzombak and morel (1990)
goethite	54	3.32e-6		Dixit and Hering (2003)
goethite	14.7	1.76e-6	3.22e-6	Muller and Sigg (1991)
kaolinite	19.53	1.02 e-8		Hizal and Apak (2006)
kaolinite	14.73	2.2e-6	3.0e-6	Lackovic, et al. (2003)
kaolinite	9.1	2.68e-7		Manning and Goldberg (1997)
illite	66.8	1.3e-6	2.27e-6	Gu and Evans (2007)
illite	123	2e-7	6e-7	Lackovic, et al. (2003)
illite	24.2	4.79e-8		Manning and Goldberg (1997)
Na-smectite	56.38	4.77e-8	9.54e-7	Bradbury and Baeyens (2005)
smectite	18.6	1.1e-6		Manning and Goldberg (1997)
albite~low	5.9	2.9e-5		Manning and Goldberg (1997)
glauconite	48.7	1.6e-6		Smith et al. (1996)

Table F6. Specific surface area and site densities used in the base model

Absorbent	Specific surface area (m^2/g)	Site density (mol/m^2)		Reference
		Strong site	Weak site	
goethite	14.7	1.76e-6	3.22e-6	Muller and Sigg, (1991)
kaolinite	14.73	2.2e-6	3.0e-6	Lackovic et al. (2003)
illite	66.8	1.3e-6	2.27e-6	Gu and Evans (2007)
Na-smectite	56.38	4.77e-8	9.54e-7	Bradbury and Baeyens (2005)